



INSTITUTO
SUPERIOR
TÉCNICO

UNIVERSIDADE TÉCNICA DE LISBOA
INSTITUTO SUPERIOR TÉCNICO

Robust Localization Algorithms in Sensor Networks with Applications on Target Tracking

Pınar Oğuz-Ekim

Supervisor: Doctor João Pedro Castilho Pereira Santos Gomes

Co-Supervisor: Doctor Paulo Jorge Coelho Ramalho Oliveira

Thesis specifically prepared to obtain the PhD Degree in
Electrical and Computer Engineering

Draft

2013

Abstract

Wireless sensor networks (WSN) are one of the most promising technologies due to their wide range of applications. Location awareness is a critical requirement of those applications as sensed information is often only meaningful if it is in conjunction with the location of the sensor. Moreover, localization and target tracking might be the main task. Therefore, with the purpose of addressing these problems, this thesis proposes several robust localization algorithms in WSN with a special focus on Target Tracking.

The first part of the thesis considers the problem of locating a single source from noisy range measurements of a set of nodes in a WSN. Several techniques are presented for two noise distributions, namely Gaussian and Laplacian, in different space dimensions. Broadly, the approaches for both noise distributions are based on formulating a range based Maximum-Likelihood (ML) estimation problem for the source position as a type of angle-of-arrival localization problem, and then using convex relaxation techniques to obtain a semidefinite program that can be globally and efficiently solved. Moreover, algorithms based on ℓ_1 -norm are used to address the Laplacian noise case, which models the presence of outliers in some practical ranging systems that adversely affect the performance of localization algorithms designed for Gaussian noise.

The second part of the thesis presents Simultaneous Localization and Tracking in WSN, which aims to determine the positions of sensor nodes and a moving target in a network, given incomplete and inaccurate range measurements between the target and each of the sensors. One of the established methods for achieving this is to iteratively maximize a likelihood function (ML) of positions given the observed ranges, which requires initialization with an approximate solution to avoid convergence towards local extrema. A modified Euclidean Distance Matrix (EDM) completion problem is solved for a block of target range measurements to approximately set up initial sensor/target positions, and the likelihood function is then iteratively refined through Majorization-Minimization. To avoid the computational burden of repeatedly solving increasingly large EDM problems in time-recursive operation, an incremental scheme is exploited whereby a new target/n-node position is estimated from previously available node/target locations to set up the iterative ML initial point for the full spatial configuration. The above methods are first derived under Gaussian noise assumptions, and modifications for Laplacian noise are then considered.

Simulation results and real indoor experiments show that the proposed algorithms significantly outperform state of the art methods in the presence of outliers as well as Gaussian noise. Additionally, they attain the Cramér Rao Lower Bound for small noise in the Gaussian case.

The third part of the thesis addresses sensor network localization problems with additional difficulties. Modified EDM completion problem is derived to estimate multiple target positions when there is no a priori information on turn-around time in two-way time of arrivals (TOA) measurements. It is assumed that targets can collaborate not only with anchors but also with each other, which leads to accurate localization even if some of those connect only to few anchors. Another EDM completion problem is examined to estimate multiple source positions in the existence of unknown transmit power in received signal strengths (RSS) measurements. Simulation results show that the proposed method outperforms the state of the art method in two ways: it is more accurate and it requires less computational operations. Additionally, it is observed that the cooperation among sources ensures accurate localization when some sources do not communicate with enough number of anchors.

Range measurements used in above algorithms are estimated from TOA or RSS. In the last part of the thesis, another range based localization problem, time difference of arrivals based source localization, is addressed. And a novel approach is proposed to solve it. The original problem is put in a more tractable mathematical form by using the square of the differences. Moreover, the exact solution of the modified problem is obtained by expressing the source location in polar coordinates instead of Cartesian coordinates.

Keywords: Source localization, sensor network localization, simultaneous localization and tracking, nonconvex and nonsmooth minimization, semidefinite programming, maximum likelihood estimation, Laplacian noise, central processing.

Resumo

As redes de sensores sem fios (RSSF) são uma das tecnologias mais promissoras pela sua utilidade num vasto número de aplicações. A informação sobre a localização dos sensores é um requisito crítico uma vez que a informação fornecida só é relevante quando combinada com a localização. Além do mais, a localização e o seguimento de alvos pode ser um objectivo por si só. Assim, com o intuito de melhorar as soluções existentes, esta tese propõe algoritmos robustos de localização em RSSF e com especial destaque em Seguimento de Alvos.

A primeira parte da tese considera o problema de encontrar uma fonte única a partir de medidas, com ruído, da distância entre a fonte e cada um dos vários nós de uma RSSF. São apresentadas várias técnicas para duas distribuições de ruído, tanto Gaussiano como Laplaciano, em espaços de diferentes dimensões. As abordagens recorrem à formulação do problema de estimação de distância baseada na máxima verossimilhança (ML do Inglês Maximum Likelihood) como uma localização de ângulo de chegada. Este problema é resolvido usando técnicas de relaxamento convexas que levam a obter um problema de programação semidefinido positivo, que pode ser global e eficientemente resolvido. Algoritmos com base na norma ℓ_1 são usados para resolver o caso de ruído Laplaciano. Este modela a presença de outliers presentes em sistemas reais e que degradam negativamente o desempenho de algoritmos de localização projectados para ruído Gaussiano.

A segunda parte da tese aborda o problema do Seguimento e Localização Simultâneos em RSSF, que visa determinar as posições dos nós da rede e de um alvo em movimento a partir de medições esparsas e imprecisas de distâncias entre o alvo e cada um dos sensores. Um dos métodos apresentados corresponde a maximizar iterativamente uma função da probabilidade dos sensores estarem numa determinada posição, dadas as distâncias observadas. O processo iterativo requer a inicialização com uma solução aproximada para evitar a convergência para um extremo local. Uma modificação ao problema de completar uma Matrix de Distância Euclidiana (EDM do Inglês Euclidean Distance Matrix) relativa ao um conjunto de medidas de distâncias ao alvo é utilizada para determinar aproximações iniciais das posições de sensores/alvos. A função de verossimilhança é então refinada iterativamente através um algoritmo de Majorização-Minimização. Para evitar a carga computacional resultante de repetidamente resolver problemas cada vez maiores da EDM, explora-se um esquema incremental pelo qual uma nova posição alvo/nó é estimada a partir de dados anteriores de posições nó/alvo para configurar o ponto inicial do ML. Os métodos referidos são inicialmente derivados assumindo ruído Gaussiano e depois modificados para o ruído Laplaciano.

Os resultados obtidos mostram que os algoritmos propostos superam significativamente os métodos de localização existentes na presença de outliers, bem como ruído Gaussiano.

A terceira parte de tese aborda problemas de localização em redes de sensores na presença de dificuldades adicionais. Em particular, propomos uma modificação ao problema de preenchimento de EDM para estimar as posições múltiplos alvos quando não temos informação a priori sobre o tempo de viagem em dupla transmissão nos tempos de chegada. Assume-se que as fontes/alvos podem colaborar não só com as âncoras mas também entre elas, o que leva a uma localização de maior acuidade na localiza ao, mesmo se esta colaboração envolver apenas poucas ligações. Propomos também um outro problema de preenchimento de EDM para estimar as posições de vários alvos quando não se sabe a potência dos sinais transmitidos. Os nossos resultados experimentais indicam que o método proposto, não só é mais preciso do que o algoritmo considerado estado-da-arte, como também requer menos operações computacionais. Para além disso, observamos que a cooperação entre fontes é suficiente para uma localização precisa quando algumas destas não comunicam com um número suficiente de âncoras.

As medições de distância que os algoritmos anteriores usam são estimadas partir da diferença de tempos de transmissão/recepção ou a partir da potência do sinal de chegada. Na última parte da tese, consideramos um outro problema de localização, baseado em diferença nos tempos de chegada, e uma propomos uma nova abordagem. O problema original é re-escrito em forma matematicamente mais tratável recorrendo ao do quadrado das diferenças. Além disso, a solução exacta do problema modificado é obtida expressando a localização da fonte em coordenadas polares em vez de coordenadas Cartesianas.

Palavras-chave: Localização de fontes, localização de rede de sensores, localização e rastreamento simultâneos, minimização não convexos e não diferenciáveis, programação semidefinida, estimativa de verosimilhança máxima, ruído Laplaciano, processamento central.

Acknowledgements

I wish to express my sincere gratitude to my advisor Professor João Pedro Gomes for his guidance, motivation and support throughout my graduate career at ISR-IST. Especially, I would like to thank him for keeping me always on the right track whenever I was miserably confused. I have learned a lot from his scientific thinking methodology and rigorous work attitude, which will continue to be good examples in my future life. I wish to express my gratitude for his constant help and support to my personal life as well as academical life. I would like to thank to my co-advisor Professor Paulo Oliveira for his comments, stimulating discussions and help on every subject.

I was very fortunate to have the opportunity to collaborate with Professor João Xavier during my PhD study. This thesis would not have been possible without his inspiration. I also thank to Professor João Paulo Costeira who brought me to ISR-IST and gave a chance to work in this excellent environment. I am obliged to Marko Stošić for the proof of Lemma [2.4.1.1](#).

There are many friends who enriched my life at ISR-IST. Some of them are my dear officemates, Ehsan Zamanizadeh, Sabina Zejnilovic, and Susana Brandão. Our “random talk” on every subject and the things we shared in both good and bad times will be sorely missed. My special thanks go to Cláudia Soares, João Mota, Dragana Bajovic, and Dusan Jakovetic for their friendship and encouragement even in distance during all these years. Without listing names and taking the risk to forget someone, I would also like to thank all my colleagues in ISR-IST, all of them great friends, for various discussions on research and the good times we shared.

Last but not least, I would like to thank my family. I would like to thank my parents-in-law, Fevziye and İlhan for their constant support and encouragement during our stay in Lisbon. It feels strange to formally thank my parents, Gülseren and Süleyman, and my sister, Şaziye, as their love and support has always felt so natural, taken for granted. Moreover, there are no words that can fully express my gratitude to them.

Lastly, I would like to express my most heartfelt gratitude to my husband, Umut. After sharing everything during the time of this PhD study – our days, our responsibilities, our successes and failures, our joys and sorrows – it is more reasonable to consider this thesis as a joint work of ours. And my dear son, Poyraz, as a futile attempt to substitute for the times that I borrowed from you, I dedicate this thesis to you.

This research was supported by Fundação para a Ciência e a Tecnologia (FCT) through grant SFRH/BD/44771/2008.

Contents

Abstract	iii
Resumo	v
Acknowledgements	vii
List of Figures	xi
List of Tables	xiii
Abbreviations	xiv
Symbols	xvi
1 Introduction	1
1.1 Wireless Sensor Networks, Localization and Tracking	1
1.2 Localization Measurements	3
1.3 Localization Algorithms	5
1.4 Contributions	8
1.5 Thesis Outline	10
2 An Angular Approach for Range Based Approximate Maximum Likelihood Source Localization Through Convex Relaxation	11
2.1 Introduction	11
2.2 Overview	12
2.3 Problem formulation	13
2.4 Source Localization in 2D	14
2.4.1 Source Localization Under Gaussian Noise: SLCP	14
2.4.1.1 Tightness and Geometry of the Constraint Set in SLCP	16
2.4.1.2 Factorization of the SDR Solution	18
2.4.2 Source localization Under Laplacian Noise: $SL-\ell_1$	19
2.5 Source Localization in Higher Dimensions	22
2.5.1 Localization under Gaussian Noise: SLNN	22
2.5.2 Localization under Laplacian Noise: $SL-\ell_1$ SD/MD	25
2.5.2.1 $SL-\ell_1$ MD	26
2.5.2.2 $SL-\ell_1$ SD	27
2.6 Complexity Analysis	29
2.7 Related Works	30
2.7.1 Squared Range Least Squares (SR-LS)	30

2.7.2	Linear Least Squares (LLS)	31
2.7.3	Two Least Squares (2LS)	32
2.8	Performance Analysis and Numerical Results	33
2.9	Real Indoor Experiments	41
2.10	Conclusion	43
3	Robust Localization of Nodes and Time-Recursive Tracking in Sensor Networks Using Noisy Range Measurements	46
3.1	Introduction	46
3.2	Overview	47
3.3	Problem Formulation	49
3.4	SLAT under Gaussian Noise	50
3.4.1	EDM with Squared Distances	50
3.4.2	Startup Initialization: EDM with Plain Distances	52
3.4.2.1	Estimation of Sensor and Target Positions from EDM	53
3.4.3	Refinement Steps: Majorization-Minimization	54
3.4.4	Updating Initialization: Recursive Position Estimation using SLCP / SLNN	55
3.5	SLAT under Laplacian Noise	56
3.5.1	Startup Initialization: EDM with Ranges and ℓ_1 -norm	56
3.5.2	Refinement Steps: Weighted Majorization Minimization	57
3.5.3	Updating Initialization: Recursive Position Estimation using SL- ℓ_1	59
3.6	Numerical Results	59
3.7	Real Indoor Experiments	65
3.8	Conclusion	67
4	Sensor Network Localization in the Presence of Unknown Turn-Around Time or Transmit Power	70
4.1	TOA based Sensor Network Localization with Unknown Turn-Around Time	70
4.1.1	Introduction	70
4.1.2	Problem Formulation	72
4.1.2.1	EDM Formulation	73
4.1.2.2	Estimate of γ_j	74
4.1.3	Simulations	75
4.1.4	Conclusion	77
4.2	RSS based Sensor Network Localization with Unknown Transmit Power	79
4.2.1	Introduction	79
4.2.2	Problem Formulation	80
4.2.3	Simulations	81
4.2.4	Conclusion	84
5	A Polar Decomposition Approach for Exact Source Localization from Squared Range Differences	85
5.1	Introduction	85
5.2	Problem Formulation	87
5.2.1	Direct Search Method	88
5.2.2	Lipschitz Optimization	88
5.2.3	Bisection Method	89

5.3	Simulations and Comparisons with Existing Methods	92
5.4	Conclusion	94
6	Conclusion and Outlook	95
6.1	Conclusion	95
6.2	Outlook	97
A	Equivalence of (2.1) and (2.2)	99
B	Proof of Lemma 2.4.1.1	100
C	Properties of Single-Source Localization using SL_{ℓ_1}	105
D	Analysis of SLNN	107
E	Derivation of CRLB for Source Localization Based on TOA	110
F	Convergence of Weighted Majorization Minimization	111
G	Derivation of CRLB for Sensor Network Localization	113
H	Derivation of CRLB for Sensor Network Localization with Unknown Turn-Around Time or Transmit Power	115
H.1	TOA based with Unknown Turn-Around Time	115
H.2	RSS based with Unknown Transmit Power	116
	Bibliography	118
	Curriculum Vitae	129

List of Figures

1.1	Geometric Techniques: Range or angle combining (reproduced from [14]).	3
1.2	The probability of successful packet transmission with respect to distance from the source in RSS case (reproduced from [3]).	5
2.1	Geometrical interpretation of terms in the source localization cost function (2.1) for $p = 1, q = 2$.	15
2.2	Minimization of a linear function over a circle.	24
2.3	RMSE Comparisons, without outliers.	35
2.4	RMSE Comparisons in the case of Selective Gaussian Noise.	37
2.5	RMSE Comparisons in the case of Laplacian Noise.	38
2.6	Speed comparisons of algorithms vs. number of anchors.	39
2.7	The sensitivity of SL- ℓ_1 MD to the penalizing term μ .	40
2.8	Range Measurement using ultrasound and radio signals (reproduced from [18]).	42
2.9	The test environment and Pioneer P3-DX: 4 Cricket sensors on the ceiling and 4 on top of tripods distributed over the lab in a 4m by 4m area. The robot or a human carries the beacon.	43
2.10	Piecewise linear/circular trajectory of Pioneer P3-DX.	44
3.1	Architecture of the SLAT algorithms.	51
3.2	Majorization Minimization Technique.	54
3.3	The value of $ \sqrt{E_{ij}} - d_{ij} $ vs E_{ij} , and the linear approximation of the concave part.	57
3.4	Comparison of initialization and refinement methods in the startup phase of SLAT.	61
3.5	Mean and uncertainty ellipsoids in the startup phase with different initialization methods. No outliers, $\sigma_{\text{gaussian}} = 0.025$.	62
3.6	Mean and uncertainty ellipsoids in the startup phase with different initialization methods. Selective Gaussian Noise (outlier), $\sigma_{\text{outlier}} = 0.8/\sigma_{\text{gaussian}} = 0.02$.	63
3.7	Evolution of Gaussian cost function $\Omega_G(\mathbf{x})$ during refinement for EDM-R+MM and SLCP+MM approaches, with $\sigma_{\text{gaussian}} = 0.04$.	64
3.8	Evolution of Laplacian cost function $\Omega_L(\mathbf{x})$ during refinement for EDM-R- ℓ_1 +wMM and SL ℓ_1 +wMM approaches, with $\sigma_{\text{laplacian}} = 0.1$.	65
3.9	Circular trajectory of Pioneer P3-DX. B-est and TR-est refer to estimation from full batch (EDM-R + MM) and the time recursive ((EDM-R + MM)+ SLNN + MM) procedures, respectively.	66

3.10	Piecewise linear/circular trajectory of Pioneer P3-DX. B-est and TR-est refer to estimation from full batch (EDM-R + MM) and the time recursive ((EDM-R + MM) + SLNN + MM) procedures, respectively.	67
3.11	Trajectory of a human target.	68
4.1	Two TW-TOAs are obtained in three communcations between target nodes. TOA measurements are estimated accurately only when the clocks of the nodes are synchronized.	73
4.2	RMSE comparisons in a fully connected randomly distributed network.	76
4.3	RMSE comparisons in a fully connected <i>structured network</i>	76
4.4	RMSE comparisons, sample mean and uncertainty ellipsoids of localization when the 5th and 6th targets of a <i>structured network</i> are connected to only two anchors.	78
4.5	RMSE comparisons for the first scenario where the sources are inside the convex hull of the anchors.	82
4.6	RMSE comparisons for the second scenario where the sources are not inside the convex hull of the anchors	82
4.7	Sample mean (shown as crosses) and uncertainty ellipsoids of EDM when sources $[\mathbf{s}_1 \ \mathbf{s}_{10}] = [2 \ 19; 18 \ 18]$ are connected to only two anchors.	83
5.1	Hyperbolas and the source position estimated by KKT and SRD-LS methods.	93
B.1	Illustration of geometrical Lemma B.0.0.2 and its application to a convex combination on the unit circle.	102
B.2	The constraint set \mathcal{S} for randomly generated $\boldsymbol{\theta}$ satisfying $ \theta_i = 1$ and different numbers of randomly placed anchors. For each set the hypothesized convex hull, computed by relaxation of \mathcal{S} , is also depicted.	104

List of Tables

2.1	Worst-case complexities of the proposed algorithms.	29
2.2	Source localization accuracy for relaxation-based methods (RMSEs listed for total and tight runs).	41
5.1	RMSE comparisons of SEARCH, KKT, SRD-LS and SI for near field case.	92
5.2	RMSE comparisons of SEARCH, KKT, SRD-LS and SI for far field case.	93

Abbreviations

WSN	W ireless S ensor N etworks
SNL	S ensor N etwork L ocalization
SL	S ource L ocalization
GPS	G lobal P ositioning S ystem
TOA	T ime O f A rrival
TDOA	T ime D ifference O f A rrival
AOA	A ngle O f A rrival
RSS	R eceived S ignal S trength
NLOS	N on L ine O f S ight
UWB	U ltra W ide- B and
ML	M aximum L ikelihood
MLE	M aximum L ikelihood E stimat(or/ion)
LS	L east S quares
NLS	N onlinear L east S quare
MM	M ajorization M inimization
SDP	S emi D efinite P rogramming
SDR	S emi D efinite R elaxation
KKT	K arush K uhn T ucker
SVD	S ingular V alue D ecomposition
EDM	E uclidean D istance M atrix
SLAT	S imultaneous L ocalisation and T racking
SLCP	S ource L ocalization in C omplex P lane
SLNN	S ource L ocalization with N uclear N orm
SL-ℓ_1	S ource L ocalization with l1 norm
SL-ℓ_1 SD	S ource L ocalization with l1 norm S ingle D imension

SL-ℓ_1 MD	S ource L ocalization with l1 norm M ultiple D imensions
CRLB	C ramér R ao L ower B ound
RMSE	R oot M ean S quare E rror
i.i.d.	i ndependent and i dentically d istributed
TW-TOA	T wo- W ay T ime- O f- A rrival
TWR	T wo W ay R anging
ATR	A symmetric T rip R anging

Symbols

x_{ij}	individual component of matrix \mathbf{X}
x_i	individual component of vector \mathbf{x}
$(\cdot)^T$	the transpose of a real vector or matrix
$(\cdot)^H$	the hermitian of a complex vector or matrix
$\langle \cdot, \cdot \rangle$	the inner product of two vectors
$\text{tr}(\cdot)$	the trace of a matrix
$\text{Re}(\cdot)$	the real part of a complex quantity
$\mathbf{X} \succeq 0$	a symmetric matrix \mathbf{X} is positive semidefinite
$\ \cdot\ _F$	the Frobenius norm
$\ \cdot\ _N$	the nuclear norm
$\ \cdot\ $ or $ \cdot $	the Euclidean norm
\mathbf{I}_m	$m \times m$ identity matrix
$\mathbf{1}_m$	the vector of m ones
$\text{co}(\mathcal{S})$	the convex hull of set \mathcal{S}
\odot	Hadamard product
\otimes	Kronecker product
$\text{sgn}(\cdot)$	the signum function
\mathbb{R}^n	set of n -dimensional column vectors with real entries
$\mathbb{R}^{n \times m}$	set of $n \times m$ matrices with real entries
\mathbb{C}^n	set of n -dimensional column vectors with complex entries
$\mathbb{C}^{n \times m}$	set of $n \times m$ matrices with complex entries

Annem'e ve Poyraz'a

Chapter 1

Introduction

1.1 Wireless Sensor Networks, Localization and Tracking

Recent advances in technology have allowed the development of low-cost, low-power and multi-functional sensors that are small in size and able to communicate at short distances. Cheap and smart sensors, which are networked through wireless links and deployed in large numbers, provide many opportunities for sensing, monitoring and controlling homes, cities, and the environment. Current and potential applications of Wireless Sensor Networks (WSN) include smart homes (home security, control of home appliances, and locating inhabitants), search and rescue (locating lost children, emergency responders, and earthquake victims), inventory control (real-time tracking of shipments and valuable items in manufacturing plants), environment monitoring (bush fire surveillance and water quality monitoring) and target tracking.

Location awareness is an essential feature of above WSN applications. Information collected or communicated by a wireless sensor node is often meaningful only in conjunction with the location of the node. For example, sensor networks used for detecting spatial variations in environmental conditions, such as temperature or pollution, require knowledge of each sensor's location. Localization is also relevant to the networks main functions: communication, geographical routing, network coverage, etc. Moreover, localization and tracking might actually be the main task of WSN such as it is the case with the applications of habitat monitoring and target tracking). Nevertheless, location awareness in WSN is far from a trivial task. Since the network can consist of a large number of sensor nodes that are deployed in an ad-hoc fashion, manually programming each sensor with its geographic information is impossible. Furthermore, any dynamic technique must take into account the low-power and low-cost constraints that govern every aspect of sensor networks. In most application scenarios, regular maintenance (and

battery recharging) is virtually impossible, making energy efficiency become a critical requirement for these nodes. These restrictions are exactly what inhibits us from using the obvious solution of incorporating a Global Positioning System (GPS) receiver in every node. Moreover, GPS-based localization is not applicable in the indoors, underground and underwater sensor deployment scenarios.

The goal of localization is to determine the physical coordinates of a group of sensor nodes. Sensor network localization algorithms estimate the locations of sensors by using knowledge of the absolute positions of a few sensors and inter-sensor measurements such as distance and bearing measurements. Sensors with known location information are called anchors and their locations can be obtained by using a GPS, or by installing anchors at points with known coordinates. In applications requiring a global coordinate system, these anchors will determine the location of the sensor network in the global coordinate system. When the relative information is sufficient, the locations of sensors are an arbitrary “rigid transformation” (rotation, reflection, translation) away from the global coordinate system. Good surveys on localization in WSN can be found in [1–5].

Sensor network localization can generally be divided into two cases: non-cooperative and cooperative. In the noncooperative case, sensor nodes can communicate only with anchor nodes [6, 7]. The lack of accessible anchor nodes and also limited connectivity among anchor nodes and sensor nodes lead to the emergence of cooperative localization in which sensor nodes are able to communicate with both anchor nodes and other sensors. Therefore, not only are measurements between sensor nodes and anchor nodes obtained, but also the sensor nodes themselves are involved and collect measurements from each other [8].

Target tracking is an important application for WSNs because of its relevance to intelligence gathering and environmental monitoring. In order to achieve good accuracy in target localization task, the nodes themselves have to be well localized. Moreover, the localization algorithm should be efficient and scalable. Although several research works have addressed the problem of target tracking in collaborative networks [9], and sensor node location estimation [10] separately, very few of them actually treat the problem of joint location estimation and target tracking, which is sometimes referred to as Simultaneous Localization and Tracking (SLAT) in the literature [11–13].

Although, the main focus of this thesis is the localization algorithms for WSN, the proposed algorithms can easily find place in cellular networks and robotics. In other words, “sensor/source/target/node” might refer to any device involved in the localization algorithms, such as a cellular phone, a base station or a robot.

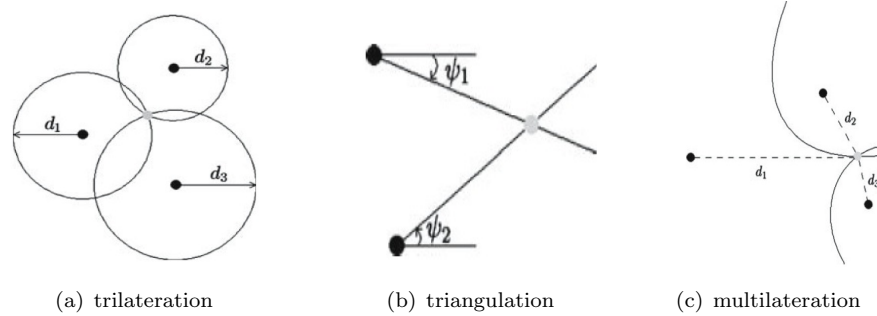


FIGURE 1.1: Geometric Techniques: Range or angle combining (reproduced from [14]).

1.2 Localization Measurements

The use of any localization algorithm is only as good as the validity of the assumptions on the underlying measurement error distribution in the actual deployment scenario. Accuracy in measurement technology affects the algorithm accuracy.

Since the sensor nodes are equipped with radios to perform communications, locating a node in a wireless system from radio signals travelling between nodes attracts lot of attention. Depending on the positioning technique, Angle of Arrival (AOA), Received Signal Strength (RSS), Time of Arrival (TOA), or Time Difference of Arrival (TDOA) information can be used.

TOA: TOA technique measures the distance between nodes using signal propagation time. In the absence of any errors, the uncertainty on TOA estimate forms a circle centered at an anchor as shown in Figure 1.1(a) [14]. In order to calculate the TOA parameter for a signal travelling between two nodes, the nodes must either have a common clock (one-way ranging approach), or exchange timing information by certain protocols such as a Two Way Ranging (TWR) protocol. The one-way ranging approach to determine TOA is less used because it requires an accurate synchronization between the sender and receiver clocks which adds cost and complexity to the WSN. TOA is susceptible to errors due to obstructions between the sender and the receiver. These obstructions, leading to so-called Non Line of Sight (NLOS) conditions, can cause a positive bias in the distance estimate. Estimating arrival times might also be hampered by noise, interference, multipath and clock drifts [15]. Among the noisy measurements upon which localization could be based, TOA provides a good tradeoff between the accuracy and implementation cost [14, 16].

TDOA: In the absence of synchronization between the sender and the receiver, the TDOA estimation can be performed if there is synchronization among the receiver nodes. TDOA estimation provides the difference in arrival times of two signals travelling between the sender node and two receiver nodes, which leads to elimination of timing offset. The noiseless TDOA between receiver nodes defines a hyperbola with foci at receiver positions (see Figure 1.1(c)). Multipath and NLOS conditions limit the accuracy of the TDOA estimation [17].

The clock synchronization is an important practical problem of TOA/TDOA based systems and it affects the accuracy of localization algorithms. Some systems sidestep this issue without resorting to the TWR protocol by using ultrasound and RF signals. The difference of those signals' arrival times to the receiver node gives an accurate estimate on the distance, between the sender and receiver nodes, which is then used in localization algorithms [18].

AOA: AOA based methods strictly speaking do not measure distance but the direction of the received signal (see Figure 1.1(b)) [19]. In these methods, several spatially separated antennas are used to discover the AOA of the signal based on measurements of the phase differences in the arrival of a wavefront. These methods can obtain accuracy to within a few degrees. Another advantage of them is that they do not require receiver or sender clock synchronization. Unfortunately, AOA hardware tends to be more expensive than the ones used in above techniques, since it requires a large receiver antenna or an antenna array. The accuracy of AOA is affected by shadowing and multipath reflections.

RSS: Among the noisy measurements upon which localization could be based, RSS is an attractive method mainly because of its low complexity and cost [16]. The power of a signal traveling between two nodes is a signal parameter that contains information related to the distance between those nodes. In theory, the energy of a radio signal diminishes with the square of the distance from the signal's source. In practice, however, it is well known that the propagation characteristics of radio signals can vary with changes in the surrounding environment (weather changes, urban/rural and indoor/outdoor settings) and can be highly non-uniform [3, 20], i.e., it is possible to retrieve the distance information from a particular direction but not from the others as shown in Figure 1.2. Multipath signals and shadowing are two major sources of environment dependence in the RSS measurement [8].

The parameters of the noise can be assumed to be known for all the previously stated methods and also it is possible to (approximately) model each noise component by a zero mean Gaussian random variable [20] for TOA, RSS and AOA based systems

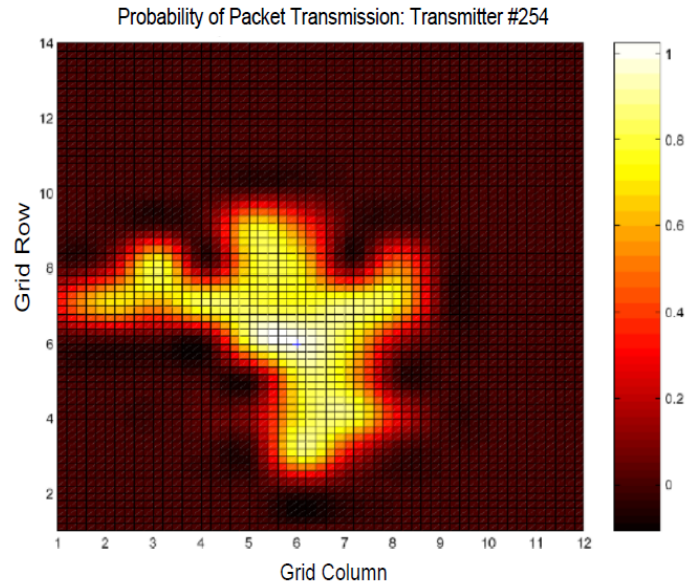


FIGURE 1.2: The probability of successful packet transmission with respect to distance from the source in RSS case (reproduced from [3]).

in Line of Sight conditions. The noise distribution in the NLOS case is commonly modeled as Rayleigh [21], Exponentially modified Gaussian [22] or Gamma distributions [20]. Algorithms based on ℓ_1 -norm are known to be robust to outliers or NLOS [23]. Therefore, ℓ_1 -norm is adopted in the cost functions of the optimization problems in this thesis. Interestingly, these problems actually become Maximum Likelihood Estimation (MLE) problems when the noise is assumed as Laplacian as shown in Chapters 2 and 3. Therefore, Laplacian noise distribution refers to outliers/NLOS throughout the thesis because of mathematical tractability.

1.3 Localization Algorithms

A detailed survey on localization algorithms can be found in [24] and a survey related with each chapter's discussion will be provided at the beginning of the chapters. However, a general look at the localization algorithms can be found next:

Geometric based techniques are appealing due to their simplicity when the noise is absent and the number of anchors is small. The most basic and intuitive method is called trilateration which locates the target node by calculating the intersection of three circles [25, 26] based on simultaneous range measurements from three nodes located at known positions as shown in Figure 1.1(a). Triangulation is used when the direction of the node instead of the distance is estimated, as in AOA systems (Figure 1.1(b)). The node positions are calculated in this case by using the trigonometry laws of sines and

cosines [26]. Multilateration is a technique based on the measurement of the difference in distance to two or more nodes at known locations which forms a hyperbolic curve. The intersection of two hyperbolas, corresponding to two TDOA measurements, determines the position of the target nodes shown in Figure 1.1(c) [26, 27].

However, when the position lines intersect at multiple points, instead of a single point, due to errors on measurements or increased number of parameters, the geometric approach does not provide a useful insight as to which intersection point to choose as the position of the target node.

If the data is known to be described well by a particular statistical model, then the MLE can be derived and implemented. That is because the variance of these estimators asymptotically (as the signal-to-noise ratio goes high) approaches the lower bound given by the Cramér Rao Lower Bound (CRLB). Even though a closed form Maximum Likelihood (ML) solution is not possible because of nonlinear dependence between the measurements and the unknown parameters, approximate and iterative ML techniques can be derived as will be discussed below.

Typically, ML solutions are obtained as the global minimum of the nonconvex objective function which is directly derived from the likelihood function of the problem. Several algorithms have been proposed which aim at finding ML solutions. For instance, the classic Nonlinear Least Squares (NLS) algorithm [28, 29] and SMACOF algorithm [30, 31] are popular due to their relatively low complexity and ease of implementation. The nonlinear optimization problem based on AOA or TDOA measurements can be solved by a Newton-Gauss iteration [32, 33]. For TOA measurements, the steepest descent [34, 35], Gauss-Newton [36, 37], Majorization-Minimization [37, 38] methods have been proposed. These methods require an initial estimate close enough to the true minimum of the cost function. Such an initial estimate may be obtained from prior information, or using a suboptimal procedure described as follows.

One way to prevent convergence to local maxima is to formulate the localization as a convex optimization problem. Localization algorithms based on global optimization such as the Semidefinite Programming (SDP) formulations are not, by design, strictly derived from the likelihood function [35, 39, 40]. However, the advantage of an SDP is that its cost function does not have local minima and thus convergence to the global minimum is guaranteed [23]. One drawback of some SDPs is their high computational complexity. Additionally, the SDP technique is sub-optimal and cannot achieve the best possible performance under all conditions. When the probability distribution of the noise is not known, least squares (LS) techniques can be used to obtain a coarse localization estimation [6, 41, 42]. Since it is computationally inexpensive, it may be

used as an initial location estimate to enhance the localization performance of more accurate (yet more complex) algorithms.

The localization algorithms can also be classified as centralized and distributed [5, 8]. Centralization requires the transfer of inter-node measurements over many hops to a sufficiently powerful central node. In distributed algorithms, each node uses its own measurements and exchanges local information with its neighbors (only one hop but possibly more than once, over multiple iterations). Centralization allows an algorithm to undertake much more complex mathematics than is possible in a distributed setting. However, distributed algorithms are more robust to node failures. Moreover, the centralized algorithms are not suitable for large scale networks due to energy efficiency. In this thesis, the centralized localization algorithms will be exploited. The main motive behind the interest in centralized localization schemes is the likelihood of providing more accurate location estimates than those provided by distributed algorithms. What is more, once the number of hops to reach the central node is less than the number of iterations to converge to a stable solution, the centralized algorithms are more energy efficient than the distributed ones [8].

To this end, while many approaches to localization based on geometric techniques or heuristic criteria can be found in the WSN literature [43, 44], the primary focus in this thesis is on optimization-based methods formally derived from the likelihood function of observations, or related cost functions [45–50]. The main tool is the ML iterative techniques with a good initialization provided by SDP techniques or convex optimization techniques alone. That's because, we can take advantage of the optimality properties of ML estimates to improve the robustness to perturbations in range measurements. Additionally, SDPs, which are derived from original problems through convex relaxations, are likely to have a good approximation (a unique minimizer of SDP) to the original solution with ease of implementation. Furthermore, as stated above, optimization based techniques provide more insights than geometric techniques or heuristics in the existence of noise and multiple parameters. With these tools, two related problems will be tackled: Source Localization (SL) and Sensor Network Localization (SNL). SNL is also examined with Target Tracking application, namely SLAT, which is not handled in a usual way as the target dynamics are not accounted for. That's because, above methods proposed for the SLAT problem need a good prior knowledge on sensor deployment and initial target position. To decrease the sensitivity to initial estimate, a novel two stage-approach (startup phase and updating phase) is proposed. Briefly, the main goal of the startup phase is to obtain an outline of the network configuration from a set of measurements between each target position and sensor/anchor positions. And it is followed by an updating phase (time recursive) where new target sightings are incrementally assimilated as they become available, while improving all previously determined locations. Each

phase consists of an initialization step to calculate approximate locations, followed by an iterative refinement step of the likelihood function. Local convergence to undesirable extrema in ML methods due to poor initialization is thus alleviated. Throughout the thesis, these algorithms are derived assuming the noise on the observations has Gaussian or Laplacian distribution.

1.4 Contributions

The original contributions of this thesis are as follows

1. *Source Localization Under Gaussian Noise (Sections 2.4.1 and 2.5.1)*: In the literature, TOA based localization algorithms mainly focus on range matching cost function or the intersection of circles. This work looks at the same problem but from a different perspective and presents a novel angular framework, called Source Localization in Complex Plane (SLCP), in Section 2.4.1 (published [45]). SLCP is a 2D source localization algorithm which manipulates the original range matching cost function, turning it into an equivalent formulation and that resembles source localization based on AOA. The framework of SLCP is also extended from 2D localization to arbitrary (real) dimensions in Section 2.5.1. The latter Semidefinite Relaxation (SDR) method is termed as Source Localization with Nuclear Norm (SLNN), as the nuclear norm arises naturally in the cost function of the relaxed optimization problem (submitted [51]). As illustrated by our simulations both SLCP and SLNN offer a tight relaxation in most problem instances, and retains a performance advantage over the most popular source localization algorithms.
2. *Source Localization Under Laplacian Noise (Sections 2.4.2 and 2.5.2)*: Laplacian noise, which represents outliers or NLOS situations, is addressed in Sections 2.4.2 and 2.5.2 by replacing ℓ_2 norms with ℓ_1 norms for various optimization subproblems. The problems are initially formulated under the assumption of Gaussian noise, and then by performing suitable manipulations, they are rewritten in a form that is amenable to general-purpose solvers. For instance, a modification of SLCP, termed Source Localization with ℓ_1 Norm (SL- ℓ_1), is introduced for ML source localization under Laplacian noise for 2D in Section 2.4.2 (published [38]). The ML formulation of a source localization problem with Laplacian noise is a more robust solution to outlier measurements, a property that was observed in simulation even for non-Laplacian range errors. Conceptually similar extensions for source localization beyond 2D, termed Source Localization with ℓ_1 Norm Single Dimension (SL- ℓ_1 SD) and Source localization with ℓ_1 Norm Multiple Dimensions

(SL- ℓ_1 MD), are provided in Section 2.5.2, consisting of a reformulation of the non-differentiable log-likelihood function for Laplacian noise as a reweighted version of the Gaussian log-likelihood (submitted [51]).

3. *SLAT with Modest Prior Knowledge (Sections 3.4.1, 3.4.2 and 3.5.1)*: This thesis emphasizes the development of a SLAT method with modest prior assumptions on the sensor/target positions (published [37], [38]). This is achieved mainly by casting SLAT as a SNL (Sections 3.4.1, 3.4.2 and 3.5.1) or SL problem during initialization in the startup and updating phases, respectively, which admit accurate convex relaxations where local extrema are absent. Anchors are still needed in refinement steps to eliminate fundamental translation and rotation ambiguities in the likelihood function.
4. *Coherent ML framework for SLAT with Moderate Complexity (Sections 3.4 and 3.5)*: The startup/time-recursive updating approach is proposed for Gaussian noise, using cost functions for the initialization steps that match *plain range* (non-squared) observations with *plain* estimated ranges. These allow for both the initialization and ML refinement steps to operate with cost functions that match plain ranges, which leads to improved robustness under strong measurement noise in Section 3.4 (published [38]). In addition to the Gaussian case, this work develops startup and updating algorithms for Laplacian noise, to model the presence of outliers in some practical ranging systems that negatively affect the performance of localization algorithms designed for Gaussian noise in Section 3.5. The details of proposed cost functions are different for Gaussian and Laplacian noise models, but in both cases robustness to range errors is gained relative to more standard Euclidean Distance Matrix (EDM) methods by matching plain distances. This is attained with a moderate complexity.

In addition to the initialization techniques, a novel ML iterative technique Majorization Minimization (MM) is proposed for the Gaussian case (Section 3.4.3) and Laplacian case (Section 3.5.2) (published [37, 38]).

5. *Real Indoor Experiments (Sections 2.9 and 3.7)*: The above contributions are also validated with a 3D real data from Cricket indoor system, from Crossbow Technologies [18], which uses both ultrasound and RF signals to estimate the ranges between sensors and a target. These devices are inexpensive and easy to deploy; however, their operating range is limited, approximately ten meters (published [52]).
6. *SNL with Unknown Turn-Around Time and Unknown Transmit Power (Sections 4.1 and 4.2)*: Chapter 4 shows the practices of similar techniques used in Chapter 3 to SNL with additional unknown parameters. An accurate SDP method which

localizes multiple targets simultaneously in the presence of unknown turn-around time in a TOA based network is presented in Section 4.1 (accepted [53]). The cooperation is assumed not only between anchors and targets but also among targets to improve the localization. For RSS based sensor network with unknown transmit power, Section 4.2 proposes a modified EDM method which is more accurate and less complex than the recently published method (submitted [54]). Accurate results are obtained even if some sources connect to few anchors due to the cooperation among themselves.

7. *Exact Source Localization from Squared TDOA (Section 5.2.3)*: Classical TDOA based localization algorithms try to minimize the inconsistencies between the measured and the estimated range differences. Due to the high nonlinearity between the measurement model and the problem parameters (and the noise), finding the exact solution of this problem is difficult. Chapter 5 proposes a novel formulation using squared range differences which leads to a nonconvex optimization problem that is solved efficiently and globally by switching from Cartesian coordinate system to polar/spherical coordinate system [55] (under preparation).

1.5 Thesis Outline

The rest of the thesis starts with addressing TOA based source localization problem in Chapter 2, which is also one of the crucial steps of the SLAT algorithm. The detailed derivations under Gaussian and Laplacian noise are given. Additionally, theoretical limitations, analyses and real setups will be mentioned. Chapter 3 presents a broader view of localization and shows simultaneous localization of nodes in sensor networks and target tracking, namely SLAT. Robust algorithms for different noise characteristics will be provided. Chapter 4 tackles sensor network localization problems with additional unknown parameters for TOA based as well as RSS based systems and explains the applications of the methods described in Chapter 3 to these harder problems. Chapter 5 returns back to source localization problem but for TDOA based systems. Conclusions will be drawn and a possible future work will be discussed in Chapter 6. Finally, some detailed analyses of the methods in Chapters 2, 3 and 4 will be provided in several Appendices.

Chapter 2

An Angular Approach for Range Based Approximate Maximum Likelihood Source Localization Through Convex Relaxation

2.1 Introduction

Locating a source from range measurements to a set of known reference points (anchors) is a classic problem in many engineering applications (e.g., radar, sonar, GPS), and has received a great deal of attention over the years. Recently, source localization from range measurements has been intensively examined in the context of WSN, where ranges are estimated from TOA.

Centralized ML algorithms for range-based source localization, which require the transmission of the full data set to a fusion node for processing, are proposed in [38, 45–50, 56, 57]. Some of these resort to SDR to alleviate the problem of algorithmic convergence to undesirable local maxima of the likelihood function [45, 50] for Gaussian noise and [38] for Laplacian noise. A related alternative approach proposed in [46] solves a constrained LS problem using squared range measurements, subject to a quadratic constraint (termed SR-LS). This was shown to outperform, on average, the ML SDR approach of [50] whose relaxed solutions sometimes fail to produce meaningful source position vectors (rank one solutions). Recently proposed SDP based methods, use either TOAs or square of them, take care of uncertainties in anchor positions [56]. Another

approach, proposed in [48], approximates the ML solution via second-order cone programming and a low-dimensional search. A linearisation based method presented in [57] solves two consecutive linear systems which exploit the constraint of squared norm of the source position in the second step.

Distributed algorithms for wireless sensor nodes, where the source location is iteratively determined through in-network processing at individual nodes and communication between neighbours, are also being very actively pursued [58–60]. These techniques, however, are not the focus of this work.

Source localization can also be viewed as a special instance of sensor network localization, where the positions of several sources/sensors are simultaneously determined from pairwise range measurements. Briefly, when a new source range measurement is obtained by the sensors, the new position is estimated by defining the previously estimated positions as reference sensors and resorting to the source localization algorithms. Related algorithms based on SDP have been developed for this class of problems [38, 61], and are relevant when there is significant uncertainty in anchor positions (see, e.g., [62] for a similar SDP approach to source localization with anchor uncertainty using range differences). This view constitutes one of the crucial steps of the SLAT algorithm which will be explained in Chapter 3.

2.2 Overview

This chapter develops algorithms for range-based source localization in arbitrary dimensions, including 2D/3D, through an ML SDR approach. The contributions and the summary of this chapter are as follows.

Section 2.4.1 presents a novel angular framework, called SLCP, which matches plain ranges using a formulation in the complex plane to attain an accurate convex relaxation as an SDP for 2D localization [45]. The framework of SLCP is also extended from 2D localization to arbitrary (real) dimensions in Section 2.5.1. The latter SDR method is termed as SLNN, as this norm arises naturally in the cost function of the relaxed optimization problem [51]. Both SLCP and SLNN offer a tight relaxation in most problem instances, and retains a performance advantage over SR-LS. Furthermore, a complete analysis of the accuracy properties of SLCP is provided, whose success in providing tight relaxations relies on certain parametrically defined sets in \mathbb{R}^2 being nearly convex. The convexity of the sets and how to trace the convex hull for any of them, from which convexity can be empirically assessed are discussed in Section 2.4.1.1. For three-anchor scenarios a search-based alternative to Singular Value Decomposition

(SVD) is also examined to extract the source coordinates from the solution of SLCP (a positive semidefinite matrix with near rank-1) in Section 2.4.1.2.

A modification of SLCP based on the same angular strategy, termed SL- ℓ_1 , is introduced for ML source localization under Laplacian noise for 2D in Section 2.4.2 [38]. This builds robustness to outlier measurements, a property that was observed in simulation even for non-Laplacian range errors. Mathematically, this stems from usage of ℓ_1 instead of ℓ_2 norms in the likelihood function, which tend to de-emphasize large discrepancies between predicted and measured ranges. In Section 2.5.2 a conceptually similar extension for source localization beyond 2D is provided, consisting of a reformulation of the non-differentiable log-likelihood function for Laplacian noise as a reweighted version of the Gaussian log-likelihood. They are SL- ℓ_1 MD which outperforms all benchmarked algorithms, and a simplified formulation (SL- ℓ_1 SD), which has slightly worse performance but is less computationally complex [51]. MD and SD refer to Multi Dimension and Single Dimension, respectively due to the dimension of the epigraph variables used in the optimization problems not because of space dimension. Section 2.6 mentions about the computational complexities of the proposed methods.

Extensive simulations were performed to compare the performance of the algorithms with the theoretical bound and several others of varying complexity and accuracy based on different criteria in Section 2.8. It is found that the proposed ones exhibit the most consistent performance over different types of range measurement noise, and relatively close to the CRLB. The complexity is comparable to that of other SDP-based methods, and appears suitable for practical implementation in several centralized scenarios of interest with current technology. The proposed algorithms are also validated with real data using an experimental 3D indoor localization setup based on Crossbow Cricket motes [18] (providing mixed RF/acoustic absolute ranging).

2.3 Problem formulation

Let $\mathbf{x} \in \mathbb{R}^n$ be the unknown source position, $\mathbf{a}_i \in \mathbb{R}^n$, $i = 1, \dots, m$ be known sensor positions (anchors), and $r_i = \|\mathbf{x} - \mathbf{a}_i\| + w_i$ be the measured range between the source and the i -th anchor, where w_i denotes a noise term. Under independent and identically distributed (i.i.d.) Gaussian or Laplacian noise maximizing the likelihood of observations for the source localization problem is equivalent to

$$\underset{\mathbf{x}}{\text{minimize}} \quad \sum_{i=1}^m \left| \|\mathbf{x} - \mathbf{a}_i\|^p - r_i^p \right|^q. \quad (2.1)$$

In this chapter it will be shown how to derive the SLCP/SLNN algorithms to (approximately) solve (2.1) under Gaussian noise ($p = 1, q = 2$), whereas SL- ℓ_1 will solve it under Laplacian noise ($p = 1, q = 1$). The case ($p = 2, q = 2$) is also of interest and corresponds to the cost function used in the SR-LS algorithm of [46], which is used to benchmark proposed algorithms. Note that the cost function for SR-LS is not a likelihood function, and it arises out of mathematical convenience.

The main difficulties of solving (2.1) lie in the fact that this cost function is, in general, nonconvex and hence multimodal. The nonconvexity of the cost function is addressed in Sections 2.4.1 and 2.5.1 by developing convex relaxations that turn out to be tight in most problem instances, thus providing a very good approximation to the global minimum of the objective function. Additional challenges are posed due to the nondifferentiability of (2.1) for $q = 1$ which is addressed in Sections 2.4.2 and 2.5.2 by rewriting it as a weighted version of the case $q = 2$, where the weights themselves become optimization variables.

2.4 Source Localization in 2D

This section presents the source localization problem specific for 2D in two parts. The first part will address the source localization problem under Gaussian noise, while the second will solve the similar problem under Laplacian noise, i.e., which is used here to model outliers in an analytically tractable way.

2.4.1 Source Localization Under Gaussian Noise: SLCP

For $p = 1, q = 2$ each term in (2.1) is viewed as the squared distance between two circles centered on \mathbf{a}_i , one with radius $\|\mathbf{x} - \mathbf{a}_i\|$, and the other with radius r_i (see Figure 2.1). This term can be replaced by the squared norm of the difference between the position vector \mathbf{x} and its closest point on the circle $\{\mathbf{y} \in \mathbb{R}^2 : \|\mathbf{y} - \mathbf{a}_i\| = r_i\}$, which is denoted by \mathbf{y}_i . Problem (2.1) can then be equivalently expressed as (a formal proof of equivalence is provided in Appendix A)

$$\begin{aligned} & \underset{\mathbf{x}, \mathbf{y}_i}{\text{minimize}} && \sum_{i=1}^m \|\mathbf{x} - \mathbf{y}_i\|^2 \\ & \text{subject to} && \|\mathbf{y}_i - \mathbf{a}_i\| = r_i \quad i = 1, \dots, m. \end{aligned} \tag{2.2}$$

If \mathbf{y}_i is fixed, the problem (2.2) with respect to \mathbf{x} is an unconstrained optimization problem whose solution is readily obtained as the center of mass of the constellation

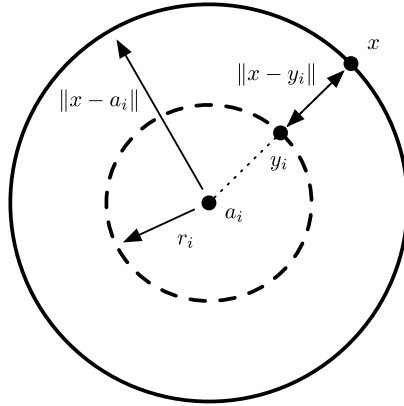


FIGURE 2.1: Geometrical interpretation of terms in the source localization cost function (2.1) for $p = 1, q = 2$.

$\mathbf{x} = \frac{1}{m} \sum_{i=1}^m \mathbf{y}_i$. Moreover, in 2D the constraints of (2.2) can be compactly described in the complex plane, yielding

$$\begin{aligned} & \underset{\mathbf{y}, \boldsymbol{\theta}}{\text{minimize}} && \left\| \frac{1}{m} \mathbf{1}_m \mathbf{1}_m^T \mathbf{y} - \mathbf{y} \right\|^2 \\ & \text{subject to} && \mathbf{y} = \mathbf{a} + \mathbf{R}\boldsymbol{\theta}, \end{aligned} \tag{2.3}$$

where $\mathbf{a} = [a_1 \ \dots \ a_m]^T \in \mathbb{C}^m$ holds the anchor coordinates, expressed as complex numbers, $\mathbf{R} = \text{diag}(r_1, \dots, r_m) \in \mathbb{R}^{m \times m}$, and $\boldsymbol{\theta} = [e^{j\phi_1} \ \dots \ e^{j\phi_m}]^T \in \mathbb{C}^m$. The problem acquires a flavor of AOA localization, as the angles ϕ_i encode a set of directions, departing from anchor nodes, that ideally intersect at the source position. The complex representation makes it simple to impose unit magnitude constraints on the elements of $\boldsymbol{\theta}$, and later relax them to obtain an SDR. Expanding the objective function and deleting constant terms yields the quadratic constrained problem

$$\begin{aligned} & \underset{\boldsymbol{\theta}}{\text{minimize}} && 2 \text{Re}(\mathbf{c}^H \boldsymbol{\theta}) - \frac{1}{m} \boldsymbol{\theta}^H \mathbf{r} \mathbf{r}^T \boldsymbol{\theta} \\ & \text{subject to} && |\theta_i| = 1, \end{aligned} \tag{2.4}$$

where $\mathbf{r} = \mathbf{R}\mathbf{1}_m$ and $\mathbf{c} = \mathbf{R}(\mathbf{I}_m - \frac{1}{m} \mathbf{1}_m \mathbf{1}_m^T) \mathbf{a}$.

To proceed one wishes to replace $\text{Re}(\mathbf{c}^H \boldsymbol{\theta})$ in (2.4) with $-|\mathbf{c}^H \boldsymbol{\theta}|$, which is readily written as a function of a quadratic form in $\boldsymbol{\theta}$ and then relaxed in the same way as the second term in the objective function. To this end, first note that if $\boldsymbol{\theta}$ is replaced with $\boldsymbol{\theta} e^{j\gamma}$ neither the second term in the objective function of (2.4) nor the constraints change for any angle γ . By proper choice of γ the complex number $\mathbf{c}^H \boldsymbol{\theta}$ may be rotated to the (negative) real axis for any feasible $\boldsymbol{\theta}$, such that $\text{Re}(\mathbf{c}^H \boldsymbol{\theta} e^{j\gamma}) = -|\mathbf{c}^H \boldsymbol{\theta}|$, thus reducing the value of the objective function relative to other values of γ . This implies that any optimal solution of (2.4) will satisfy $\text{Re}(\mathbf{c}^H \boldsymbol{\theta}) = -|\mathbf{c}^H \boldsymbol{\theta}|$, which justifies replacing $\text{Re}(\cdot)$

with $-|\cdot|$ in the cost function. It should be kept in mind, however, that once a solution $\boldsymbol{\theta}$ to the modified optimization problem is obtained it should be rotated to obtain the actual vector of phases $\boldsymbol{\theta}e^{j\gamma}$ such that $\text{Re}(\mathbf{c}^H \boldsymbol{\theta}e^{j\gamma}) = -|\mathbf{c}^H \boldsymbol{\theta}|$.

Now the modified problem is equivalently written as

$$\begin{aligned} & \underset{\boldsymbol{\theta}}{\text{maximize}} && 2\sqrt{\text{tr}(\mathbf{c}\mathbf{c}^H \boldsymbol{\theta}\boldsymbol{\theta}^H)} + \frac{1}{m}\text{tr}(\mathbf{r}\mathbf{r}^T \boldsymbol{\theta}\boldsymbol{\theta}^H) \\ & \text{subject to} && |\theta_i| = 1, \end{aligned} \tag{2.5}$$

and standard manipulations are followed, i.e., the new variable $\boldsymbol{\Phi} = \boldsymbol{\theta}\boldsymbol{\theta}^H$ and an associated (nonconvex) constraint $\text{rank}(\boldsymbol{\Phi}) = 1$ are introduced. Finally, a SDR formulation of SLCP is obtained by introducing the hypograph variable t such that $0 \leq t \leq 2\sqrt{\text{tr}(\mathbf{c}\mathbf{c}^H \boldsymbol{\Phi})}$ and dropping the rank constraint

$$\begin{aligned} & \underset{\boldsymbol{\Phi}, t}{\text{maximize}} && t + \frac{1}{m}\text{tr}(\mathbf{r}\mathbf{r}^T \boldsymbol{\Phi}) \\ & \text{subject to} && \boldsymbol{\Phi} \succeq 0, \quad \phi_{ii} = 1, \quad 4\mathbf{c}^H \boldsymbol{\Phi} \mathbf{c} \geq t^2. \end{aligned} \tag{2.6}$$

Remark that the solution of (2.6) is a positive semidefinite matrix, which should have a clearly dominant eigenvalue in problem instances where the SDR is an accurate approximation to the initial problem (2.2). In such cases $\boldsymbol{\Phi} \approx \lambda_1 \mathbf{u}_1 \mathbf{u}_1^H$, where λ_1 is the highest eigenvalue of $\boldsymbol{\Phi}$ and \mathbf{u}_1 the corresponding eigenvector, and the vector of complex phases is estimated as $\boldsymbol{\theta} = \sqrt{\lambda_1} \mathbf{u}_1$ [63]. An alternative approach for computing $\boldsymbol{\theta}$ is examined in Section 2.4.1.2. Algorithm 1 summarizes SLCP.

Algorithm 1 Summary of the SLCP algorithm

- 1: Given the anchor positions and range measurements, solve the SDR (2.6)
 - 2: Compute a rank-1 approximation of the SDR solution as $\boldsymbol{\Phi} \approx \boldsymbol{\theta}\boldsymbol{\theta}^H$
 - 3: Compute a rotation angle γ such that $\text{Re}(\mathbf{c}^H \boldsymbol{\theta}e^{j\gamma}) = -|\mathbf{c}^H \boldsymbol{\theta}|$ in (2.4)
 - 4: Obtain the vector of circle projections $\mathbf{y} = \mathbf{a} + \mathbf{R}\boldsymbol{\theta}e^{j\gamma}$
 - 5: Estimate the source position as the centroid $\mathbf{x} = \frac{1}{m} \mathbf{1}_m^T \mathbf{y}$
-

2.4.1.1 Tightness and Geometry of the Constraint Set in SLCP

The source localization problem prior to relaxation (2.5) can be written as

$$\begin{aligned} & \underset{u, v}{\text{maximize}} && 2\sqrt{u} + \frac{1}{m}v \\ & \text{subject to} && (u, v) \in \mathcal{S}, \end{aligned} \tag{2.7}$$

where

$$\mathcal{S} = \{(|\mathbf{c}^H \boldsymbol{\theta}|^2, |\mathbf{r}^T \boldsymbol{\theta}|^2) : \boldsymbol{\theta} \in \mathbb{C}^m, |\theta_i| = 1\}. \tag{2.8}$$

The objective function in (2.7) is concave with respect to u and v , and the optimization problem would be convex if the set \mathcal{S} , over which this function should be maximized, were convex. Then, the SDR used in SLCP (2.6) would always find a rank-1 solution Φ , from which the vector of phases θ would readily follow by factorization. In practice it was found that, even for a moderate number of anchors, the set \mathcal{S} is likely to have the required shape along part of its border, as discussed below, so that the SDR solution has indeed rank-1. Now, some of the properties of \mathcal{S} and the optimal solution will be examined.

Given the separable form of the cost function (2.7) it is clear that, for fixed v , it can be maximized by choosing u as large as possible within \mathcal{S} , and vice-versa. This implies the following property for the optimal points of (2.7):

Proposition 2.1. *The optimal points of (2.7) lie on the “upper right” boundary of set \mathcal{S} , i.e., optimal points of (2.7) are maximal elements of \mathcal{S} with respect to the standard cone \mathbb{R}_+^2 [23].*

Regarding the convexity properties of \mathcal{S} , recall that the cost function of (2.7) was designed to be invariant to rotations of θ so that, without loss of generality, the first element may be taken as unity. For $m = 2$ anchors and $\theta_1 = 1$, $\theta_2 = e^{j\phi}$ we then have

$$u = |c_1^* + c_2^* e^{j\phi}|^2 = |c_1|^2 + |c_2|^2 + 2|c_1||c_2| \cos(\phi + \alpha) \quad (2.9)$$

$$v = |r_1 + r_2 e^{j\phi}|^2 = r_1^2 + r_2^2 + 2r_1 r_2 \cos \phi, \quad (2.10)$$

where $\alpha = \angle c_1 - \angle c_2$. Set \mathcal{S} is an ellipse centered on $(|c_1|^2 + |c_2|^2, r_1^2 + r_2^2)$, therefore clearly nonconvex. Given the definitions of \mathbf{c} and \mathbf{r} in (2.4), for $m > 2$ anchors it is always possible to zero out elements $3, \dots, m$ in these vectors if $r_3 = \dots = r_m = 0$ in the diagonal of \mathbf{R} , thus reverting to the case $m = 2$. In summary:

Proposition 2.2. *Depending on the specific range measurements, set \mathcal{S} may be non-convex for any number of anchors.*

In spite of the lack of convexity guarantees for \mathcal{S} , the simulation results suggest that for $m \geq 3$ anchors and typical range measurements this set usually does have a convex-like shape. Even when \mathcal{S} is not convex all that is required for the SDR to provide a rank-1 solution is “local convexity” along the “upper right” boundary of \mathcal{S} where the optimal point of (2.7) is known to be located. More formally, it is required that the intersection of \mathcal{S} with any supporting hyperplane defined by a normal direction with nonnegative components be a compact subset (a single point or a line segment) [23]. Figure B.2 depicts some examples of \mathcal{S} for different numbers of anchors and randomly generated \mathbf{c} , \mathbf{r} .

The practical test for local (non)convexity of \mathcal{S} consists of tracing multiple supporting hyperplanes with nonnegative normal elements, and assessing whether any of them intersect \mathcal{S} at two well-separated points. Supporting hyperplanes are built not on \mathcal{S} directly, which is a hard problem, but on the related relaxed convex set

$$\mathcal{T} = \{(\text{tr}(\mathbf{c}\mathbf{c}^H \Phi), \text{tr}(\mathbf{r}\mathbf{r}^T \Phi)) : \Phi \in \mathbb{C}^{m \times m}, \Phi \succeq 0, \phi_{ii} = 1\}. \quad (2.11)$$

Specifically, for a supporting hyperplane with normal $(\cos \beta, \sin \beta)$, $0 \leq \beta \leq \frac{\pi}{2}$, an intersection point with \mathcal{T} is determined by solving the convex optimization problem

$$\begin{aligned} & \underset{\Phi}{\text{maximize}} && \langle (\cos \beta, \sin \beta), (\text{tr}(\mathbf{c}\mathbf{c}^H \Phi), \text{tr}(\mathbf{r}\mathbf{r}^T \Phi)) \rangle \\ & \text{subject to} && \Phi \succeq 0, \phi_{ii} = 1, \end{aligned} \quad (2.12)$$

and setting the intersection point as $u = \text{tr}(\mathbf{c}\mathbf{c}^H \Phi)$, $v = \text{tr}(\mathbf{r}\mathbf{r}^T \Phi)$. This procedure is justified by the following result, proved in Appendix B.

Lemma 2.4.1.1. For $m \leq 3$ anchors the sets \mathcal{S} and \mathcal{T} have the same set of supporting hyperplanes with nonnegative normal elements. Equivalently, in the relevant portion of its boundary \mathcal{T} coincides with the convex hull of \mathcal{S} .

Although this result is only proved up to $m = 3$, the empirical evidence suggests that it is also valid for higher m , at least up to some maximum order (see Figure B.2). This is left as a conjecture and apply the procedure for $m > 3$ as well, noting, however, that the case $m = 3$ has major practical significance as the minimum number of anchors that are necessary to recover a general 2D source position based on range measurements. It is also conjectured that \mathcal{T} is actually the convex hull of \mathcal{S} , so (2.12) may be used to trace the full boundary of $\text{co}(\mathcal{S})$, and not just the portion where the supporting hyperplanes have nonnegative normal elements. This assumption is not required for the analysis, but was used for generating the set boundaries shown in Figure B.2.

2.4.1.2 Factorization of the SDR Solution

The solution of the relaxed SLCP optimization problem (2.6) is a positive semidefinite matrix, Φ , from which the vector of complex exponentials θ is calculated by rank-1 factorization. The latter is needed to form the vector of circle projections $\mathbf{y} = \mathbf{a} + \mathbf{R}\theta$ (see (2.3)) and, ultimately, the source position vector as the centroid $\mathbf{x} = \frac{1}{m} \mathbf{1}_m^T \mathbf{y}$. The rank-1 factorization method advocated in Section 2.4.1 is truncation of the eigenvalue decomposition of Φ at the highest eigenvalue. This subsection examines a more exact search-based alternative for the practically relevant case of $m = 3$ anchors, which will also be useful to assess the accuracy of the factorization based on eigenvalue truncation.

For a given positive semidefinite matrix $\Phi \in \mathbf{C}^{m \times m}$ one wishes to find vector $\theta \in \mathbf{C}^m$ satisfying

$$\begin{aligned} & \underset{\theta}{\text{minimize}} \quad \|\Phi - \theta\theta^H\|_F^2 \\ & \text{subject to} \quad |\theta_i| = 1. \end{aligned} \tag{2.13}$$

The objective function in (2.13) is expanded as

$$\|\Phi - \theta\theta^H\|_F^2 = \text{tr}((\Phi - \theta\theta^H)^H(\Phi - \theta\theta^H)) = \|\Phi\|_F^2 + \underbrace{\|\theta\|^4}_{m^2} - \text{tr}(\Phi^H\theta\theta^H) - \text{tr}(\theta\theta^H\Phi). \tag{2.14}$$

Ignoring constant terms the optimization problem is equivalently reformulated as

$$\begin{aligned} & \underset{\theta}{\text{maximize}} \quad \theta^H\Phi\theta \\ & \text{subject to} \quad |\theta_i| = 1. \end{aligned} \tag{2.15}$$

The cost function of (2.15) is insensitive to a global rotation of all elements of θ by a common factor, hence for $m = 3$ anchors θ can be written as $\theta = \begin{bmatrix} 1 & e^{j\alpha} & e^{j(\alpha+\delta)} \end{bmatrix}^T$ and (2.15) becomes

$$\underset{\alpha, \delta}{\text{maximize}} \quad \text{Re}(\phi_{12}e^{j\alpha} + \phi_{23}e^{j\delta} + \phi_{13}e^{j(\alpha+\delta)}). \tag{2.16}$$

For fixed α the maximum is attained for $\delta = -\angle(\phi_{23} + \phi_{13}e^{j\alpha})$, yielding for (2.16)

$$\underset{\alpha}{\text{maximize}} \quad \text{Re}(\phi_{12}e^{j\alpha}) + |\phi_{23} + \phi_{13}e^{j\alpha}|. \tag{2.17}$$

The solution to (2.17) is found by searching for the maximum value over the interval $[0, 2\pi)$.

Referring to the definitions of the 2D sets \mathcal{S} in (2.8) and \mathcal{T} in (2.11), similar criteria to the above were considered for finding θ such that the induced point in \mathcal{S} is closest in Euclidean norm to the one induced by Φ in \mathcal{T} . However, the many-to-one nature of the mapping of θ onto points in \mathcal{S} makes this formulation intrinsically ambiguous.

2.4.2 Source localization Under Laplacian Noise: SL- ℓ_1

When disturbances are Laplacian and i.i.d., thus heavier tailed than Gaussian, maximizing the likelihood amounts to solving (2.1) for $p = q = 1$,

$$\underset{\mathbf{x}}{\text{minimize}} \quad \sum_{i=1}^m \left| \|\mathbf{x} - \mathbf{a}_i\| - r_i \right|. \tag{2.18}$$

or

$$\underset{\mathbf{x}}{\text{minimize}} \quad \left(\sum_{i=1}^m \left| \|\mathbf{x} - \mathbf{a}_i\| - r_i \right| \right)^2, \quad (2.19)$$

where \mathbf{x} , \mathbf{a}_i and r_i are defined in Section 2.4.1. The presence of $|\cdot|$ in each summation term of (2.18), rather than $(\cdot)^2$, de-emphasizes the contributions of measurements r_i corrupted by large noise values. The optimal point of (2.18) is thus less biased by these outlier measurements than the cost function (2.1) for the Gaussian case $p = 1$, $q = 2$. However, a major difficulty in solving (2.18) is the fact that the cost function is not differentiable, making it less amenable to the types of analytic manipulations that are used to develop SDR.

Ideas from [64] are used to express the minimization of (2.19) as a weighted sum of squares.

Lemma 2.4.2.1. The following problem is equivalent to (2.19)

$$\begin{aligned} & \underset{\mathbf{x}}{\text{minimize}} \quad \underset{\boldsymbol{\lambda} \in \mathbb{R}^m}{\text{minimize}} \quad \sum_{i=1}^m \frac{(\|\mathbf{x} - \mathbf{a}_i\| - r_i)^2}{\lambda_i}, \\ & \text{subject to} \quad \lambda_i > 0, \quad \mathbf{1}^T \boldsymbol{\lambda} = 1. \end{aligned} \quad (2.20)$$

A proof is given in Appendix C. As claimed in Section 2.4.1 and shown in Appendix A, the difference between the true range and observed range is actually equivalent to the distance between the source position and the closest point on the circle with center \mathbf{a}_i and radius r_i . An equivalent formulation is therefore

$$\begin{aligned} & \underset{\mathbf{x}, \mathbf{y}_i, \boldsymbol{\lambda}}{\text{minimize}} \quad \sum_{i=1}^m \frac{\|\mathbf{x} - \mathbf{y}_i\|^2}{\lambda_i} \\ & \text{subject to} \quad \|\mathbf{y}_i - \mathbf{a}_i\| = r_i, \quad \lambda_i > 0, \quad \mathbf{1}^T \boldsymbol{\lambda} = 1. \end{aligned} \quad (2.21)$$

If the \mathbf{y}_i and λ_i are fixed, the problem (2.21) with respect to \mathbf{x} is an unconstrained optimization problem whose solution is readily obtained by invoking the optimality conditions

$$\sum_{i=1}^m \frac{(\mathbf{x} - \mathbf{y}_i)}{\lambda_i} = 0 \Rightarrow \mathbf{x}^* = \frac{\sum_{i=1}^m \frac{\mathbf{y}_i}{\lambda_i}}{\sum_{i=1}^m \frac{1}{\lambda_i}}. \quad (2.22)$$

Geometrically, the first constraint of (2.21) defines circle equations, which can be compactly described in the complex plane as $y_i = a_i + r_i e^{j\phi_i}$. These are collected into a vector $\mathbf{y} = \mathbf{a} + \mathbf{R}\mathbf{u}$, where \mathbf{a} and \mathbf{R} are defined as in Section 2.4.1 and $\mathbf{u} = \left[e^{j\phi_1} \quad \dots \quad e^{j\phi_m} \right]^T \in \mathbb{C}^m$. Using the optimal \mathbf{x} , we get

$$\begin{aligned} & \underset{\mathbf{u}, \boldsymbol{\lambda}}{\text{minimize}} \quad \mathbf{y}^H \boldsymbol{\Pi} \mathbf{y} = (\mathbf{a} + \mathbf{R}\mathbf{u})^H \boldsymbol{\Pi} (\mathbf{a} + \mathbf{R}\mathbf{u}) \\ & \text{subject to} \quad \lambda_i > 0, \quad \mathbf{1}^T \boldsymbol{\lambda} = 1, \quad |u_i| = 1, \end{aligned} \quad (2.23)$$

where

$$\begin{aligned} \mathbf{\Pi} &= \begin{bmatrix} \frac{1}{\lambda_1} & 0 & 0 \\ 0 & \ddots & 0 \\ 0 & 0 & \frac{1}{\lambda_m} \end{bmatrix} - \frac{1}{\sum_{i=1}^m \frac{1}{\lambda_i}} \begin{bmatrix} \frac{1}{\lambda_1} \\ \vdots \\ \frac{1}{\lambda_m} \end{bmatrix} \begin{bmatrix} \frac{1}{\lambda_1} & \cdots & \frac{1}{\lambda_m} \end{bmatrix} \\ &= \mathbf{\Lambda}^{-1} - \mathbf{\Lambda}^{-1} \mathbf{1} (\mathbf{1}^T \mathbf{\Lambda}^{-1} \mathbf{1})^{-1} \mathbf{1}^T \mathbf{\Lambda}^{-1}, \end{aligned} \quad (2.24)$$

with $\mathbf{\Lambda} = \text{diag}(\lambda_1, \dots, \lambda_m)$.

Matrix $\mathbf{\Pi}$ resembles an orthogonal projector. Using the matrix inversion lemma¹, it is seen to be the limiting case $\mathbf{\Pi} = \lim_{\eta \rightarrow \infty} (\mathbf{\Lambda} + \eta \mathbf{1} \mathbf{1}^T)^{-1}$ and thus positive semidefinite. This format is more amenable to analytic manipulations in optimization problems and will be used throughout this chapter. The parameter η is taken as a sufficiently large constant (see Appendix C), although it could also be regarded as an additional optimization variable to ensure adequate approximation accuracy.

An epigraph variable $t \in \mathbb{R}$ in (2.23) is introduced, i.e., one minimizes over t and add the constraint $t - (\mathbf{a} + \mathbf{R}\mathbf{u})^H \mathbf{\Pi} (\mathbf{a} + \mathbf{R}\mathbf{u}) \geq 0$. Applying Schur complements the constraint may be successively written as

$$\begin{bmatrix} t & (\mathbf{a} + \mathbf{R}\mathbf{u})^H \\ \mathbf{a} + \mathbf{R}\mathbf{u} & \mathbf{\Pi}^{-1} \end{bmatrix} \succeq 0 \quad \Leftrightarrow \quad \mathbf{\Pi}^{-1} - \frac{(\mathbf{a} + \mathbf{R}\mathbf{u})(\mathbf{a} + \mathbf{R}\mathbf{u})^H}{t} \succeq 0. \quad (2.25)$$

The formulation becomes

$$\begin{aligned} &\underset{\mathbf{u}, t, \boldsymbol{\lambda}}{\text{minimize}} && t \\ &\text{subject to} && \lambda_i > 0, \mathbf{1}^T \boldsymbol{\lambda} = 1, |u_i| = 1, \\ &&& t\mathbf{\Lambda} + t\eta \mathbf{1} \mathbf{1}^T \succeq (\mathbf{a} + \mathbf{R}\mathbf{u})(\mathbf{a} + \mathbf{R}\mathbf{u})^H. \end{aligned} \quad (2.26)$$

Finally, $\mathbf{A} = [\mathbf{a} \ \mathbf{R}]$, $\mathbf{v}^H = [1 \ \mathbf{u}^H]$, $\mathbf{V} = \mathbf{v}\mathbf{v}^H$ are defined, and the rank-1 constraint on the new variable \mathbf{V} is dropped to obtain the relaxed SDP

$$\begin{aligned} &\underset{\boldsymbol{\beta}, t, \mathbf{V}}{\text{minimize}} && t \\ &\text{subject to} && \beta_i > 0, \mathbf{1}^T \boldsymbol{\beta} = t, V_{ii} = 1, \mathbf{V} \succeq 0, \\ &&& \text{diag}(\boldsymbol{\beta}) + t\eta \mathbf{1} \mathbf{1}^T \succeq \mathbf{A}\mathbf{V}\mathbf{A}^H. \end{aligned} \quad (2.27)$$

The solution of the optimization problem (2.27) includes the positive semidefinite matrix \mathbf{V} from whose first row or column \mathbf{u} can be extracted directly² to obtain $\mathbf{y} = \mathbf{a} + \mathbf{R}\mathbf{u}$ and the target coordinates from (2.22). Algorithm 2 summarizes SL- ℓ_1 .

¹ $(A + BCD)^{-1} = A^{-1} - A^{-1}B(DA^{-1}B + C^{-1})^{-1}DA^{-1}$.

²Alternatively, \mathbf{u} can be obtained by rank 1 factorization of the lower right submatrix of \mathbf{V} corresponding to $\mathbf{u}\mathbf{u}^H$, as in [35, 65].

Algorithm 2 Summary of the SL- ℓ_1 algorithm

- 1: Given the anchor positions and range measurements, solve the SDP (2.27)
 - 2: Compute a rank-1 approximation of the SDP solution from first row or column of \mathbf{V}
 - 3: Obtain the vector of circle projections $\mathbf{y} = \mathbf{a} + \mathbf{R}\mathbf{u}$
 - 4: Estimate the source position as $\mathbf{x} = \frac{\sum_{i=1}^m \frac{\mathbf{y}_i}{\lambda_i}}{\sum_{i=1}^m \frac{1}{\lambda_i}}$
-

2.5 Source Localization in Higher Dimensions

In this section, the 3D and higher dimension extensions of the algorithms in Section 2.4.1 and in Section 2.4.2 are derived for Gaussian and Laplacian noise assumptions, respectively. The first part describes the SLNN algorithm for Gaussian noise. The second part will present SL- ℓ_1 MD and SL- ℓ_1 SD which, similarly to the 2D case, express the Laplacian likelihood function as a variable-weighted Gaussian likelihood.

2.5.1 Localization under Gaussian Noise: SLNN

To extend the approach used in SLCP to $n > 2$ dimensions, the circle/sphere equations in (2.2) are written using an equivalent parametric form with real coordinates

$$\begin{aligned} & \underset{\mathbf{x}, \mathbf{y}_i, \mathbf{u}_i}{\text{minimize}} && \sum_{i=1}^m \|\mathbf{x} - \mathbf{y}_i\|^2 \\ & \text{subject to} && \mathbf{y}_i = \mathbf{a}_i + r_i \mathbf{u}_i, \quad \|\mathbf{u}_i\| = 1, \end{aligned} \quad (2.28)$$

where $\mathbf{x}, \mathbf{y}_i, \mathbf{a}_i$ and \mathbf{u}_i are now vectors in \mathbb{R}^n , rather than complex scalars used in SLCP. In (2.28) $\mathbf{u}_i \in \mathbb{R}^n$ is a unit-norm vector that plays the same role as the complex phase shift $e^{j\phi_i}$ in SLCP. Equivalently,

$$\begin{aligned} & \underset{\mathbf{x}, \mathbf{y}_i, \mathbf{u}_i}{\text{minimize}} && \|\mathbf{1}_m \mathbf{x}^T - \mathbf{Y}\|_F^2 \\ & \text{subject to} && \underbrace{\begin{bmatrix} \mathbf{y}_1^T \\ \vdots \\ \mathbf{y}_m^T \end{bmatrix}}_{\mathbf{Y}} = \underbrace{\begin{bmatrix} \mathbf{a}_1^T \\ \vdots \\ \mathbf{a}_m^T \end{bmatrix}}_{\mathbf{A}} + \mathbf{R} \underbrace{\begin{bmatrix} \mathbf{u}_1^T \\ \vdots \\ \mathbf{u}_m^T \end{bmatrix}}_{\mathbf{U}}, \quad \|\mathbf{u}_i\| = 1, \end{aligned} \quad (2.29)$$

where $\mathbf{R} = \text{diag}(r_1, \dots, r_m)$ as in (2.3). For fixed $\mathbf{y}_i, \mathbf{u}_i$ (2.29) describes n uncoupled least-squares problems whose variables are the components of the source location vector \mathbf{x} . The optimal solutions may be jointly written compactly as

$$\mathbf{x}^T = (\mathbf{1}_m^T \mathbf{1}_m)^{-1} \mathbf{1}_m^T \mathbf{Y} = \frac{1}{m} \mathbf{1}_m^T \mathbf{Y}. \quad (2.30)$$

After replacing \mathbf{x} in (2.29) with (2.30), the objective function becomes $\|\mathbf{\Pi Y}\|_F^2 = \text{tr}(\mathbf{Y}^T \mathbf{\Pi Y})$, where $\mathbf{\Pi} = \mathbf{I}_m - \frac{1}{m} \mathbf{1}_m \mathbf{1}_m^T$ is a projection matrix (hence idempotent). Similarly to (2.3)–(2.4), variable \mathbf{Y} and the first set of equality constraints might be eliminated by replacing \mathbf{Y} in the cost function of (2.29). Afterwards, its definition in the objective function can be expanded and constant terms are ignored to obtain

$$\begin{aligned} & \underset{\mathbf{U}}{\text{minimize}} && 2 \text{tr}(\mathbf{C}^T \mathbf{U}) - \frac{1}{m} \text{tr}(\mathbf{U}^T \mathbf{r} \mathbf{r}^T \mathbf{U}) \\ & \text{subject to} && \|\mathbf{u}_i\| = 1, \end{aligned} \tag{2.31}$$

where $\mathbf{C} = \mathbf{R} \mathbf{\Pi A}$ and, as in (2.4), $\mathbf{r} = \mathbf{R} \mathbf{1}_m$.

Nuclear Norm Approximation

As in the complex formulation it is required to rewrite the first term in the objective function of (2.31) in a form that is more amenable to SDR. In the optimization problem \mathbf{U} is thus replaced with the product $\mathbf{U V}$, where \mathbf{V} is an $n \times n$ orthogonal matrix such that $\mathbf{V}^T \mathbf{V} = \mathbf{V V}^T = \mathbf{I}_n$, yielding

$$\begin{aligned} & \underset{\mathbf{U}, \mathbf{V}}{\text{minimize}} && 2 \text{tr}(\mathbf{C}^T \mathbf{U V}) - \frac{1}{m} \text{tr}(\mathbf{V}^T \mathbf{U}^T \mathbf{r} \mathbf{r}^T \mathbf{U V}) \\ & \text{subject to} && \|\mathbf{u}_i\| = 1, \quad \mathbf{V}^T \mathbf{V} = \mathbf{I}_n. \end{aligned} \tag{2.32}$$

Note that, due to the orthogonality of \mathbf{V} , each line of $\mathbf{U V}$ still has unit norm, so for any feasible \mathbf{U} in (2.31) $\mathbf{U V}$ is also feasible. Regarding (2.32), \mathbf{V} may be interpreted as an inner optimization variable that, for each candidate \mathbf{U} , minimizes the value of the objective function. Noting that the second term in the objective function (2.32) does not depend on \mathbf{V} , as $\text{tr}(\mathbf{V}^T \mathbf{U}^T \mathbf{r} \mathbf{r}^T \mathbf{U V}) = \text{tr}(\mathbf{r} \mathbf{r}^T \mathbf{U V V}^T \mathbf{U}^T) = \text{tr}(\mathbf{r} \mathbf{r}^T \mathbf{U U}^T)$, the inner optimization problem simply becomes

$$\begin{aligned} & \underset{\mathbf{V}}{\text{minimize}} && \text{tr}(\mathbf{C}^T \mathbf{U V}) = \langle \mathbf{V}, \mathbf{U}^T \mathbf{C} \rangle \\ & \text{subject to} && \mathbf{V}^T \mathbf{V} = \mathbf{I}_n. \end{aligned} \tag{2.33}$$

This involves the minimization of a linear function on the set of orthogonal matrices, which resembles the known problem of minimizing a linear function of a vector \mathbf{v} , say, $\langle \mathbf{v}, \mathbf{a} \rangle$, on the unit sphere $\|\mathbf{v}\|^2 = \mathbf{v}^T \mathbf{v} = 1$. Invoking the Karush Khun Tucker (KKT) conditions [23] the latter problem is readily seen to yield the optimal cost $-\|\mathbf{a}\|$, attained at the point on the sphere along vector $-\mathbf{a}$ (illustration is given on a circle in Figure 2.2). One would therefore expect the solution of (2.33) to be $-\|\mathbf{C}^T \mathbf{U}\|$ which involves some matrix norm of $\mathbf{C}^T \mathbf{U}$. In Appendix D, (2.33) is solved by invoking the KKT conditions and it is shown that this is indeed the case, and the appropriate norm to consider is the *nuclear norm*, defined for matrix \mathbf{X} as $\|\mathbf{X}\|_N = \text{tr}((\mathbf{X}^H \mathbf{X})^{\frac{1}{2}})$ which equals to the

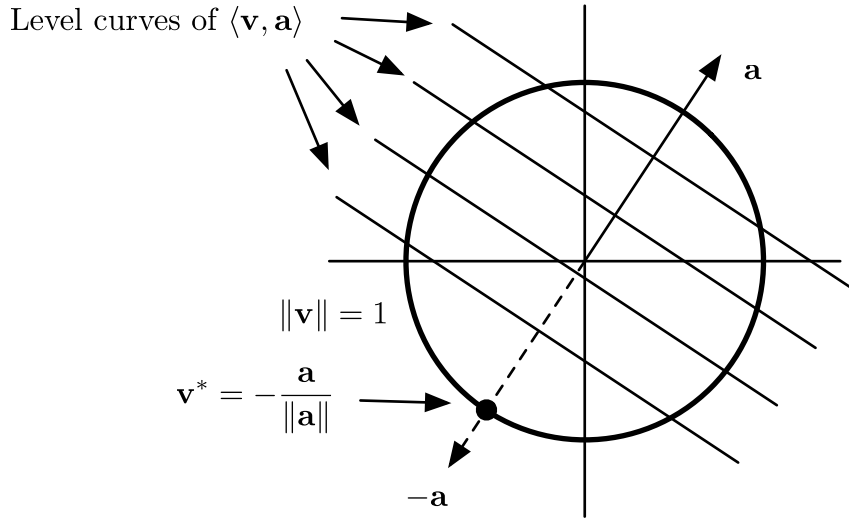


FIGURE 2.2: Minimization of a linear function over a circle.

sum of its singular values [66]. The optimization problem (2.32) is therefore equivalently rewritten as

$$\begin{aligned} \underset{\mathbf{U}}{\text{minimize}} \quad & -2\|\mathbf{C}^T\mathbf{U}\|_N - \frac{1}{m}\text{tr}(\mathbf{r}\mathbf{r}^T\mathbf{U}\mathbf{U}^T) \\ \text{subject to} \quad & \|\mathbf{u}_i\| = 1, \end{aligned} \tag{2.34}$$

or

$$\begin{aligned} \underset{\mathbf{U}}{\text{maximize}} \quad & 2\text{tr}((\mathbf{C}^T\mathbf{U}\mathbf{U}^T\mathbf{C})^{\frac{1}{2}}) + \frac{1}{m}\text{tr}(\mathbf{r}\mathbf{r}^T\mathbf{U}\mathbf{U}^T) \\ \text{subject to} \quad & \|\mathbf{u}_i\| = 1. \end{aligned} \tag{2.35}$$

The variable $\mathbf{W} = \mathbf{U}\mathbf{U}^T$ is introduced and the associated nonconvex constraint $\text{rank}(\mathbf{W}) = n$ is ignored to obtain the SDR

$$\begin{aligned} \underset{\mathbf{W}}{\text{maximize}} \quad & 2\text{tr}((\mathbf{C}^T\mathbf{W}\mathbf{C})^{\frac{1}{2}}) + \frac{1}{m}\text{tr}(\mathbf{r}\mathbf{r}^T\mathbf{W}) \\ \text{subject to} \quad & \mathbf{W} \succeq 0, \quad w_{ii} = 1. \end{aligned} \tag{2.36}$$

The objective function of (2.36) is the sum of a concave³ function of \mathbf{W} with a linear term, and is therefore concave. The constraint set of (2.36) is convex, thus establishing that this is indeed a convex optimization problem. It is expressed in standard SDP form as

$$\begin{aligned} \underset{\mathbf{W}, \mathbf{Z}}{\text{maximize}} \quad & 2\text{tr}(\mathbf{Z}) + \frac{1}{m}\text{tr}(\mathbf{r}\mathbf{r}^T\mathbf{W}) \\ \text{subject to} \quad & \mathbf{W} \succeq 0, \quad w_{ii} = 1, \quad \mathbf{Z} \succeq 0, \\ & \begin{bmatrix} \mathbf{C}^T\mathbf{W}\mathbf{C} & \mathbf{Z} \\ \mathbf{Z} & \mathbf{I}_n \end{bmatrix} \succeq 0. \end{aligned} \tag{2.37}$$

³The first term is the composition of the linear map $\mathbf{X} = \mathbf{C}^T\mathbf{W}\mathbf{C}$ with $\text{tr}(\mathbf{X}^{\frac{1}{2}})$, which is known to be concave in \mathbf{X} [23].

The equivalence between (2.36) and (2.37) is proved in Appendix D.

Similarly to the complex 2D formulation, the solution of the proposed SDR is a $m \times m$ matrix \mathbf{W} that should have approximately rank n when the relaxation is tight. The matrix \mathbf{U} of unit-norm vectors is obtained by SVD factorization of \mathbf{W} [63] and, after accounting for the inner rotation of \mathbf{U} , it is used to build the \mathbf{y}_i and, ultimately, the source position vector \mathbf{x} . Algorithm 3 summarizes the SLNN.

Algorithm 3 Summary of the SLNN algorithm

- 1: Given the anchor positions and range measurements, solve the SDR (2.37)
 - 2: Compute a rank- n approximation of the SDR solution as $\mathbf{W} \approx \mathbf{U}\mathbf{U}^T$
 - 3: Solve the inner optimization problem (2.33) to get the rotation matrix \mathbf{V} , Appendix D
 - 4: Obtain the matrix of sphere projections as $\mathbf{Y} = \mathbf{A} + \mathbf{R}\mathbf{U}\mathbf{V}$
 - 5: Estimate the source position as the centroid of the rows of \mathbf{Y} , $\mathbf{x} = \frac{1}{m}\mathbf{Y}^T\mathbf{1}_m$
-

2.5.2 Localization under Laplacian Noise: SL- ℓ_1 SD/MD

The strategy adopted to circumvent the nondifferentiability parallels the one used in Section 2.4.2 for 2D sources, and as a key ingredient involves squaring the cost function of (2.18) (which does not affect the location of extremal points), and then rewriting it as

$$\begin{aligned} & \underset{\mathbf{x}, \boldsymbol{\lambda}}{\text{minimize}} && \sum_{i=1}^m \frac{(\|\mathbf{x} - \mathbf{a}_i\| - r_i)^2}{\lambda_i} \\ & \text{subject to} && \lambda_i > 0, \quad \mathbf{1}_m^T \boldsymbol{\lambda} = 1. \end{aligned} \tag{2.38}$$

The cost function is thus reduced to a weighted version of the more tractable Gaussian log-likelihood, where the real weighting coefficients λ_i become optimization variables themselves. See Appendix C for a proof of this result (also [67]). Now, the manipulations used earlier in Section 2.5.1 for the development of SLNN can be replicated here to reformulate the problem as

$$\begin{aligned} & \underset{\mathbf{x}, \mathbf{y}_i, \mathbf{u}_i, \boldsymbol{\lambda}}{\text{minimize}} && \sum_{i=1}^m \frac{\|\mathbf{x} - \mathbf{y}_i\|^2}{\lambda_i} \\ & \text{subject to} && \mathbf{y}_i = \mathbf{a}_i + r_i \mathbf{u}_i, \quad \|\mathbf{u}_i\| = 1 \\ & && \lambda_i > 0, \quad \mathbf{1}_m^T \boldsymbol{\lambda} = 1. \end{aligned} \tag{2.39}$$

For given \mathbf{y}_i , \mathbf{u}_i , and $\boldsymbol{\lambda}$, (2.39) has a least-squares cost function whose unconstrained optimal solution with respect to \mathbf{x} is readily found in closed form from the first-order

stationary condition

$$\sum_{i=1}^m \frac{\mathbf{x} - \mathbf{y}_i}{\lambda_i} = 0, \quad \mathbf{x}^* = \frac{\sum_{i=1}^m \frac{\mathbf{y}_i}{\lambda_i}}{\sum_{i=1}^m \frac{1}{\lambda_i}}. \quad (2.40)$$

Substituting the optimal \mathbf{x} in (2.21), and using matrix notation, the cost function becomes $\text{tr}(\mathbf{Y}^T \mathbf{\Xi} \mathbf{Y})$, where $\mathbf{\Xi}$ is the modified projector as in (2.24).

\mathbf{Y} and the related constraint can be eliminated to obtain

$$\begin{aligned} & \underset{\mathbf{U}, \boldsymbol{\lambda}}{\text{minimize}} && \text{tr}((\mathbf{A} + \mathbf{R}\mathbf{U})^T \mathbf{\Xi} (\mathbf{A} + \mathbf{R}\mathbf{U})) \\ & \text{subject to} && \|\mathbf{u}_i\| = 1, \lambda_i > 0, \quad \mathbf{1}_m^T \boldsymbol{\lambda} = 1. \end{aligned} \quad (2.41)$$

2.5.2.1 SL- ℓ_1 MD

An epigraph variable t_i for each term contributing to $\text{tr}(\cdot)$ in the cost function of (2.41) is introduced

$$\begin{aligned} & \underset{\mathbf{U}, \boldsymbol{\lambda}, \mathbf{t}}{\text{minimize}} && \mathbf{t} \mathbf{1}_n \\ & \text{subject to} && \mathbf{e}_i^T (\mathbf{A} + \mathbf{R}\mathbf{U})^T \mathbf{\Xi} (\mathbf{A} + \mathbf{R}\mathbf{U}) \mathbf{e}_i \leq t_i \\ & && \|\mathbf{u}_i\| = 1, \quad \lambda_i > 0, \quad \mathbf{1}_m^T \boldsymbol{\lambda} = 1, \end{aligned} \quad (2.42)$$

where $\mathbf{t} = [t_1 \ \dots \ t_n]$ and \mathbf{e}_i is the standard coordinate vector with 1 in the i -th position and zeros elsewhere. As in Section 2.4.2 the matrix inversion lemma is invoked to express $\mathbf{\Xi}$ as the limiting case of (positive semidefinite) $\mathbf{\Xi} = \lim_{\eta \rightarrow \infty} (\boldsymbol{\Lambda} + \eta \mathbf{1}_m \mathbf{1}_m^T)^{-1}$, which is more amenable to analytic manipulations in optimization problems. Using Schur complements the inequality constraint in (2.42) may be successively written as

$$\begin{bmatrix} t_i & \mathbf{e}_i^T (\mathbf{A} + \mathbf{R}\mathbf{U})^T \\ (\mathbf{A} + \mathbf{R}\mathbf{U}) \mathbf{e}_i & \mathbf{\Xi}^{-1} \end{bmatrix} \succeq 0 \quad (2.43)$$

$$t_i (\boldsymbol{\Lambda} + \eta \mathbf{1}_m \mathbf{1}_m^T) - (\mathbf{A} + \mathbf{R}\mathbf{U}) \mathbf{e}_i \mathbf{e}_i^T (\mathbf{A} + \mathbf{R}\mathbf{U})^T \succeq 0. \quad (2.44)$$

The last inequality is bilinear in t_i and $\lambda_1, \dots, \lambda_m$, and it is linearized by replacing the optimization variable $\boldsymbol{\lambda}$ with a new $\boldsymbol{\beta}_i = t_i \boldsymbol{\lambda}$. Now, the $\boldsymbol{\beta}_i$ can be assembled into a matrix

$$\boldsymbol{\beta} = [\boldsymbol{\beta}_1 \ \dots \ \boldsymbol{\beta}_n] = \boldsymbol{\lambda} \mathbf{t}, \quad (2.45)$$

which, as shown above, should have rank 1 and satisfy $\beta_{ij} > 0$, $\mathbf{1}_m^T \boldsymbol{\beta} = \mathbf{t}$. However, the rank-1 constraint for $\boldsymbol{\beta}$ cannot be directly imposed in convex formulations, and a common technique is resorted to indirectly induce low rank in optimal solutions by adding to the cost function the (scaled) nuclear norm $\|\boldsymbol{\beta}\|_N$. The sensitivity of the algorithm to the scaling parameter, μ , and its value will be discussed in Section 2.8.

Regarding the second term on the left-hand side of (2.44), first note that

$$(\mathbf{A} + \mathbf{R}\mathbf{U})\mathbf{e}_i = \begin{bmatrix} \mathbf{A}\mathbf{e}_i & \mathbf{R} \end{bmatrix} \begin{bmatrix} 1 \\ \mathbf{U}\mathbf{e}_i \end{bmatrix} = \begin{bmatrix} \boldsymbol{\alpha}_i & \mathbf{R} \end{bmatrix} \begin{bmatrix} 1 \\ \mathbf{v}_i \end{bmatrix}, \quad (2.46)$$

where $\boldsymbol{\alpha}_i$ and \mathbf{v}_i denote the i -th columns of matrices \mathbf{A} and \mathbf{U} , respectively. Now, consider the following variable, obtained from the stacked rotation vectors that makes up \mathbf{U} ,

$$\mathbf{W} = \begin{bmatrix} 1 \\ \text{vec}(\mathbf{U}^T) \end{bmatrix} \begin{bmatrix} 1 & \text{vec}(\mathbf{U}^T)^T \end{bmatrix} = \begin{bmatrix} 1 & \mathbf{u}_1^T & \dots & \mathbf{u}_m^T \\ \mathbf{u}_1 & \underbrace{\mathbf{u}_1\mathbf{u}_1^T}_{\mathbf{W}_{11}} & & \\ \vdots & & \ddots & \\ \mathbf{u}_m & & & \underbrace{\mathbf{u}_m\mathbf{u}_m^T}_{\mathbf{W}_{mm}} \end{bmatrix}. \quad (2.47)$$

Further, let I_i denote the set of row indices that extracts the elements of $[1 \ \mathbf{v}_i^T]^T$ in (2.46) from the first column of \mathbf{W} . Then, the dyad below is readily obtained by selecting the submatrix formed from the I_i rows and I_i columns of \mathbf{W}

$$\mathbf{W}_{I_i I_i} = \begin{bmatrix} 1 \\ \mathbf{v}_i \end{bmatrix} \begin{bmatrix} 1 & \mathbf{v}_i^T \end{bmatrix}, \quad (2.48)$$

and this carries over to (2.44) through (2.46), which can therefore be written in terms of submatrix $\mathbf{W}_{I_i I_i}$. The positive semidefinite matrix \mathbf{W} will replace \mathbf{U} as an optimization variable, retaining the constraints along the diagonal blocks in (2.47), namely, $\text{tr}(\mathbf{W}_{ii}) = 1$. Finally, the full convex relaxation of (2.42) is obtained by combining all the above elements and dropping the rank-1 constraint for \mathbf{W} that is implied by (2.47)

$$\begin{aligned} & \underset{\mathbf{W}, \boldsymbol{\beta}, \mathbf{t}}{\text{minimize}} && \mathbf{t}\mathbf{1}_n + \mu\|\boldsymbol{\beta}\|_N \\ & \text{subject to} && \text{diag}(\boldsymbol{\beta}_i) + t_i\eta\mathbf{1}_m\mathbf{1}_m^T \succeq \begin{bmatrix} \boldsymbol{\alpha}_i & \mathbf{R} \end{bmatrix} \mathbf{W}_{I_i I_i} \begin{bmatrix} \boldsymbol{\alpha}_i^T \\ \mathbf{R} \end{bmatrix} \\ & && \mathbf{W} \succeq 0, \quad w_{11} = 1, \quad \text{tr}(\mathbf{W}_{ii}) = 1 \\ & && \beta_{ij} > 0, \quad \mathbf{1}_m^T \boldsymbol{\beta} = \mathbf{t}. \end{aligned} \quad (2.49)$$

2.5.2.2 SL- ℓ_1 SD

The simulation results suggest that in most scenarios the accuracy of the solution obtained from (2.49) is nearly identical to that of a simplified formulation where a single

epigraph variable, t , is used. Referring to (2.42), we now minimize $\text{tr}(t\mathbf{I}_n)$ or, equivalently, t , and replace the first constraint for all $i = 1, \dots, n$ with the single matrix inequality $(\mathbf{A} + \mathbf{R}\mathbf{U})^T \mathbf{\Xi} (\mathbf{A} + \mathbf{R}\mathbf{U}) \preceq t\mathbf{I}_n$. Applying Schur complements as in (2.43)–(2.44) yields

$$t(\mathbf{A} + \eta \mathbf{1}_m \mathbf{1}_m^T) - \begin{bmatrix} \mathbf{A} & \mathbf{R} \end{bmatrix} \begin{bmatrix} \mathbf{I}_n \\ \mathbf{U} \end{bmatrix} \begin{bmatrix} \mathbf{I}_n & \mathbf{U}^T \end{bmatrix} \begin{bmatrix} \mathbf{A}^T \\ \mathbf{R} \end{bmatrix} \succeq 0, \quad (2.50)$$

and again variable $\boldsymbol{\lambda}$ is replaced with $\boldsymbol{\beta} = t\boldsymbol{\lambda}$ such that $\beta_i > 0$, $\mathbf{1}_m^T \boldsymbol{\beta} = t$. Now, however, there is no need to assemble a matrix as in (2.45) and to include its nuclear norm as a penalization term in the cost function. Finally, to obtain a convex relaxation \mathbf{U} is replaced with the new variable

$$\mathbf{W} = \begin{bmatrix} \mathbf{I}_n \\ \mathbf{U} \end{bmatrix} \begin{bmatrix} \mathbf{I}_n & \mathbf{U}^T \end{bmatrix} = \begin{bmatrix} \mathbf{I}_n & \mathbf{U}^T \\ \underbrace{\mathbf{W}_{11}} & \\ \mathbf{U} & \mathbf{U}\mathbf{U}^T \end{bmatrix}, \quad (2.51)$$

and drop the rank- n constraint on \mathbf{W} that follows from (2.51). The simplified SDP formulation for SL- ℓ_1 MD, denoted by SL- ℓ_1 SD, is given by

$$\begin{aligned} & \underset{\mathbf{W}, \boldsymbol{\beta}, t}{\text{minimize}} && t \\ & \text{subject to} && \text{diag}(\boldsymbol{\beta}) + t\eta \mathbf{1}_m \mathbf{1}_m^T \succeq \begin{bmatrix} \mathbf{A} & \mathbf{R} \end{bmatrix} \mathbf{W} \begin{bmatrix} \mathbf{A}^T \\ \mathbf{R} \end{bmatrix} \\ & && \mathbf{W} \succeq 0, \quad \mathbf{W}_{11} = \mathbf{I}_n, \quad w_{ii} = 1 \\ & && \beta_i > 0, \quad \mathbf{1}_m^T \boldsymbol{\beta} = t. \end{aligned} \quad (2.52)$$

Note that the optimization variables \mathbf{W} and $\boldsymbol{\beta}$ in (2.49) have size $(mn+1) \times (mn+1)$ and $m \times n$, respectively, whereas the corresponding sizes in (2.52) are only $(m+n) \times (m+n)$ and $m \times 1$. For ambient dimension $n = 2$ or 3 and for $m \approx 5$ anchors used in the simulations problem (2.52) has considerably fewer variables than (2.49), and the gap increases as m and n grow.

Given the configuration for variable \mathbf{W} in both formulations of SL- ℓ_1 (2.47), (2.51), the required elements of the rotation vectors that make up \mathbf{U} can be obtained from the rightmost (block) column of \mathbf{W} or by factorizing submatrices along the block diagonal. The former approach is usually more accurate [61]. SL- ℓ_1 MD and SL- ℓ_1 SD are summarized in Algorithm 4.

Algorithm 4 Summary of the SL- ℓ_1 MD/SD algorithms

- 1: Given the anchor positions and range measurements, solve the SDR (2.49) or (2.52)
- 2: Compute a rank- n approximation of the SDR solution from the rightmost (block) column of \mathbf{W} or by factorizing submatrices along the block diagonal
- 3: Obtain the matrix of sphere projections as $\mathbf{Y} = \mathbf{A} + \mathbf{R}\mathbf{U}$
- 4: Estimate the source position as $\mathbf{x} = \frac{\sum_{i=1}^m \frac{y_i}{\lambda_i}}{\sum_{i=1}^m \frac{1}{\lambda_i}}$

TABLE 2.1: Worst-case complexities of the proposed algorithms.

Algorithms	Operation per iteration
\mathcal{O}_{SLCP}	$(2m^2)^2$
\mathcal{O}_{SLNN}	$(m^2)^2$
$\mathcal{O}_{SL-\ell_1-MD}$	$((mn + 1)^2 + mn + n)^2(mn)^2$
$\mathcal{O}_{SL-\ell_1-SD}$	$((m + n)^2 + m + 1)^2 m^2$

2.6 Complexity Analysis

Consider the general form of a SDP [68]

$$\begin{aligned} & \underset{\mathbf{x}}{\text{minimize}} && \mathbf{c}^T \mathbf{x} \\ & \text{subject to} && \mathbf{F}(\mathbf{x}) \succeq 0, \end{aligned} \tag{2.53}$$

where $\mathbf{x} \in \mathbb{R}^k$ and $\mathbf{F}(\mathbf{x}) = \mathbf{F}_0 + \sum_{i=1}^k x_i \mathbf{F}_i$. The available data includes the vector $\mathbf{c} \in \mathbb{R}^k$ and $k + 1$ symmetric matrices $\mathbf{F}_0, \dots, \mathbf{F}_k \in \mathbb{R}^{l \times l}$. An SDP problem can be solved by iterative optimization techniques, e.g., interior-point methods. The worst-case computational complexity of solving SDP in each iteration is $\mathcal{O}(k^2 l^2)$ [68]. The number of iterations is also bounded by $\mathcal{O}(\sqrt{l} \log(1/\epsilon))$, where ϵ is the accuracy of the SDP solution [68].

The proposed methods involve formulating and solving a single SDP, so their worst-case computational complexities can be readily estimated from the above results. For SLCP, SLNN, SL- ℓ_1 MD and SL- ℓ_1 SD, the (k, l) pairs are $(k \simeq 2m^2, l \simeq 1)$, $(k \simeq m^2, l \simeq 1)$, $(k \simeq (mn + 1)^2 + mn + n, l \simeq mn)$ and $(k \simeq (m + n)^2 + m + 1, l \simeq m)$, respectively. Note that m and n are the number of anchors and the space dimension, respectively. Additionally, note that SVD should be applied to the results of SLCP and SLNN and this operation brings additional cost. However, the asymptotic complexity of SVD is much smaller than SDP and it is ignored. The worst-case complexities of the proposed methods per iteration are given in Table 2.1.

2.7 Related Works

This section surveys related methods with varying complexities and accuracies that may be used as benchmarks to the proposed algorithms. They are representatives of different classes and some of them are originally derived for different measurement models, but adapted here for TOA-based source localization as discussed in the sequel.

2.7.1 Squared Range Least Squares (SR-LS)

The first state-of-the-art localization algorithm of interest is the exact optimization method proposed in [47]. This technique relies on a variation of the ML localization problem given in (2.1), in which range measurements are squared. Specifically, the problem solved in [47] is

$$\underset{\mathbf{x}}{\text{minimize}} \quad \sum_{i=1}^m (\|\mathbf{x} - \mathbf{a}_i\|^2 - r_i^2)^2. \quad (2.54)$$

Since the range measurements r_i are squared, this problem differs from the original ML source localization problem. However, squaring measurements is a very popular approach (also in TDOA) because it makes optimization-based source localization problems more tractable. Because, it was shown in [47] that the exact solution of (2.54) can be derived as follows. Write the equivalent form

$$\begin{aligned} & \underset{\mathbf{y}}{\text{minimize}} \quad \|\mathbf{A}\mathbf{y} - \mathbf{b}\|^2 \\ & \text{subject to} \quad \mathbf{y}^T \mathbf{H}\mathbf{y} + 2\mathbf{c}^T \mathbf{y} = 0, \end{aligned} \quad (2.55)$$

where $\mathbf{A} = \begin{bmatrix} -2\mathbf{a}_1^T & 1 \\ \vdots & \vdots \\ -2\mathbf{a}_m^T & 1 \end{bmatrix}$, $\mathbf{b} = \begin{bmatrix} r_1^2 - \|\mathbf{a}_1\|^2 \\ \vdots \\ r_m^2 - \|\mathbf{a}_m\|^2 \end{bmatrix}$, $\mathbf{H} = \begin{bmatrix} \mathbf{I}_n & \mathbf{0}_n \\ \mathbf{0}_1 & 0 \end{bmatrix}$, and $\mathbf{c} = \begin{bmatrix} \mathbf{0}_n \\ -0.5 \end{bmatrix}$.

Next, compute α^* as the root of

$$\hat{\mathbf{y}}(\alpha)^T \mathbf{H}\hat{\mathbf{y}}(\alpha) + 2\mathbf{c}^T \hat{\mathbf{y}}(\alpha) = 0, \quad \text{with} \quad \alpha \in \left(-\frac{1}{\alpha_1}, \infty\right) \quad (2.56)$$

where α_1 is the maximum of the generalized eigenvalues [63] of $(\mathbf{H}, \mathbf{A}^T \mathbf{A})$ and

$$\hat{\mathbf{y}}(\alpha) = (\alpha \mathbf{H} + \mathbf{A}^T \mathbf{A})^{-1} (\mathbf{A}^T \mathbf{b} - \alpha \mathbf{c}). \quad (2.57)$$

Finally, the minimizer of the objective in (2.54) is given by the n first component of $\hat{\mathbf{y}}(\alpha^*) \in \mathbb{R}^{n+1}$. This method will be called SR-LS from now on. In spite of the fact that the solution is exact, the formulation of the problem is suboptimal with respect to

the ML formulation, since squaring the distances amplifies errors on the measurements, fundamentally increasing the achievable mean square location error [69].

The weighted version of (2.54), designated as WSR-LS, is

$$\underset{\mathbf{x}}{\text{minimize}} \quad \sum_{i=1}^m w_i (\|\mathbf{x} - \mathbf{a}_i\|^2 - r_i^2)^2 \quad (2.58)$$

where w_i s are positive constants. And the equivalent problem is

$$\begin{aligned} \underset{\mathbf{y}}{\text{minimize}} \quad & (\mathbf{A}\mathbf{y} - \mathbf{b})^T \mathbf{W} (\mathbf{A}\mathbf{y} - \mathbf{b}) \\ \text{subject to} \quad & \mathbf{y}^T \mathbf{H}\mathbf{y} + 2\mathbf{c}^T \mathbf{y} = 0, \end{aligned} \quad (2.59)$$

Weighting Scheme

The weighting scheme is similar to [41, 70]. Let us discuss the disturbances in \mathbf{b} , which suggest a criterion for choosing \mathbf{W} . For sufficiently small measurement error, the squared value of r_i can be approximated as $r_i^2 = (d_i + n_i)^2 \approx d_i^2 + 2d_i n_i$, where $d_i = \|\mathbf{x} - \mathbf{a}_i\|$ is the true range. As a result, the disturbance between the true and measured squared distances is $\varepsilon = r_i^2 - d_i^2 \approx 2d_i n_i$. In vector form $\boldsymbol{\varepsilon} = [2d_1 n_1, \dots, 2d_m n_m]^T$. The covariance matrix of the disturbance is thus of the form $\boldsymbol{\Psi} = \mathbf{B}\mathbf{A}\mathbf{B}$, where $\mathbf{B} = \text{diag}(2d_1, \dots, 2d_m)$ and $\mathbf{A} = \text{diag}(\sigma_1^2, \dots, \sigma_m^2)$. The optimum weighting matrix is $\mathbf{W} = \boldsymbol{\Psi}^{-1}$ [70]. Since it depends on the unknown d_i , it is approximated as $\boldsymbol{\Psi} = \hat{\mathbf{B}}\mathbf{A}\hat{\mathbf{B}}$, where $\hat{\mathbf{B}} = \text{diag}(2r_1, \dots, 2r_m)$.

2.7.2 Linear Least Squares (LLS)

LLS method solves two linear system of equations sequentially. It was originally proposed for RSS in [57], but it is adapted for TOA in this section. The first system of linear equations is solved by using the same cost function of WSR-LS. The optimal source position is calculated from the first n components of

$$\hat{\boldsymbol{\theta}} = (\mathbf{A}^T \mathbf{W} \mathbf{A})^{-1} \mathbf{A}^T \mathbf{W} \mathbf{b}. \quad (2.60)$$

This unconstrained solution ignores the constraint that ties the last component of $\boldsymbol{\theta}$, denoted by R , to its remaining elements,

$$R = \sum_{i=1}^n x_i^2. \quad (2.61)$$

Based on [70], the solution obtained in first step of LLS algorithm is therefore improved by solving another linear system of equations to approximately enforce (2.61). When $\hat{\boldsymbol{\theta}}_{1:n}$ is sufficiently close to \mathbf{x} ,

$$\hat{\theta}_i^2 - x_i^2 = (\hat{\theta}_i + x_i)(\hat{\theta}_i - x_i) \approx 2x_i(\hat{\theta}_i - x_i), \quad i = 1, \dots, n. \quad (2.62)$$

Based on (2.61) and (2.62), a linear system is constructed

$$\mathbf{h} = \mathbf{G}\mathbf{z} + \mathbf{q}, \quad (2.63)$$

where $\mathbf{h} = [\hat{\theta}_1^2, \dots, \hat{\theta}_n^2, \hat{\theta}_{n+1}]^T$, $\mathbf{G} = \begin{bmatrix} \mathbf{I}_n \\ \mathbf{1}_n^T \end{bmatrix}$, $\mathbf{z} = [x_1^2, \dots, x_n^2]^T$ and $\mathbf{q} = [2x_1(\hat{\theta}_1 - x_1), \dots, 2x_n(\hat{\theta}_n - x_n), \hat{\theta}_{n+1} - R]^T$.

To determine the parameter vector \mathbf{z} , the weighted LS criterion is used again. The weight matrix \mathbf{C}_q is calculated by using the covariance matrix of $\hat{\boldsymbol{\theta}}$, $(\mathbf{A}^T \mathbf{W} \mathbf{A})^{-1}$, such that $\mathbf{C}_q = \text{diag}(2x_1, \dots, 2x_n, 1)(\mathbf{A}^T \mathbf{W} \mathbf{A})^{-1} \text{diag}(2x_1, \dots, 2x_n, 1)$. In practice, x_i is substituted with $\hat{\theta}_i$. As a result, $\hat{\mathbf{z}} = (\mathbf{G}^T \mathbf{C}_q \mathbf{G})^{-1} \mathbf{G}^T \mathbf{C}_q^{-1} \mathbf{h}$.

There is a sign ambiguity when \mathbf{x} is estimated from \mathbf{z} . Therefore, the improved position estimate is obtained as $\hat{\mathbf{x}} = \text{sgn}((\hat{\boldsymbol{\theta}})_{1:n}) \odot \sqrt{\hat{\mathbf{z}}}$, $\sqrt{\cdot}$ operation is used for each element of the vector.

2.7.3 Two Least Squares (2LS)

The formulation of 2LS in [56] is originally derived for TOA with unknown initial transmission time. The authors tackle the following problem where unknown r_0 refers to the distance corresponding to the unknown initial transmission time

$$\underset{\mathbf{x}, r_0}{\text{minimize}} \quad \sum_{i=1}^m (\|\mathbf{x} - \mathbf{a}_i\| + r_0 - r_i)^2. \quad (2.64)$$

Since the proposed algorithms are derived for the source localization problem using TOA with no synchronization problem, r_0 is assumed to be a known parameter and chosen to be 0 for fairness. Define an auxiliary variable for $\tau_i = \|\mathbf{a}_i - \mathbf{x}\|$ and denote $\mathbf{r} = [r_1, \dots, r_m]^T$, $\boldsymbol{\tau} = [\tau_1 \dots \tau_m]^T$, $\mathbf{Q} = \boldsymbol{\tau} \boldsymbol{\tau}^T$ to write the objective function of (2.64) as $\text{tr}[\mathbf{Q} - 2\mathbf{t}\boldsymbol{\tau}^T + \mathbf{t}\mathbf{t}^T]$. Clearly, the objective function is a linear function of both \mathbf{Q} and $\boldsymbol{\tau}$ and thus it is convex. However, because the constraints $\tau_i = \|\mathbf{a}_i - \mathbf{x}\|$ and $\mathbf{Q} = \boldsymbol{\tau} \boldsymbol{\tau}^T$ are nonconvex, the optimization problem is nonconvex. To obtain a convex optimization problem note that $(\mathbf{a}_i - \mathbf{x})^T (\mathbf{a}_i - \mathbf{x}) = \begin{bmatrix} \mathbf{x}_i \\ -1 \end{bmatrix}^T \begin{bmatrix} \mathbf{I} & \mathbf{x} \\ \mathbf{x}^T & x_s \end{bmatrix} \begin{bmatrix} \mathbf{x}_i \\ -1 \end{bmatrix}$, where $x_s = \mathbf{x}^T \mathbf{x}$.

Use this and Cauchy-Schwarz inequality to yield

$$\mathbf{Q}_{ii} = \tau_i^2 = (\mathbf{a}_i - \mathbf{x})^T (\mathbf{a}_i - \mathbf{x}) = \begin{bmatrix} \mathbf{x}_i \\ -1 \end{bmatrix}^T \begin{bmatrix} \mathbf{I} & \mathbf{x} \\ \mathbf{x}^T & x_s \end{bmatrix} \begin{bmatrix} \mathbf{x}_i \\ -1 \end{bmatrix}$$

and

$$\mathbf{Q}_{ij} = \tau_i \tau_j = \|\mathbf{a}_i - \mathbf{x}\| \|\mathbf{a}_j - \mathbf{x}\| \geq \left| \begin{bmatrix} \mathbf{x}_i \\ -1 \end{bmatrix}^T \begin{bmatrix} \mathbf{I} & \mathbf{x} \\ \mathbf{x}^T & x_s \end{bmatrix} \begin{bmatrix} \mathbf{x}_j \\ -1 \end{bmatrix} \right|$$

which are convex in terms of \mathbf{Q} , \mathbf{x} and x_s . There are still two nonlinear and nonconvex constraints, $\mathbf{Q} = \boldsymbol{\tau} \boldsymbol{\tau}^T$ and $x_s = \mathbf{x}^T \mathbf{x}$. Through semidefinite relaxations and linear matrix inequalities the following convex optimization problem is obtained

$$\begin{aligned} & \underset{\mathbf{x}, x_s, \boldsymbol{\tau}, \mathbf{Q}}{\text{minimize}} && \text{tr}[\mathbf{Q} - 2\mathbf{t}\boldsymbol{\tau}^T + \mathbf{t}\mathbf{t}^T] \\ & \text{subject to} && \begin{bmatrix} \mathbf{Q} & \boldsymbol{\tau} \\ \boldsymbol{\tau}^T & 1 \end{bmatrix} \geq 0, \quad \begin{bmatrix} \mathbf{I} & \mathbf{x} \\ \mathbf{x}^T & x_s \end{bmatrix} \geq 0, \\ & && \mathbf{Q}_{ii} = \begin{bmatrix} \mathbf{x}_i \\ -1 \end{bmatrix}^T \begin{bmatrix} \mathbf{I} & \mathbf{x} \\ \mathbf{x}^T & x_s \end{bmatrix} \begin{bmatrix} \mathbf{x}_i \\ -1 \end{bmatrix}, \\ & && \mathbf{Q}_{ij} \geq \left| \begin{bmatrix} \mathbf{x}_i \\ -1 \end{bmatrix}^T \begin{bmatrix} \mathbf{I} & \mathbf{x} \\ \mathbf{x}^T & x_s \end{bmatrix} \begin{bmatrix} \mathbf{x}_j \\ -1 \end{bmatrix} \right|, \\ & && i = 1, \dots, m, \quad j = i + 1, \dots, m. \end{aligned} \tag{2.65}$$

2.8 Performance Analysis and Numerical Results

In this section, the performance and the computational complexity of several algorithms are analyzed. They are compared with CRLB, simulated data and real test bed data. The algorithms, SLCP (Algorithm 1), SL- ℓ_1 (Algorithm 2), SLNN (Algorithm 3) and SL- ℓ_1 MD/SD (Algorithm 4) are benchmarked against the following algorithms in 2D and 3D scenarios under various noise assumptions: *i*) SR-LS and its weighted version WSR-LS in [47] directly optimize the source coordinates using an iterative root-finding procedure (Section 2.7.1). The weighting procedure penalizes larger ranges more and assumes prior knowledge on the variance of disturbances, as described in Section 2.7.1. *ii*) 2LS in [56] approximates the ML estimate of the source position with a SDP formulation (Section 2.7.3). *iii*) SDR, another popular formulation based on semidefinite relaxation is chosen for benchmarking [50]. *iv*) LLS in [57] solves sequentially two linear systems, where the second step improves the source position estimate by exploiting the constraint on the squared norm of the source position (Section 2.7.2).

In each reported simulation M Monte Carlo runs are performed, where in each run the source and anchor locations were randomly generated from a uniform distribution over a square or cube. The observed ranges, corrupted by i.i.d. noise, were generated as described in Section 2.3 under appropriate noise probability densities. Figures show Root Mean Square Error (RMSE), computed as

$$\sqrt{\frac{1}{M} \sum_{i=1}^M \|\mathbf{x}_i - \hat{\mathbf{x}}_i\|^2}, \quad (2.66)$$

where \mathbf{x}_i and $\hat{\mathbf{x}}_i$ denote the actual and estimated source positions in the i -th Monte Carlo run, respectively.

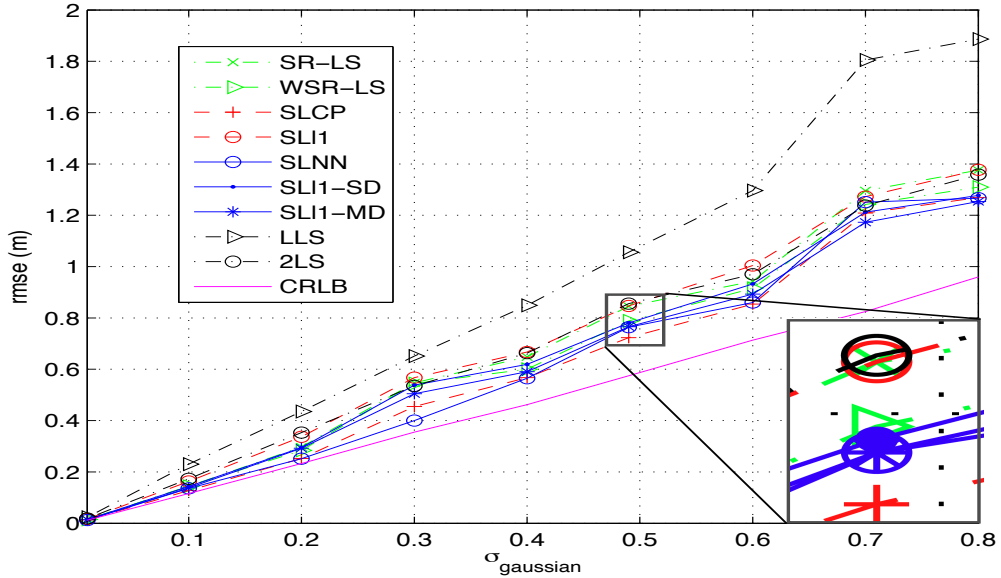
The CRLB gives a lower bound on the variance attainable by any unbiased estimators [71]. Although it is loose compared to the performance of the ML estimator in the presence of large perturbations [72] and there exists no efficient unbiased estimate for the source position due to the nonlinearity between the variable and the observation [73], it is still of interest as a benchmark [41, 70] and it is derived briefly in Appendix E in terms of the notation adopted in this thesis. Thus, the error plots for Gaussian noise also show CRLB, calculated as

$$\sqrt{\frac{1}{M} \sum_{k=1}^M \text{trace}(\text{CRLB}_k)} \quad (2.67)$$

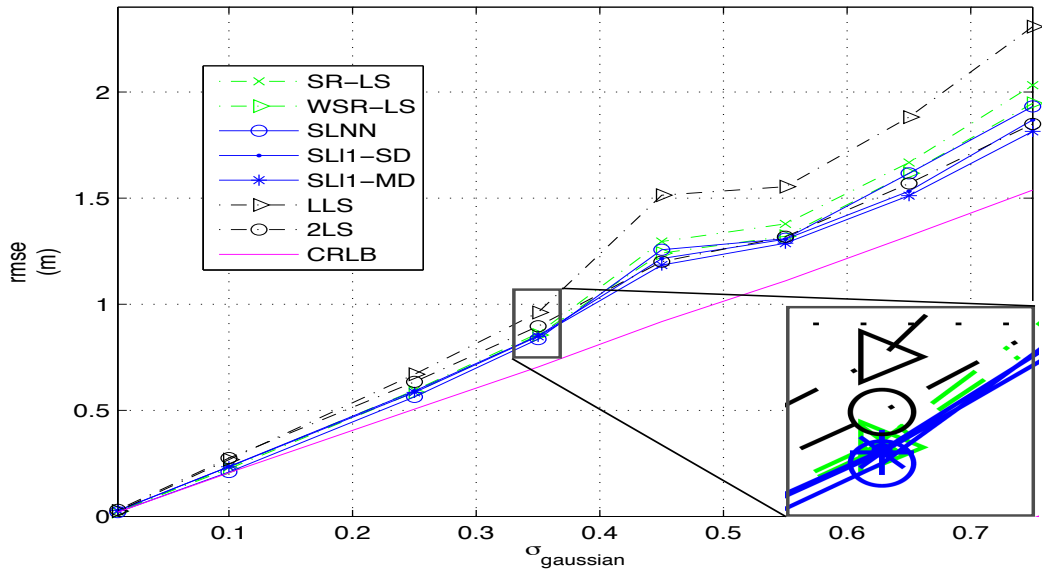
for each noise variance, where CRLB_k denotes matrix lower bound at the k -th Monte Carlo iteration.

Example 1 [Localization in 2D and 3D under Gaussian noise] $M = 1000$ Monte Carlo runs are performed, where in each run the source and anchor locations were randomly generated from a uniform distribution over a square or cube whose sides are $[0, 10]$ m. The observed ranges, corrupted by i.i.d. Gaussian noise whose $\sigma_{\text{gaussian}} \in [10^{-2} \ 0.8]$ m, were generated as described in Section 2.3.

Figure 2.3 shows the RMSE of the algorithms for 5 and 6 anchors in 2D and 3D, respectively. The worst performances, both in 2D and 3D, are attained by SR-LS and LLS. The former squares measurements ($p = 2, q = 2$ in (2.1)), and thus becomes more sensitive to the presence of (Gaussian) noise in range measurements. The latter resorts to linearization, which is not very accurate for this observation model and becomes less so as the noise power increases. The weighted version (WSR-LS) performs significantly better than SR-LS, as it de-emphasizes long ranges where the impact of squared disturbances is strongest. However, in practice this method requires some form



(a) RMSE Comparisons in 2D without outlier for 5 anchors



(b) RMSE Comparisons in 3D without outlier for 6 anchors

FIGURE 2.3: RMSE Comparisons, without outliers.

of calibration to estimate the variances of the disturbances. The remaining algorithms behave similarly, with $SL-\ell_1$ MD providing slightly better performance at higher noise levels. Note also how the RMSE of the simplified formulation $SL-\ell_1$ SD (2.52) is quite close to that of $SL-\ell_1$ MD (2.49). $SLCP$ and $SL-\ell_1$ are absent from Figure 2.3(b), as these two algorithms are specific for 2D localization. The RMSE gap to the CRLB is significant (about 0.3 m for $\sigma_{\text{gaussian}} = 0.8$ m), but it seems unlikely that it could be closed by alternative algorithms.

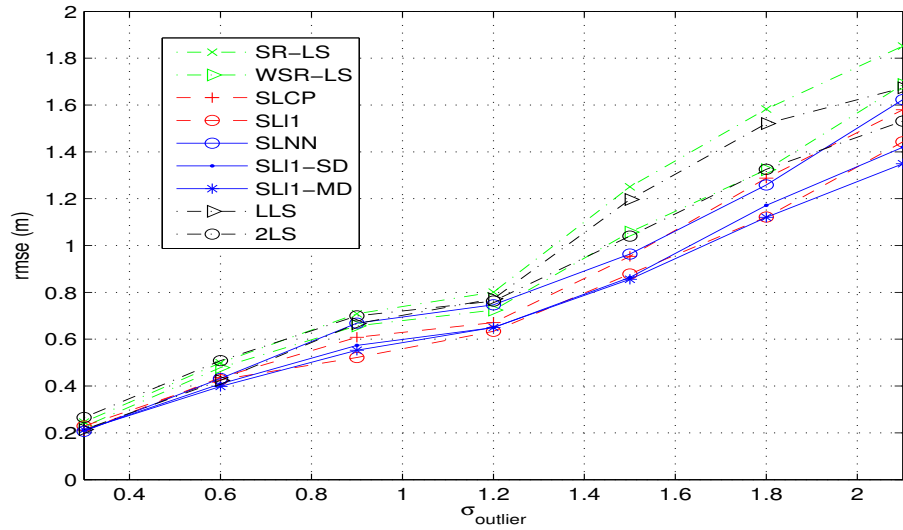
Example 2 [Localization in 2D and 3D in the presence of outliers] The same setup for Gaussian noise is adopted here, except that ranges are contaminated either by Laplacian noise with $\sigma_{\text{laplacian}} \in [0.4 \text{ } 1.8]$ m, or by what is designated here as *selective Gaussian noise*. Range measurements for the latter are created as

$$r_i = \|\mathbf{x} - \mathbf{a}_i\| + w_i + |\epsilon|, \quad (2.68)$$

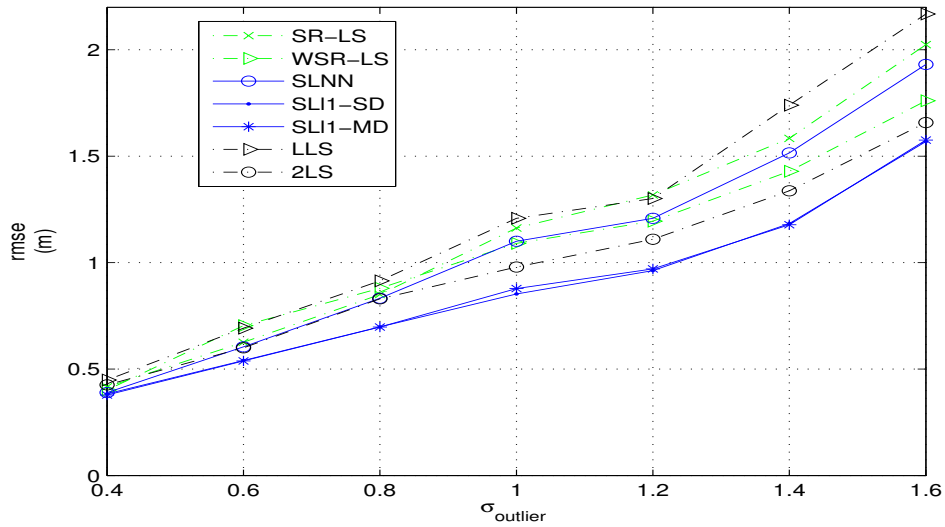
where w_i is a Gaussian noise term with $\sigma_{\text{gaussian}} = 0.04$ m that is present in all observations and ϵ is also a Gaussian disturbance, but with higher standard deviation $\sigma_{\text{outlier}} \in [0.3, 2.1]$ m, that contaminates only one measured range (i.e., $\epsilon = 0$ for all other observations). This statistical model is less tractable than the Laplacian noise model, but it is included in some of the simulations as it more realistically reflects how outliers occur in real ranging systems [24, 74].

Figures 2.4 and 2.5 depict RMSEs for 2D and 3D source localization under both outlier generation models. There are now more substantial disparities between different classes of algorithms. Broadly, the RMSE curves in these figures can be divided into 3 groups: As before, LLS and SR-LS attain the highest RMSEs. An intermediate group is formed by algorithms designed for Gaussian likelihoods (SLCP/SLNN and 2LS), as well as WSR-LS. Finally, the algorithms designed for Laplacian noise (SL- ℓ_1 in 2D and SL- ℓ_1 MD/SD in 2D or 3D) outperform all others. Interestingly, their superiority is even more evident under selective Gaussian noise, which does not match the underlying cost (likelihood) function of Section 2.4.2. Overall, the ℓ_1 -based algorithms show the most consistent behavior across all noise models.

Example 3 [Practical Computational complexity of algorithms vs. the number of anchors and the space dimension] Several authors have examined the theoretical (worst-case) complexity of localization algorithms, e.g., [56, 75]. The computational complexities of the proposed algorithms are discussed in Section 2.6 and given in Table 2.1. The emphasis here is on demonstrating the practical feasibility of the algorithms in centralized scenarios with moderate computational power, so actual running times are focused on, knowing that many technological factors related to hardware and software architectures may influence it. Note, however, that SLCP, SLNN, SL- ℓ_1 MD/SD, as well as 2LS, are single-shot formulations that essentially require a single invocation of the same general-purpose solver, and the running times for these algorithms should therefore closely reflect the relative operations count. These times are evaluated in 2D and 3D for variable numbers of anchors that encompass those that one would reasonably expect to find within range of a given target position in practice. The experiments were conducted on a machine powered by an Intel Xeon 3.2 GHz Quad-Core



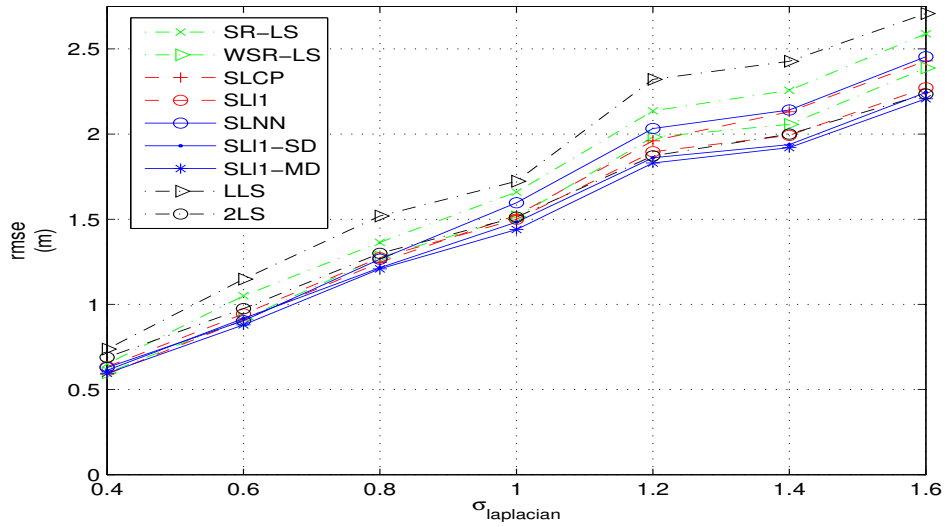
(a) RMSE Comparisons in 2D with Selective Gaussian Noise for 5 anchors



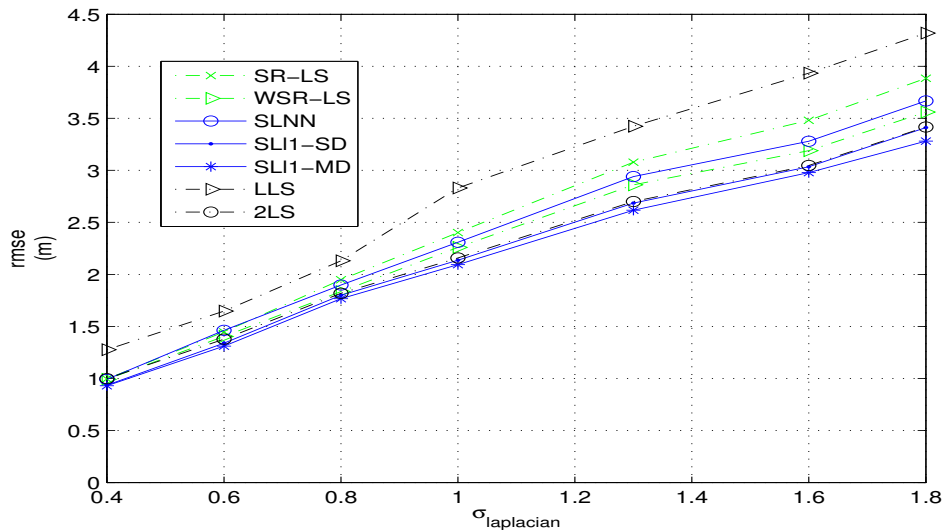
(b) RMSE Comparisons in 3D with Selective Gaussian Noise for 6 anchors

FIGURE 2.4: RMSE Comparisons in the case of Selective Gaussian Noise.

CPU and 8 GB of RAM, using Matlab R2010b and CVX/SeDuMi as a general-purpose SDP solver. Figure 2.6(a) shows that SR-LS, WSR-LS and LLS are much faster than the other algorithms (average times are 0.2 ms for LLS, 3 ms for SR-LS, and 2.5 ms for WSR-LS), but their larger RMSEs would make them preferred mainly under severe temporal or computational constraints. The running times of SLCP and SLNN are almost constant in the figure (about 0.2 s), suggesting that the fixed overhead from the software implementation plays an important role (the variable component becomes significant above 15 anchors). Regarding SL- l_1 and SL- l_1 SD, the times increase moderately, remain below 0.5 s, and are similar in 2D and 3D (Figure 2.6(b)). The largest



(a) RMSE Comparisons in 2D with Laplacian Noise for 5 anchors

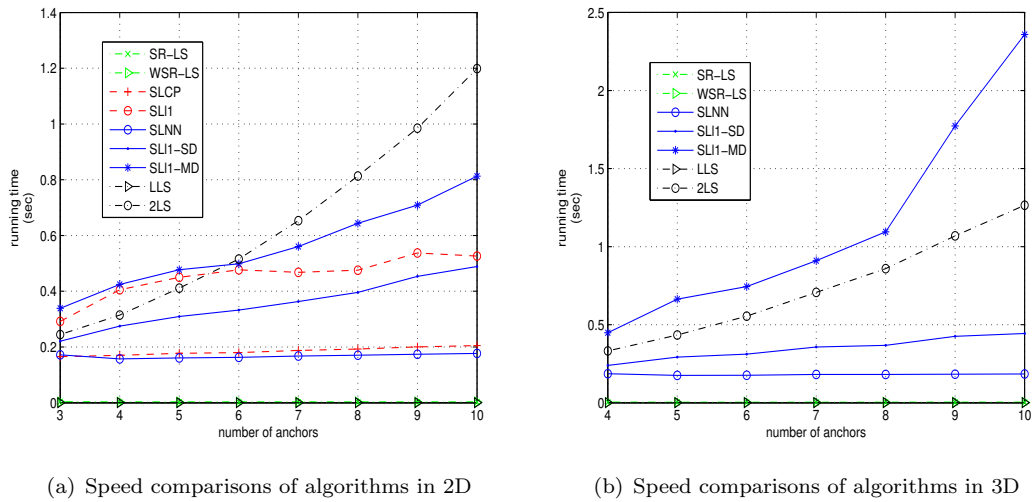


(b) RMSE Comparisons in 3D with Laplacian Noise for 6 anchors

FIGURE 2.5: RMSE Comparisons in the case of Laplacian Noise.

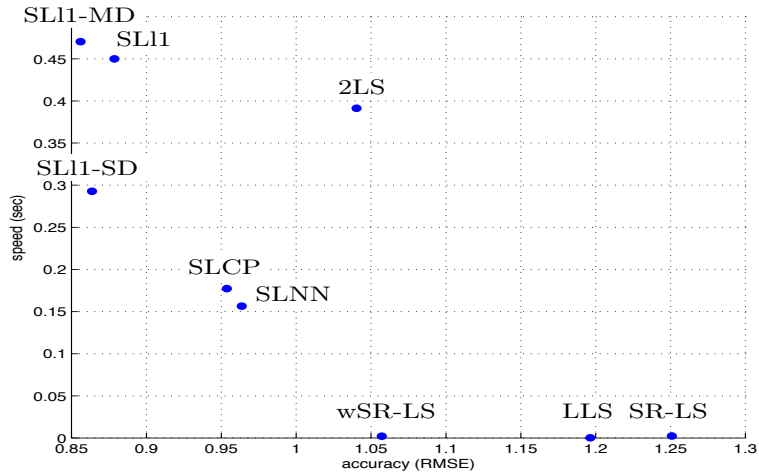
times and increase rates are attained by 2LS in 2D and $SL-\ell_1$ MD in 3D. Note that in $SL-\ell_1$ MD the number of variables is affected *multiplicatively* by the ambient space dimension, leading to larger effort in 3D. Notice that the ordering of proposed algorithms according to the operations count given in Table 2.1 agrees with the results for execution time given in Figures 2.6(a) and 2.6(b).

The above results show that $SL-\ell_1$ SD has nearly the same performance of $SL-\ell_1$ MD at a fraction of the complexity. The running times for these algorithms, even with more modest hardware, may enable tracking of relatively slow targets with practical numbers



(a) Speed comparisons of algorithms in 2D

(b) Speed comparisons of algorithms in 3D



(c) Speed vs Accuracy in 2D

FIGURE 2.6: Speed comparisons of algorithms vs. number of anchors.

of anchors. Figure 2.6(c) summarizes the RMSE vs. speed tradeoff of the considered algorithms in 2D for 5 anchors and Selective Gaussian noise with $\sigma_{\text{outlier}} = 1.5$.

Example 4 [The sensitivity of SL- ℓ_1 MD to μ] SL- ℓ_1 MD has a penalizing term μ for the norm of the variable β which is constrained to be rank-1. Figure 2.7 shows the (in)sensitivity of the method to the penalizing term for two scenarios where the ranges were corrupted with white Gaussian noises having $\sigma = 1$ m and $\sigma = 0.5$ m, respectively. The source and five anchors were uniformly distributed over a square whose sides are $[0, 10]$ m at each Monte Carlo run. It is chosen to be equal to 10 throughout the simulations.

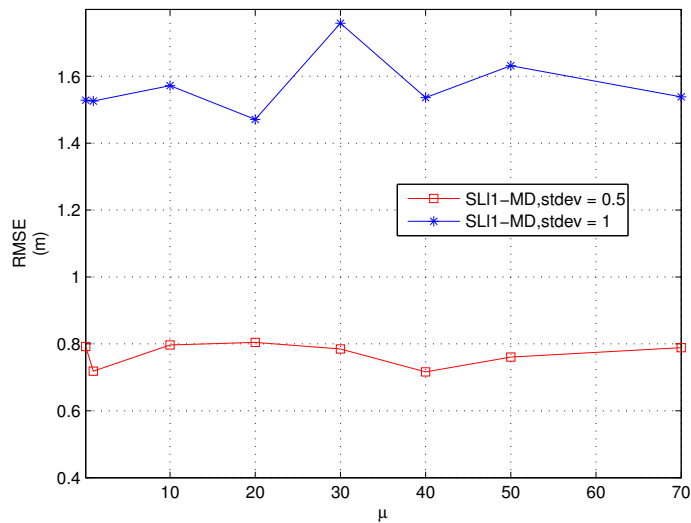


FIGURE 2.7: The sensitivity of SL- ℓ_1 MD to the penalizing term μ

Example 5 [Convexity and tightness of SLCP] In this example we characterize the accuracy of the convex relaxation used in SLCP and compare its performance to that of the SDR algorithm of [50]. Range measurements to a variable number of randomly placed anchors in a square whose sides are $[-10, 10]$ m were generated over $M = 1000$ Monte Carlo runs, and corrupted by white Gaussian noise.

First, it is estimated how often the constraint set \mathcal{S} (2.8), which appears in the formulation of the source localization problem prior to relaxation (2.7), is convex along its “upper right” boundary where the optimal solution lies. As discussed in Section 2.4.1.1, when this property holds the relaxed solution Φ obtained by SLCP (2.6) will have rank 1 and can be factorized to yield the optimal point for the non-relaxed problem (2.7) on the boundary of \mathcal{S} . Convexity of \mathcal{S} is empirically assessed by tracing the boundary of the (partially hypothesized) convex hull \mathcal{T} (2.11) and searching for line segments that delimit regions where the boundaries of \mathcal{S} and \mathcal{T} depart due to local concavity of \mathcal{S} . Specifically, the support hyperplane problem (2.12) is solved for a grid of angles $0 \leq \beta \leq \frac{\pi}{2}$ and detect the presence of a line segment when the distance between the intersection points $(u(\beta), v(\beta))$ for two consecutive angles β exceeds a threshold. For a noise standard deviation $\sigma_{\text{gaussian}} = 10^{-2}$ m, \mathcal{S} passed the convexity test in 80% of runs for three anchors. The percentage increased to 84% for five anchors, in line with the reasoning in Section 2.4.1.1 that \mathcal{S} is more likely to be convex as the number of anchors increases.

Next, the RMSEs of SDR and SLCP are compared. As in [47] Monte Carlo runs are provided for SDR, SLCP and also for so-called *tight runs* (denoted by SDRt, SLCPt) where the solution for the relaxed localization problem is close to having rank 1, as

TABLE 2.2: Source localization accuracy for relaxation-based methods (RMSEs listed for total and tight runs).

σ_{gaussian}	N_{SDR}	N_{SLCP}	SDR [50]	SDRt [50]	SLCP	SLCPt
10^{-3}	490	921	0.0045	0.0014	0.0020	0.0015
10^{-2}	444	815	0.0162	0.0107	0.0112	0.0108
10^{-1}	478	527	0.1503	0.0960	0.1207	0.0959
1	538	526	1.6070	1.1885	1.2169	1.1885

desired for subsequent factorization to obtain the actual source coordinates. A solution matrix is considered to be tight when the ratio between its first and second eigenvalues is at least 10^2 . Table 2.2 lists the RMSEs and the number of tight runs (N_{SDR} , N_{SLCP}) over 1000 trials for five anchors and Gaussian noise standard deviations of 1 m, 10^{-1} m, 10^{-2} m, and 10^{-3} m. SLCP is clearly superior over the full set of trials, but the gap to SDR closes in the subset of tight runs, indicating that the advantage is mostly due to a much higher probability of its solution having near rank 1. Even for the highest noise power, where the number of tight runs in both algorithms is comparable, the ratio of first to second eigenvalues is usually higher in SLCP, leading to lower RMSE.

Under the same simulation setup as above, but using only three anchors, the alternative search-based method described in Section 2.4.1.2 to obtain the vector of rotation factors θ from the relaxed solution matrix of SLCP, Φ is tested. Improvements in total RMSE are under 1% for all noise variances using 2×10^5 grid points on the interval $[0, 2\pi)$ to evaluate (2.17). Foremost, this suggests that rank-1 factorization by SVD, which is adopted as the technique of choice to efficiently extract rotation factors, yields results that are indeed very close to the best possible strategy for finding θ .

2.9 Real Indoor Experiments

There is a large and growing list of practical works related to localization systems (mostly for target (self)-localization, but not for joint sensor/target localization) which rely on infrared (IR), RSS, Ultra Wideband (UWB) and ultrasound signals, etc. Many such systems rely on RSS, but these are impractical to use when indoor propagation conditions are complicated [76]. The overall performance of IR degrades under direct sunlight or high ambient temperature. On the other hand, these systems are appropriate for spaces in which other technologies do not perform properly [77]. The Active Bat [78] is based on ultrasonic pulses which rely on TOA measurements, requiring very accurate clock synchronization in the system. UWB based systems are an emerging indoor localization technology which provides an accuracy on the order of a few centimeters. However, they are still expensive [79]. In this work, a Cricket system from Crossbow Technologies

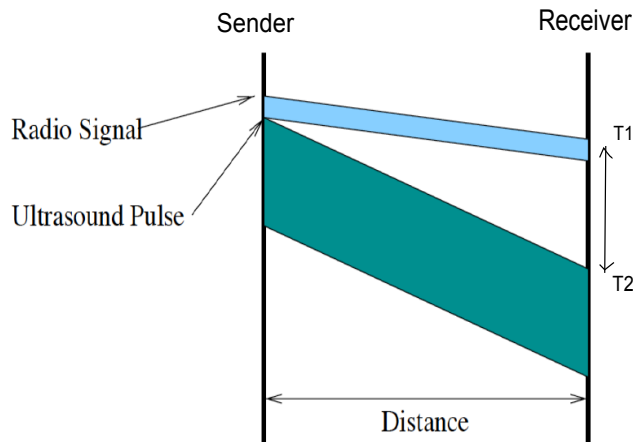


FIGURE 2.8: Range Measurement using ultrasound and radio signals (reproduced from [18]).

[18] is employed, using both ultrasound and RF signals to estimate the ranges between sensors and a target. These devices are inexpensive and easy to deploy; however, their operating range is limited, approximately ten meters.

To estimate ranges, a mobile Cricket Node (beacon/target) simultaneously emits a radio and an ultrasound pulse every second. Since the difference in arrival time of these two pulses to a sensor node (listener) is proportional to the range between the sensor node and the target, Crickets compute ranges from these arrival times as shown in Figure 2.8. Note that this scheme does not require TWR or clock synchronization.

Since the algorithms scheme entirely rely on distance estimates, any inaccuracies or spurious estimates will result in erroneous positions. Therefore, in the sequel the uncertainties are described in the setup. The line-of-sight operating range of ultrasonic listener-beacon pairs is around 10 meters, when both the listener and the beacon are facing each other. It is observed in [80] that approximately within 5 m range when a listener and beacon face each other at $0 - 40^\circ$ angles, the error in range estimation remains quite stable within 2 cm boundaries. From 40° on up to 75° , the error rises to 9 cm. From 75° onwards, the listener is no longer able to detect the ultrasonic signal. In the setup similar behaviour was experienced; for up to 4 m range measurements the uncertainties in measurements can go up to 6 cm due to the variable facing angle between sensors and the beacon along the trajectory. Secondly, the ultrasound sensor on a Cricket occupies an area of 1 cm x 2 cm on the circuit board, so it is difficult to estimate the ground truth for its location below those dimensions. Additionally, the anchor nodes are normally assumed to be fixed at known positions. However, in practice, there are uncertainties in anchor node positions due to imperfect deployment etc.



FIGURE 2.9: The test environment and Pioneer P3-DX: 4 Cricket sensors on the ceiling and 4 on top of tripods distributed over the lab in a 4m by 4m area. The robot or a human carries the beacon.

Results will be presented relative to tracking a Pioneer P3-DX robot in a test environment shown in Figure 2.9, where 8 listeners were deployed around the lab and on the ceiling in a 4 m by 4 m area and the beacon was attached to a Pioneer P3-DX mobile robot programmed to follow a desired path for approximately 2 minutes, generating 24 target positions. As the robot moves, the beacon periodically emits signals which allow the anchors to measure their distances to the robot. Anchor positions were manually measured to a precision of about 2 cm. For ground truth, the initial point for the beacon path was similarly determined, and the remaining ones were set relative to it according to the planned trajectory (the robot's navigation system is very precise under the test conditions). Figure 2.10 shows an estimated representative trajectory (a straight line, followed by a half circle, a straight line, and a full circle) by the best three methods (SLNN, SL- ℓ_1 MD and 2LS) and their average RMSEs for all 24 target/source positions. Results for SLNN and SL- ℓ_1 MD are very similar, slightly outperforming 2LS. As there are no obvious outlier range measurements here (noise statistics are unknown) ℓ_1 -based algorithms are on a par with those based on Gaussian assumptions. On a final practical note, producing the trajectories shown in Figure 2.10 required no tuning of parameters.

2.10 Conclusion

Approximate ML algorithms have been proposed for range-based source localization through convex relaxation of likelihood functions for Gaussian or Laplacian noise. These centralized algorithms yield excellent localization accuracy with moderate computational

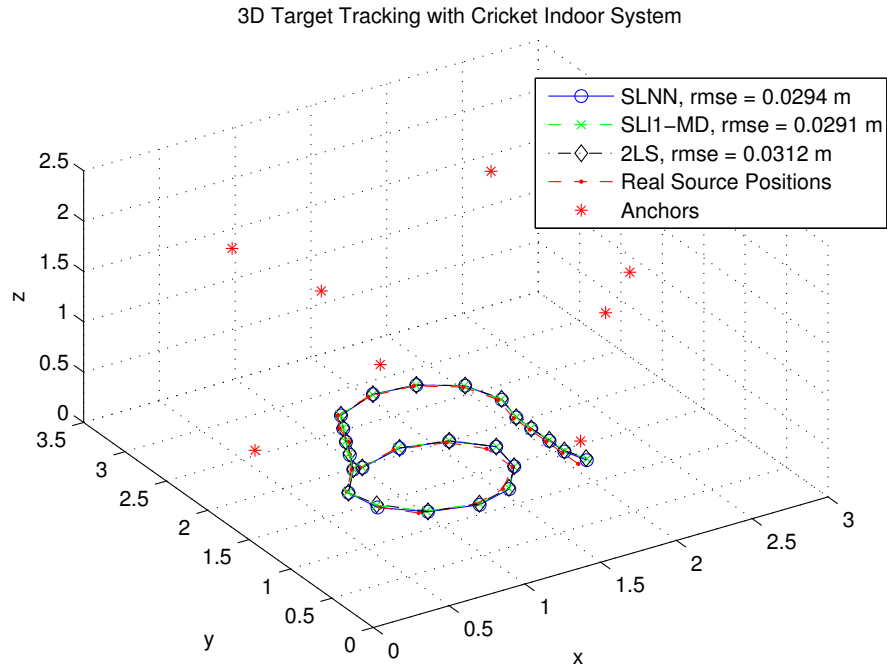


FIGURE 2.10: Piecewise linear/circular trajectory of Pioneer P3-DX.

cost. The fact that they solve a single convex optimization problem and do not require setting critical parameters *a priori* makes them robust and very convenient for practical use, if execution times on the order of 1 second or less using contemporary generic computers can be tolerated.

SLCP and SLNN are proposed as an ML-based source localization approach under Gaussian noise by resorting to complex plane and nuclear norms, respectively. $SL-\ell_1$ localization algorithms for Laplacian noise are also developed. The simulation results show that the proposed algorithms are very accurate compared to other optimization-based localization methods that operate on range measurements with a moderate computational complexity. In 3D scenarios with Gaussian noise SLNN delivered solutions that were about 5% more accurate than those of $SL-\ell_1$, whereas in the presence of outlier range measurements the situation was reversed and $SL-\ell_1$ proved to be about 5–20% more accurate under either Laplacian or selective Gaussian models. $SL-\ell_1$ MD/SD are developed as 3D extensions of $SL-\ell_1$, which exhibited comparable performance, with a slight advantage of $SL-\ell_1$ MD. However, $SL-\ell_1$ SD is a lot faster. Complexity considerations (e.g., computational load, maximum admissible problem size) will then play an important role when selecting one of those algorithms for a particular application. Experimental results demonstrated the feasibility of the proposed algorithms in a practical centralized indoor localization testbed.

An analysis of the geometry of the 2D formulation for ML localization under Gaussian

noise (SLCP) is carried out, and it is found that the high probability that a certain portion of the (outer) border of its constraint set is convex justifies the observed strong tightness of the relaxation. The simulation results for random anchor configurations indicate that another well-known SDR relaxation for the same problem has a significantly higher chance of yielding optimal solutions that do not have the necessary properties (unit rank) to accurately recover source positions. Regarding the extraction of spatial coordinates from the positive semidefinite matrix computed by SLCP, a search-based alternative to standard rank-1 factorization using the SVD is examined. This strategy is feasible for the practically important case of range-based localization using three anchors, but was found to yield only minor improvements relative to the SVD-based factorization.

Chapter 3

Robust Localization of Nodes and Time-Recursive Tracking in Sensor Networks Using Noisy Range Measurements

3.1 Introduction

This chapter addresses the problem of tracking a single target from distance-like measurements taken by nodes in a sensor network whose positions are not precisely known. The goal is to estimate the positions of all sensors and of the target, given partial or no *a priori* information regarding the spatial configuration of the network. As the ability to track a target is a key component in several scenarios of WSNs, methods that avoid the need for careful calibration of sensor positions are practically relevant. Since target dynamics are not considered in the proposed approach, the target tracking is not handled in the usual sense and the proposed method might be better framed in the group of SNL. Nevertheless, the problem tackled in this chapter is viewed as simultaneous localization and tracking (SLAT) due to the functional similarities with the approaches originally presented in [11, 81].

In [11, 81] SLAT is formulated in a Bayesian framework that exploits the connections with the well-studied problem of simultaneous localization and mapping (SLAM) in robotics. The *a posteriori* probability density function of sensor/target positions and calibration parameters is recursively propagated in time as new target sightings become available. The observations in [11] are true range measurements obtained through a

combination of transmitted acoustic and radio pulses. Some alternatives to range include pseudorange and bearing information estimated from camera images [81] or the (somewhat unreliable) RSS of radio transmissions [82]. In [83] the SLAT problem is also formulated in a Bayesian framework as a general state evolution model under a binary proximity model and solved in a decentralized way using binary sensor networks. Another SLAT-like approach using localization techniques (calibration) is presented in [84], where positions and orientations of unknown sources and sensors are centrally obtained via ML based on TOA and AOA measurements.

In the presented approach target dynamics are not accounted for; therefore the SLAT problem may be thought of as a special type of SNL, with a limited set of intersensor measurements, for a network comprising the original set of nodes and the sensed target positions. The proposed approach resorts to EDM methods based on SDP, which were previously adopted for static SNL (see [35] and references therein). EDM completion for SLAT is discussed in [82], although the authors pursued an alternative approximate completion approach based on a variant of Multidimensional Scaling (MDS). Underwater and underground scenarios with uncertainty in anchor positions are considered in [85], and edge-based SDP is proposed to reduce the computational complexity of SNL. In [74] static SNL is formulated as a problem of ML phase retrieval.

In addition to centralized SNL approaches such as [35, 74, 85], enumerated above, a wealth of results are available on distributed approaches for scenarios where the existence of a central node is inconvenient, e.g., due to congested communications in its vicinity or excessive vulnerability of the whole infrastructure to failure of that single node [31, 59, 82, 86–88]. A two-step approach based on second-order cone programming relaxation with inaccurate anchor positions is introduced in [86]. In [59] a weighted least-squares algorithm with successive refinement provides both position estimates and their covariances in partially connected scenarios. A distributed weighted MDS method with majorization approximations is applied in [31]. The cost function and the majorization technique are similar to those used in this chapter for ML iterative refinement under Gaussian noise, but initialization relies on prior estimates of sensor positions.

3.2 Overview

The summary and the contributions of the chapter are highlighted as follows.

This part of the thesis focuses on centralized SLAT based on plain ML estimation which is formulated in Section 3.3. A two-stage approach, consisting of a *startup phase* and *updating phase*, is proposed. The main goal of the startup phase is to obtain an outline

of the network configuration from a block of measurements (as in [11], the term *batch* is often used for such a block, or to qualify the associated processing algorithms). It is followed by an *updating phase* where new target sightings are incrementally assimilated as they become available, while improving all previously determined locations. Each phase consists of an *initialization step* to calculate approximate locations, followed by an iterative *refinement step* of the likelihood function using MM [89]. Local convergence to undesirable extrema in ML methods due to poor initialization is thus alleviated.

During startup the initialization step solves an EDM completion problem for range data from multiple target sightings, which requires little *a priori* knowledge of sensor/-target positions. The updating phase, carried out for each new target sighting after startup, aims to bypass the need for EDM initialization with increasingly large matrices as time progresses and more range measurements become available. Initialization in this phase uses source localization algorithms that fix all previously estimated positions and attempt to determine the location for the most recently observed target. The computational load of this simplified recursive initialization scheme is scalable with time.

This work develops startup and updating algorithms for Gaussian noise and also for Laplacian noise which models the presence of outliers in some practical ranging systems that adversely affect the performance of localization algorithms designed for Gaussian noise [11, 90]. The proposed methods for the initialization steps are novel and relevant for SNL and SL applications. In particular, for startup initialization EDM completion methods are developed that depart from related approaches [35, 65] in which squared range measurements are matched. The details of the proposed cost functions are different for Gaussian and Laplacian noise models, but in both cases robustness to range errors is gained relative to more standard EDM methods by matching plain distances. With regard to the updating phase, the initialization step under Gaussian noise is carried out by the SLCP or SLNN methods proposed in Sections 2.4.1 and 2.5.1. Under Laplacian noise ℓ_1 norm based methods addressed in Sections 2.4.2 and 2.5.2 are used.

To this end, Section 3.4 presents the proposed localization algorithms that use range measurements corrupted by Gaussian noise, namely, EDM initialization, iterative likelihood refinement by MM, and time-recursive updating through incremental estimation of target/sensor positions. Section 3.5 develops similar methods for Laplacian noise.

Section 3.6 provides simulation results for the performances of startup and updating algorithms under both types of measurement noise. Additionally, theoretical performance limits and asymptotic complexity are assessed. This work experimentally evaluates the proposed algorithms for solving SLAT real-world problems in 3D indoor environments using a Cricket-based positioning system [52] in Section 3.7.

3.3 Problem Formulation

The network comprises sensors at unknown positions $\{\mathbf{x}_1, \mathbf{x}_2, \dots, \mathbf{x}_h\} \in \mathbb{R}^n$, a set of reference sensors (anchors) at known positions $\{\mathbf{a}_1, \mathbf{a}_2, \dots, \mathbf{a}_m\} \in \mathbb{R}^n$, and unknown target positions $\mathcal{S} = \{\mathbf{e}_1, \mathbf{e}_2, \dots, \mathbf{e}_l\} \in \mathbb{R}^n$, where n is the ambient space dimension ($n = 2$ or 3 for 2D or 3D scenarios, respectively). A central processing node has access to range measurements between target positions and sensors/anchors, namely,

$$d_{ij} = \|\mathbf{x}_i - \mathbf{e}_j\| + w_{ij} \quad i \in \mathcal{C}_j, \quad d_{ij} = \|\mathbf{a}_i - \mathbf{e}_j\| + w_{ij} \quad i \in \mathcal{B}_j, \quad \text{and} \quad j \in \mathcal{S},$$

where w_{ij} denotes noise terms and the sets B and C are defined as

$$\mathcal{B}_j = \{ i \mid \text{anchor } i \text{ can communicate with target } j \}, \quad (3.1)$$

$$\mathcal{C}_j = \{ i \mid \text{sensor } i \text{ can communicate with target } j \}. \quad (3.2)$$

A practical system that provides such range measurements is used, e.g., in [11].

SLAT Under Gaussian Noise: If disturbances are Gaussian, i.i.d., then maximizing the likelihood for the full batch of observations is equivalent to minimizing the cost function

$$\Omega_G(\mathbf{x}) = \sum_{j \in \mathcal{S}} \sum_{i \in \mathcal{C}_j} (\|\mathbf{x}_i - \mathbf{e}_j\| - d_{ij})^2 + \sum_{j \in \mathcal{S}} \sum_{i \in \mathcal{B}_j} (\|\mathbf{a}_i - \mathbf{e}_j\| - d_{ij})^2. \quad (3.3)$$

The set of unknown sensor and target positions is concatenated into column vector $\mathbf{x} \in \mathbb{R}^{n(h+l)}$, the argument of Ω_G . The goal of the proposed SLAT approach is to find the set of coordinates in \mathbf{x} which minimize (3.3).

SLAT Under Laplacian Noise: When the disturbances are Laplacian and i.i.d., thus heavier tailed than Gaussian, maximizing the likelihood amounts to minimizing the cost function

$$\Omega_L(\mathbf{x}) = \sum_{j \in \mathcal{S}} \sum_{i \in \mathcal{C}_j} \|\|\mathbf{x}_i - \mathbf{e}_j\| - d_{ij}\| + \sum_{j \in \mathcal{S}} \sum_{i \in \mathcal{B}_j} \|\|\mathbf{a}_i - \mathbf{e}_j\| - d_{ij}\|. \quad (3.4)$$

When compared with (3.3), the absence of squares in the summation terms of (3.4) renders the function less sensitive to outlier measurements d_{ij} with large deviations from the true ranges.

Since the Euclidean distance metric in both problem setups is invariant to global rotation, translation, and reflection, so are the functions Ω_G and Ω_L in the absence of anchors. To remove most of those ambiguities¹ in the solutions, a minimum of $m = 3$ or 4

¹Some geometrical configurations for sensor and target positions have intrinsic rotation/reflection ambiguities for range-based localization that cannot be resolved by anchors.

non collinear anchors must be considered. As in many other ML problems, the functions Ω_G and Ω_L are in general nonconvex and multimodal, hence their (approximate) minimization proceeds in two steps: initialization and refinement. The former provides suitable initial points, through EDM completion (startup) or source localization (updating), for target/sensor positions which tend to avoid convergence towards undesirable local minimizers of the ensuing iterative refinement algorithms based on MM or weighted-MM. Sections 3.4 and 3.5 develop algorithms for the operations listed in Algorithm 5 under Gaussian and Laplacian noise, respectively. Figure 3.1 shows the flow of the algorithms.

Algorithm 5 Summary of the proposed SLAT algorithm

Goal: Given incomplete and inaccurate range measurements, find sensor and target positions which (locally) maximize the likelihood function (3.3) for Gaussian noise or (3.4) for Laplacian noise

Startup phase (Batch algorithms)

Collect a block of range measurements for target sightings at times $t = 1, \dots, T$

Initialization step: Solve EDM completion problem using (3.10) or (3.20)

Factorize EDM matrix to get spatial coordinates

Refinement step: Improve the likelihood of sensor/target positions by iterative MM using (3.15) or (3.25)

Updating phase (Time-recursive algorithms)

Collect range measurements for a new target sighting at time $t > T$

Initialization step: Solve source localization problem for new target position using SLCP/SLNN in Sections 2.4.1/2.5.1 or $SL\ell_1$ SD/MD in Sections 2.4.2/2.5.2

Refinement step: Repeat likelihood refinement as in startup

3.4 SLAT under Gaussian Noise

This section develops algorithms for EDM initialization, MM refinement, and time-recursive estimation in SLAT under the assumption that measurement noise is i.i.d. and Gaussian. First, a basic formulation of EDM completion with squared distances is provided to form the basis for the initialization methods described in Sections 3.4.2 and 3.5.1.

3.4.1 EDM with Squared Distances

The basic EDM completion problem, described below, operates on squared ranges [23, 91]. Even though it is not matched to the likelihood function (3.3), it is useful for

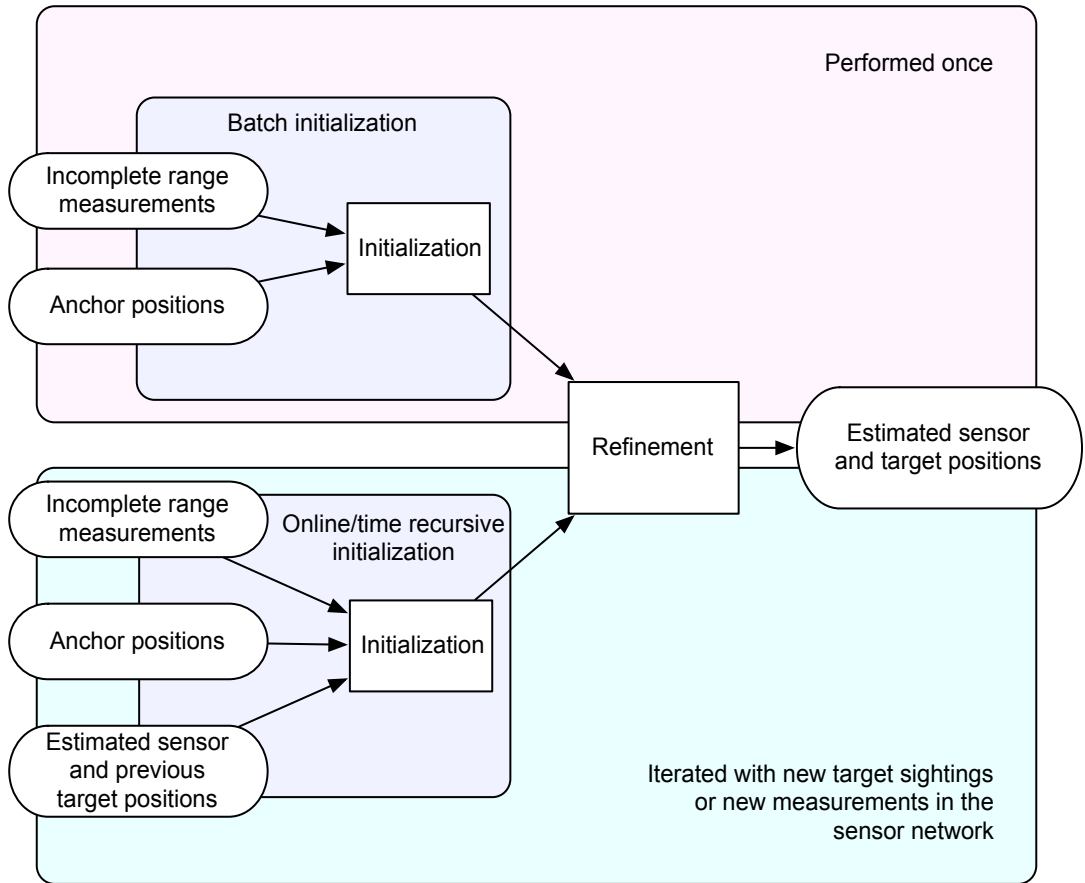


FIGURE 3.1: Architecture of the SLAT algorithms.

benchmarking in Section 3.6, as its performance is representative of other popular SNL methods [35, 65] and the SLAT approach of [37].

A partial pre-distance matrix \mathbf{D} is a matrix with zero diagonal entries and with certain nonnegative elements equal to the squares of observed distances, $D_{ij} = d_{ij}^2$. The remaining elements are considered free. The nearest EDM problem is to find an EDM \mathbf{E} that is nearest in the least-squares sense to matrix \mathbf{D} , when the free variables are not considered and the elements of \mathbf{E} satisfy $E_{ij} = \|\mathbf{y}_i - \mathbf{y}_j\|^2$ for a set of points \mathbf{y}_i . The geometry and properties of EDM (a convex cone) have been extensively studied in the literature [23, 91]. The nearest EDM problem is formulated as

$$\begin{aligned}
 & \underset{\mathbf{E}}{\text{minimize}} && \sum_{j \in \mathcal{S}} \sum_{i \in \mathcal{B}_j \cup \mathcal{C}_j} (E_{ij} - d_{ij}^2)^2 \\
 & \text{subject to} && \mathbf{E} \in \mathcal{E}, \mathbf{E}(\mathcal{A}) = \mathbf{A} \\
 & && \text{rank}(\mathbf{J}\mathbf{E}\mathbf{J}) = n,
 \end{aligned} \tag{3.5}$$

where $\mathbf{J} = (\mathbf{I}_\rho - \frac{1}{\rho} \mathbf{1}_\rho \mathbf{1}_\rho^T)$, $\rho = h + m + l$, is a centering operator which subtracts the mean of a vector from each of its components. The constraint $\mathbf{E}(\mathcal{A}) = \mathbf{A}$, where \mathcal{A} is the index set of anchor/anchor distances and $\mathbf{A}_{ij} = \|\mathbf{a}_i - \mathbf{a}_j\|^2$ is the corresponding EDM submatrix, enforces the known *a priori* spatial information. Matrix \mathbf{E} belongs to the EDM cone \mathcal{E} if it satisfies the properties

$$E_{ii} = 0, \quad E_{ij} \geq 0, \quad -\mathbf{J}\mathbf{E}\mathbf{J} \succeq 0. \quad (3.6)$$

The rank constraint in (3.5) ensures that the solution is compatible with a constellation of sensor/anchor/target points in \mathbb{R}^n . Extraction of the set \mathbf{y}_i from \mathbf{E} is described below. Problem (3.5) is also known as the penalty function approximation [23] due to the form of the cost function $\varphi_1(\mathbf{E}) = \sum_{i,j} (E_{ij} - d_{ij}^2)^2$. By expressing (3.5) in terms of full matrices and dropping the rank constraint, a compact relaxed SDP formulation is obtained as

$$\begin{aligned} & \underset{\mathbf{E}}{\text{minimize}} && \|\mathbf{W} \odot (\mathbf{E} - \mathbf{D})\|_F^2 \\ & \text{subject to} && \mathbf{E} \in \mathcal{E}, \mathbf{E}(\mathcal{A}) = \mathbf{A}, \end{aligned} \quad (3.7)$$

where \mathbf{W} is a mask matrix with zeros in the entries corresponding to free elements of $D_{ij} = d_{ij}^2$ and ones elsewhere. When combined with the Hadamard product \odot , the Frobenius norm $\|\cdot\|_F$ replaces the summation in (3.5) over the observed index sets $j \in \mathcal{S}$, $i \in \mathcal{B}_j \cup \mathcal{C}_j$. From here on, this method will be called EDM with squared ranges (EDM-SR).

3.4.2 Startup Initialization: EDM with Plain Distances

Instead of trying to match squared distances, EDM completion can be applied to plain distances as

$$\begin{aligned} & \underset{\mathbf{E}}{\text{minimize}} && \sum_{j \in \mathcal{S}} \sum_{i \in \mathcal{B}_j \cup \mathcal{C}_j} (\sqrt{E_{ij}} - d_{ij})^2 \\ & \text{subject to} && \mathbf{E} \in \mathcal{E}, \mathbf{E}(\mathcal{A}) = \mathbf{A} \\ & && \text{rank}(\mathbf{J}\mathbf{E}\mathbf{J}) = n. \end{aligned} \quad (3.8)$$

For this method the penalty function is $\varphi_2(\mathbf{E}) = \sum_{i,j} (\sqrt{E_{ij}} - d_{ij})^2$, which more closely resembles the terms in the likelihood function (3.3), and (3.8) is thus expected to inherit some of the robustness properties of ML estimation. Expanding the objective function

in (3.8) results in

$$\begin{aligned}
 & \underset{\mathbf{E}}{\text{minimize}} && \sum_{j \in \mathcal{S}} \sum_{i \in \mathcal{B}_j \cup \mathcal{C}_j} (E_{ij} - 2\sqrt{E_{ij}}d_{ij} + d_{ij}^2) \\
 & \text{subject to} && \mathbf{E} \in \mathcal{E}, \mathbf{E}(\mathcal{A}) = \mathbf{A} \\
 & && \text{rank}(\mathbf{J}\mathbf{E}\mathbf{J}) = n.
 \end{aligned} \tag{3.9}$$

A relaxed SDP is obtained by introducing an epigraph-like variable \mathbf{T} and dropping the rank constraint

$$\begin{aligned}
 & \underset{\mathbf{E}, \mathbf{T}}{\text{minimize}} && \sum_{j \in \mathcal{S}} \sum_{i \in \mathcal{B}_j \cup \mathcal{C}_j} (E_{ij} - 2T_{ij}d_{ij}) \\
 & \text{subject to} && T_{ij}^2 \leq E_{ij} \\
 & && \mathbf{E} \in \mathcal{E}, \mathbf{E}(\mathcal{A}) = \mathbf{A}.
 \end{aligned} \tag{3.10}$$

From here on, this method will be called EDM with plain ranges (EDM-R).

3.4.2.1 Estimation of Sensor and Target Positions from EDM

Note that the solutions of the initialization techniques described here and in Sections 3.4.1 and 3.5.1 are distance matrices. To estimate the spatial coordinates of the sensors and target positions from EDM, define a matrix \mathbf{Y} whose columns hold all sensor, anchor and target coordinates, globally translated so that their average is located at the origin. Then the Gram matrix $\mathbf{Y}^T\mathbf{Y}$ is obtained from the EDM matrix \mathbf{E} by a linear transformation [23], Sec. 8.3, from which spatial coordinates \mathbf{Y} are extracted by SVD up to a unitary matrix. In most cases the SVD will return a coordinate matrix whose rank is greater than the embedding dimension (2 or 3 in this work) so valid coordinates are obtained by truncating the SVD to the appropriate rank. The anchors are then used to estimate the residual unitary matrix \mathbf{Q} after SVD by solving the Procrustes problem, [63]

$$\begin{aligned}
 & \underset{\mathbf{Q}}{\text{minimize}} && \|\mathbf{A} - \mathbf{Q}\mathbf{Y}_{\mathbf{A}}\|_F^2 \\
 & \text{subject to} && \mathbf{Q}^T\mathbf{Q} = \mathbf{I},
 \end{aligned} \tag{3.11}$$

where the columns of \mathbf{A} hold the anchor positions, and $\mathbf{Y}_{\mathbf{A}}$ denotes the relevant subset of the columns of the truncated SVD output \mathbf{Y} (the anchor set and the subconstellation are also centered to the origin as explained above.). This problem has a closed-form solution.

Observation noise can significantly disrupt the estimated sensor/target coordinates through EDM completion and rank truncation, and it was found that much more accurate results

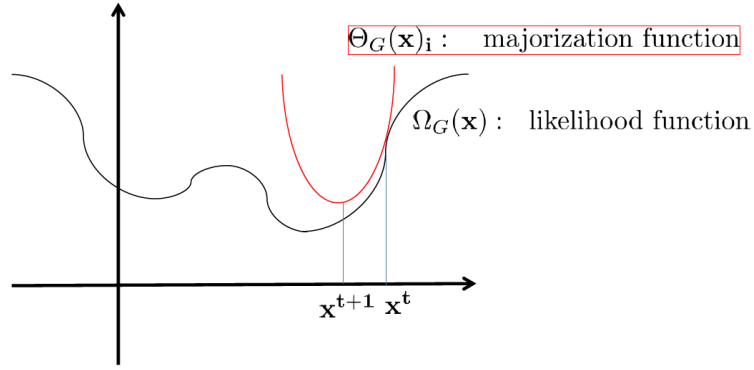


FIGURE 3.2: Majorization Minimization Technique.

are obtained by using those as a starting point for likelihood maximization. Next, MM algorithms are proposed for iterative likelihood maximization.

3.4.3 Refinement Steps: Majorization-Minimization

The key idea of MM is to find, at a certain point \mathbf{x}^t , a simpler function that has the same function value at \mathbf{x}^t and anywhere else is larger than or equal to the objective function to be minimized. Such a function is called a majorization function. By minimizing the majorization function the next point of the algorithm is obtained, while decreasing the cost function [89] as shown in Figure 3.2.

Define two convex functions as

$$f_{ij}(\mathbf{x}) = \|\mathbf{x}_i - \mathbf{e}_j\|, \quad g_{ij}(\mathbf{x}) = \|\mathbf{a}_i - \mathbf{e}_j\|. \quad (3.12)$$

and assume that sensors and targets are not at the same positions, i.e., $\mathbf{x}_i \neq \mathbf{e}_j$ and $\mathbf{a}_i \neq \mathbf{e}_j$.

Expanding f and g in (3.3) and using first-order conditions on convexity [23],

$$\begin{aligned} \Omega_G(\mathbf{x}) \leq & \sum_{j \in \mathcal{S}} \sum_{i \in \mathcal{C}_j} (f_{ij}^2(\mathbf{x}) - 2d_{ij}(f_{ij}(\mathbf{x}^t) + \langle \nabla f_{ij}(\mathbf{x}^t), (\mathbf{x} - \mathbf{x}^t) \rangle) + d_{ij}^2) \\ & + \sum_{j \in \mathcal{S}} \sum_{i \in \mathcal{B}_j} (g_{ij}^2(\mathbf{x}) - 2d_{ij}(g_{ij}(\mathbf{x}^t) + \langle \nabla g_{ij}(\mathbf{x}^t), (\mathbf{x} - \mathbf{x}^t) \rangle) + d_{ij}^2), \end{aligned} \quad (3.13)$$

where $\langle u, v \rangle = u^T v$, the proposed majorization function is on the right side of (3.13), which is quadratic in \mathbf{x} and easily minimized. The MM iteration

$$\mathbf{x}^{t+1} = \arg \min_{\mathbf{x}} \sum_{j \in \mathcal{S}} \sum_{i \in \mathcal{C}_j} (f_{ij}^2(\mathbf{x}) - 2d_{ij} \langle \nabla f_{ij}(\mathbf{x}^t), \mathbf{x} \rangle) + \sum_{j \in \mathcal{S}} \sum_{i \in \mathcal{B}_j} (g_{ij}^2(\mathbf{x}) - 2d_{ij} \langle \nabla g_{ij}(\mathbf{x}^t), \mathbf{x} \rangle) \quad (3.14)$$

turns out to be obtained as the solution of the following linear system of equations

$$\left[\sum_{j \in \mathcal{S}} \sum_{i \in \mathcal{C}_j} \mathbf{M}_{ij}^T \mathbf{M}_{ij} + \sum_{j \in \mathcal{S}} \sum_{i \in \mathcal{B}_j} \mathbf{N}_j^T \mathbf{N}_j \right] \mathbf{x}^{t+1} = \sum_{j \in \mathcal{S}} \sum_{i \in \mathcal{C}_j} d_{ij} \nabla f_{ij}(\mathbf{x}^t) + \sum_{j \in \mathcal{S}} \sum_{i \in \mathcal{B}_j} d_{ij} \nabla g_{ij}(\mathbf{x}^t) - \sum_{j \in \mathcal{S}} \sum_{i \in \mathcal{B}_j} \mathbf{N}_j \mathbf{a}_i^T, \quad (3.15)$$

where the selection matrices \mathbf{M}_{ij} and \mathbf{N}_j are defined in Appendix G and

$$\nabla f_{ij}(\mathbf{x}^t) = \frac{\mathbf{M}_{ij}^T \mathbf{M}_{ij} \mathbf{x}^t}{\|\mathbf{M}_{ij} \mathbf{x}^t\|}, \quad \nabla g_{ij}(\mathbf{x}^t) = \frac{\mathbf{N}_j^T (\mathbf{a}_i + \mathbf{N}_j \mathbf{x}^t)}{\|\mathbf{a}_i + \mathbf{N}_j \mathbf{x}^t\|}.$$

3.4.4 Updating Initialization: Recursive Position Estimation using SLCP / SLNN

Suppose that a batch of observations have been processed and a new target position is to be estimated. One idea is to repeat MM refinement with EDM-R initialization acting on an expanded batch that concatenates all previous range measurements and those for the new target sighting. However, this would be computationally expensive due to the EDM completion step. Also, previously estimated positions would be ignored and could not contribute to computational complexity reduction. To alleviate the load a simple methodology is proposed to obtain a good initial point for MM which avoids the EDM step. This consists of fixing the previous positions at their estimated values and only estimating the new target position. More precisely, the following cost function is minimized

$$\Psi_G(\mathbf{y}) = \sum_{i=1}^{m+h} (\|\mathbf{b}_i - \mathbf{y}\| - d_i)^2, \quad (3.16)$$

where \mathbf{y} is the new target position, \mathbf{b}_i denotes the previously estimated position of a sensor or anchor, and d_i is the corresponding range measurement. SLCP or SLNN proposed in Section 2.4.1 or Section 2.5.1 can be used to minimize (3.16).

After an optimal target position is obtained through SLCP/SLNN, the cost function (3.3) is resorted to iteratively refine all estimates using (3.15). In SNL this incremental procedure could also be applied as new sensors become available.

In a previous paper [37], the source localization method derived in [46], termed SR-LS, was proposed for initialization during the updating phase. Note that in [46] squared distances are matched, leading to a Trust Region optimization problem. However, as demonstrated in [45] and in Chapter 2, SLCP is a more accurate source localization method and its cost function (3.16) is better matched to the likelihood function (3.3).

This makes it more convenient for initialization of iterative refinement algorithms, which will then require fewer iterations to converge and/or will be less likely to get trapped in undesirable local extrema.

3.5 SLAT under Laplacian Noise

3.5.1 Startup Initialization: EDM with Ranges and ℓ_1 -norm

Among the penalty function approximation methods, the ℓ_1 -norm approximation is known to be robust to outliers [23]. Therefore, the penalty function of the third SLAT startup initialization method is chosen as $\varphi_3(\mathbf{E}) = \sum_{i,j} |\sqrt{E_{ij}} - d_{ij}|$, and the associated optimization problem becomes

$$\begin{aligned} & \underset{\mathbf{E}}{\text{minimize}} && \sum_{j \in \mathcal{S}} \sum_{i \in \mathcal{B}_j \cup \mathcal{C}_j} |\sqrt{E_{ij}} - d_{ij}| \\ & \text{subject to} && \mathbf{E} \in \mathcal{E}, \mathbf{E}(\mathcal{A}) = \mathbf{A}, \\ & && \text{rank}(\mathbf{J}\mathbf{E}\mathbf{J}) = n. \end{aligned} \tag{3.17}$$

The terms $|\sqrt{E_{ij}} - d_{ij}|$ in the objective function for this problem are convex when $\sqrt{E_{ij}} - d_{ij} < 0$, but concave for $\sqrt{E_{ij}} - d_{ij} > 0$. To obtain a convex approximation each of those terms is replaced by a linear approximation

$$c_{ij}E_{ij} + s_{ij}, \quad c_{ij} = \frac{1}{\sqrt{E_{\max}} + d_{ij}}, \quad s_{ij} = -\frac{d_{ij}^2}{\sqrt{E_{\max}} + d_{ij}} \tag{3.18}$$

in part of the domain where it is concave, as shown in Figure 3.3. The two functions coincide for $E_{ij} = d_{ij}^2$ and $E_{ij} = E_{\max}$, where the constant E_{\max} is a practical upper bound on (squared) range measurements. Thus $|\sqrt{E_{ij}} - d_{ij}|$ is replaced by its convex envelope $\max\{d_{ij} - \sqrt{E_{ij}}, c_{ij}E_{ij} + s_{ij}\}$ and the epigraph variable \mathbf{T} is used to obtain

$$\begin{aligned} & \underset{\mathbf{E}, \mathbf{T}}{\text{minimize}} && \sum_{j \in \mathcal{S}} \sum_{i \in \mathcal{B}_j \cup \mathcal{C}_j} T_{ij} \\ & \text{subject to} && \max\{d_{ij} - \sqrt{E_{ij}}, c_{ij}E_{ij} + s_{ij}\} \leq T_{ij} \\ & && \mathbf{E} \in \mathcal{E}, \mathbf{E}(\mathcal{A}) = \mathbf{A} \\ & && \text{rank}(\mathbf{J}\mathbf{E}\mathbf{J}) = n. \end{aligned} \tag{3.19}$$

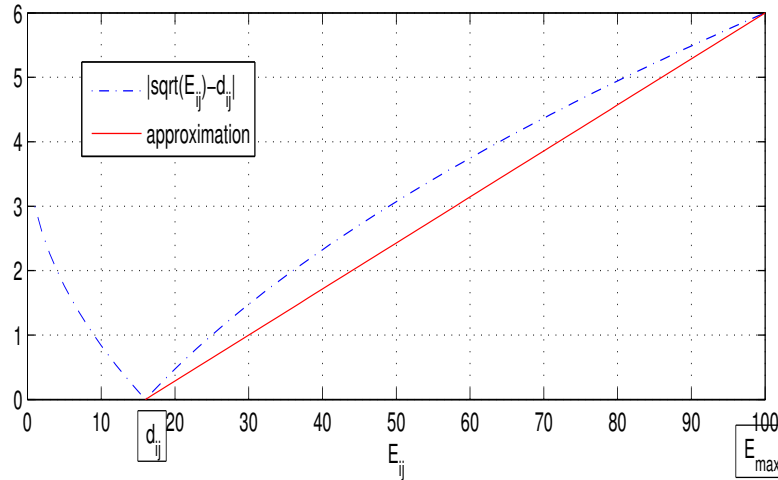


FIGURE 3.3: The value of $|\sqrt{E_{ij}} - d_{ij}|$ vs E_{ij} , and the linear approximation of the concave part.

A relaxation of (3.19) after dropping the rank constraint is

$$\begin{aligned}
 & \underset{\mathbf{E}, \mathbf{T}}{\text{minimize}} && \sum_{j \in \mathcal{S}} \sum_{i \in \mathcal{B}_j \cup \mathcal{C}_j} T_{ij} \\
 & \text{subject to} && (d_{ij} - T_{ij})^2 \leq E_{ij}, \quad c_{ij} E_{ij} + s_{ij} \leq T_{ij} \\
 & && \mathbf{E} \in \mathcal{E}, \quad \mathbf{E}(\mathcal{A}) = \mathbf{A}.
 \end{aligned} \tag{3.20}$$

Note that the first constraint in (3.20) is not equivalent to $d_{ij} - \sqrt{E_{ij}} \leq T_{ij}$, but rather to $-\sqrt{E_{ij}} \leq d_{ij} - T_{ij} \leq \sqrt{E_{ij}}$, which amounts to intersecting the original epigraph with the parabolic hypograph $d_{ij} + \sqrt{E_{ij}} \geq T_{ij}$. This preserves the convexity of the feasible set and does not change its lower boundary for $E_{ij} \in [0, E_{\max}]$, where the optimal point will be found. The constraint can now be readily expressed in standard form without introducing additional variables, e.g., as an LMI or a second-order cone constraint [92]

$$\begin{bmatrix} 1 & d_{ij} - T_{ij} \\ d_{ij} - T_{ij} & E_{ij} \end{bmatrix} \succeq 0 \quad \text{or} \quad \left\| \begin{bmatrix} 2(d_{ij} - T_{ij}) \\ E_{ij} - 1 \end{bmatrix} \right\| \leq E_{ij} + 1. \tag{3.21}$$

This technique will be called EDM with ranges and ℓ_1 -norm (EDM-R- ℓ_1).

3.5.2 Refinement Steps: Weighted Majorization Minimization

Robustness to outliers in the cost function (3.4) for Laplacian noise is gained at the expense of differentiability. To circumvent this shortcoming the well-known re-weighted least squares approach will be resorted [93], which replaces the minimization of (3.4) with a sequence of minimizations of smooth approximation functions that converge to

$\Omega_L(\mathbf{x})$. Specifically, (3.4) is first written as

$$\Omega_L(\mathbf{x}) = \sum_{j \in \mathcal{S}} \sum_{i \in \mathcal{C}_j} u_{ij} (\|\mathbf{x}_i - \mathbf{e}_j\| - d_{ij})^2 + \sum_{j \in \mathcal{S}} \sum_{i \in \mathcal{B}_j} v_{ij} (\|\mathbf{a}_i - \mathbf{e}_j\| - d_{ij})^2, \quad (3.22)$$

with

$$u_{ij} = \frac{1}{|\|\mathbf{x}_i - \mathbf{e}_j\| - d_{ij}|}, \quad v_{ij} = \frac{1}{|\|\mathbf{a}_i - \mathbf{e}_j\| - d_{ij}|}.$$

At time t the minimization function becomes $\Omega_L^t(\mathbf{x})$, which has the same form of (3.22) but the *functions* u_{ij} , v_{ij} above are now replaced by *constants* based on the estimated positions after the previous iteration

$$u_{ij}^t = \frac{1}{|\|\mathbf{x}_i^t - \mathbf{e}_j^t\| - d_{ij}|}, \quad v_{ij}^t = \frac{1}{|\|\mathbf{a}_i - \mathbf{e}_j^t\| - d_{ij}|}. \quad (3.23)$$

An inner optimization loop could now be used to minimize $\Omega_L^t(\mathbf{x})$ for every t but, as shown in Appendix F, a single iteration suffices to ensure convergence. With fixed u_{ij}^t , v_{ij}^t the same majorization technique of Section 3.4.3 yields the weighted-MM iteration

$$\mathbf{x}^{t+1} = \arg \min_{\mathbf{x}} \sum_{j \in \mathcal{S}} \sum_{i \in \mathcal{C}_j} u_{ij}^t (f_{ij}^2(\mathbf{x}) - 2d_{ij} \langle \nabla f_{ij}(\mathbf{x}^t), \mathbf{x} \rangle) + \sum_{j \in \mathcal{S}} \sum_{i \in \mathcal{B}_j} v_{ij}^t (g_{ij}^2(\mathbf{x}) - 2d_{ij} \langle \nabla g_{ij}(\mathbf{x}^t), \mathbf{x} \rangle). \quad (3.24)$$

Thus, the new point is obtained by solving the linear system

$$\left[\sum_{j \in \mathcal{S}} \sum_{i \in \mathcal{C}_j} u_{ij}^t \mathbf{M}_{ij}^T \mathbf{M}_{ij} + \sum_{j \in \mathcal{S}} \sum_{i \in \mathcal{B}_j} v_{ij}^t \mathbf{N}_j^T \mathbf{N}_j \right] \mathbf{x}^{t+1} = \sum_{j \in \mathcal{S}} \sum_{i \in \mathcal{C}_j} u_{ij}^t d_{ij} \nabla f_{ij}(\mathbf{x}^t) + \sum_{j \in \mathcal{S}} \sum_{i \in \mathcal{B}_j} v_{ij}^t d_{ij} \nabla g_{ij}(\mathbf{x}^t) - \sum_{j \in \mathcal{S}} \sum_{i \in \mathcal{B}_j} v_{ij}^t \mathbf{N}_j \mathbf{a}_i^T, \quad (3.25)$$

where $\nabla f_{ij}(\mathbf{x}^t)$, $\nabla g_{ij}(\mathbf{x}^t)$, \mathbf{M}_{ij} and \mathbf{N}_j are the same as in (3.15).

In practice the weights u_{ij}^t and v_{ij}^t must be modified to avoid the possibility of division by zero [94], which in this thesis is achieved by saturating them at 10^5 when computing (3.24). Hence, truncating the weights, which are the Huber thresholds, is equivalent to using the Huber function.

3.5.3 Updating Initialization: Recursive Position Estimation using SL- ℓ_1

The ML source localization problem under Laplacian noise is equivalent to

$$\underset{\mathbf{y}}{\text{minimize}} \quad \Psi_L(\mathbf{y}) = \sum_{i=1}^{h+m} \left| \|\mathbf{y} - \mathbf{b}_i\| - d_i \right| \quad (3.26)$$

where \mathbf{y} , \mathbf{b}_i and d_i are defined in Section 3.4.4. The ideas of Sections 2.4.2 and 2.5.2 are followed to express the minimization of Ψ_L^2 as a weighted sum of squares.

As in Section 3.4.4, after an optimal target position is obtained, the cost function (3.4) is resorted to iteratively refine all the estimates using (3.25). Section 3.6 and Section 2.8 demonstrate in simulations that SL- ℓ_1 and its 3D extensions are more robust to outliers than the SLCP/SLNN algorithms of Section 2.4.1 and Section 2.5.1, as the cost function (3.26) is better matched to the likelihood function (3.4).

3.6 Numerical Results

Example 1 [Comparison of Initialization Methods for the Startup Phase (EDM Completion)] To investigate the accuracy of the methods, a physical scenario that contains four anchors, five unknown sensors, and six target positions in a $[0, 2] \text{ m} \times [0, 2] \text{ m}$ area is set. Range measurements are corrupted by additive spatio-temporally white noise with standard deviation $\sigma_{\text{gaussian}} \in [0.005, 0.03] \text{ m}$. This noisy observation model may lead to near-zero or negative range measurements, in which case normal practice [35] is followed and they are set to be equal to a small positive constant (10^{-5} in the simulations). With the chosen noise variances this occurs sufficiently seldom (up to 0.04% of measurements) for its impact on estimation accuracy to be unimportant. Several algorithms are tested (EDM-SR, EDM-R, EDM-R- ℓ_1 , MM initialized by EDM-SR (EDM-SR+MM), MM initialized by EDM-R (EDM-R+MM) and MM initialized by EDM-R- ℓ_1 (EDM-R- ℓ_1 +MM)), and their performances are compared according to the total RMSE

$$\sqrt{\frac{1}{K} \frac{1}{h+l} \sum_{k=1}^K \sum_{i=1}^{h+l} \|\mathbf{x}_i - \hat{\mathbf{x}}_i^k\|^2}, \quad (3.27)$$

where $\hat{\mathbf{x}}_i^k$ denotes the i -th estimated sensor or target position in the k -th Monte Carlo run for the specific noise realization. The RMSE defined in (3.27) and (2.66) are the same with only one difference that (3.27) is the mean of all target and sensor positions hence it is called total RMSE. In each of $K = 150$ Monte Carlo runs, a random network is generated according to the physical scenario described above. To assess the fundamental

hardness of position estimation, error plots for Gaussian noise also show the total CRLB, calculated as

$$\sqrt{\frac{1}{K} \frac{1}{h+l} \sum_{k=1}^K \text{trace}(\text{CRLB}_k)} \quad (3.28)$$

for each noise variance, where CRLB_k denotes the matrix lower bound at the k -th Monte Carlo run. The CRLB for anchored and anchor-free localization using ranging information has been studied in [16, 95, 96] for different variance models of range estimation noise. For convenience, the CRLB for the SLAT problem under Gaussian noise is rederived in Appendix G in terms of the notation adopted in this thesis. To fully justify benchmarking against the CRLB, the unbiasedness of the proposed estimators, a mathematically challenging endeavor, should be proved. In the experimental results, however, no clear evidence of bias for small noise levels is found, where convergence to undesirable extrema of the cost functions is avoided. Figure 3.4(a) shows that plain EDM-R has better accuracy than EDM-SR and EDM-R- l_1 , although the performance gap closes after iterative refinement by MM. Moreover, MM initialized by the various methods nearly touches the CRLB except when the noise variance is large.

To compare the total RMSE of the algorithms in the presence of outliers, modified range measurements are created according to a “selective Gaussian” model defined in (2.68). The disturbance ϵ_i with $\sigma_{\text{outlier}} \in [0.4, 2]$ m randomly affects only two range measurements, whereas w_i with $\sigma_{\text{gaussian}} = 0.01$ m is present in all observations. This outlier generating model deviates from the earlier Laplacian assumption, but it is arguably representative of observed range measurements in practical systems [74]. Numerical results under a pure Laplacian model will be presented in Examples 3 and 4. In the presence of high noise and/or outliers, Figure 3.4(b) shows that weighted-MM refinement does not close the performance gap between EDM-R- l_1 , EDM-R and EDM-SR initialization because in the latter cases the algorithms converge more often to local minima, thus producing a larger total RMSE.

Example 2 [Uncertainty Ellipsoids] To further examine the accuracy of MM and weighted-MM with different initialization methods in the startup phase, two networks of 10 sensors, 4 anchors and 11 target positions are randomly generated. 100 Monte Carlo runs were used to find the mean and (1σ) uncertainty ellipsoids of the positions estimated by the methods. The mean and uncertainty ellipsoids for $\sigma_{\text{gaussian}} = 0.025$ m and $\sigma_{\text{gaussian}} = 0.02$ m / $\sigma_{\text{outlier}} = 0.8$ m are shown in Figures 3.5 and 3.6, respectively. Again, outliers are randomly added to two range measurements in Figure 3.6.

Without outliers (Figure 3.5) using EDM-SR, EDM-R, or EDM-R- l_1 as an initialization to MM makes the uncertainty ellipsoids shrink dramatically after refinement, yielding

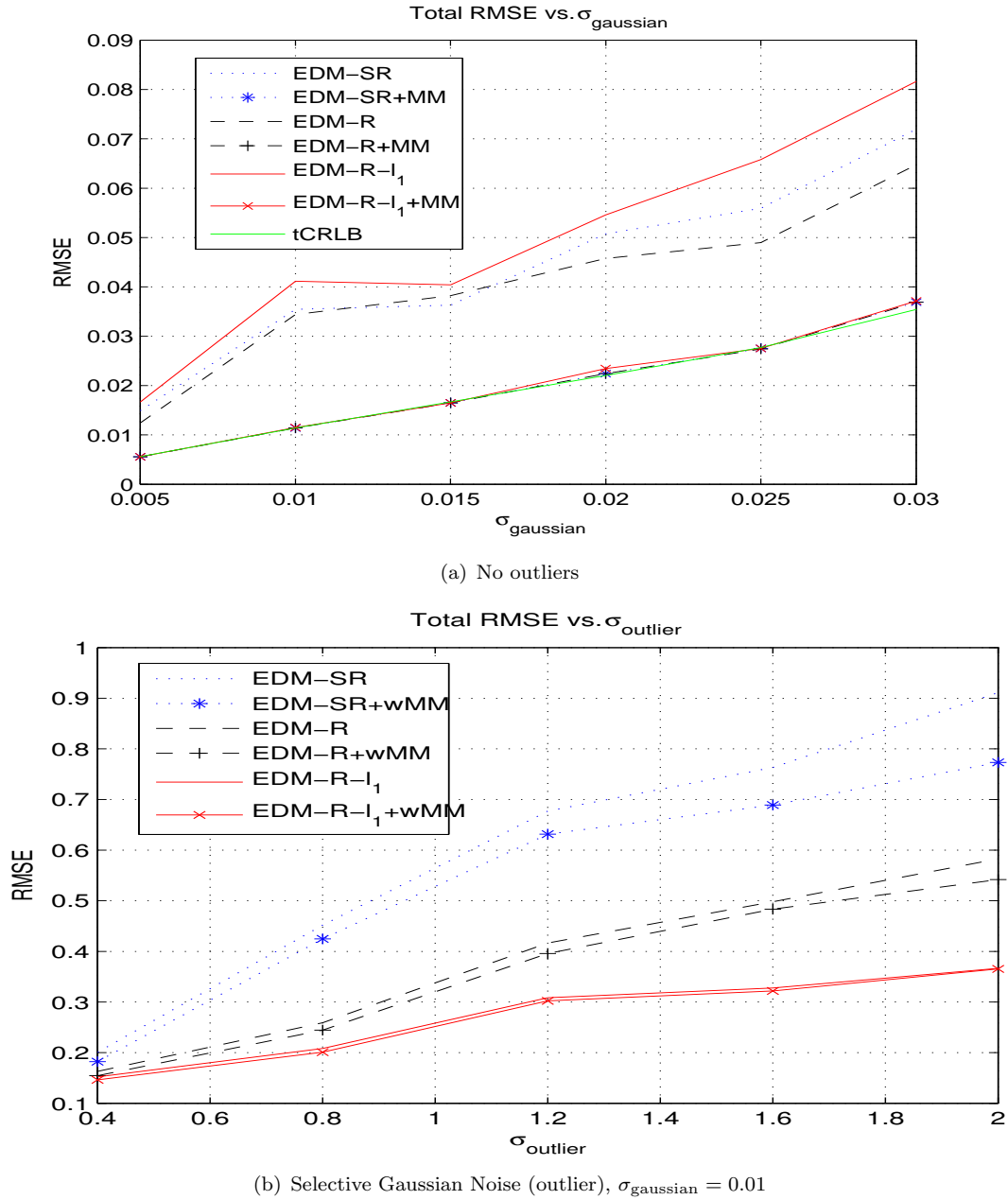
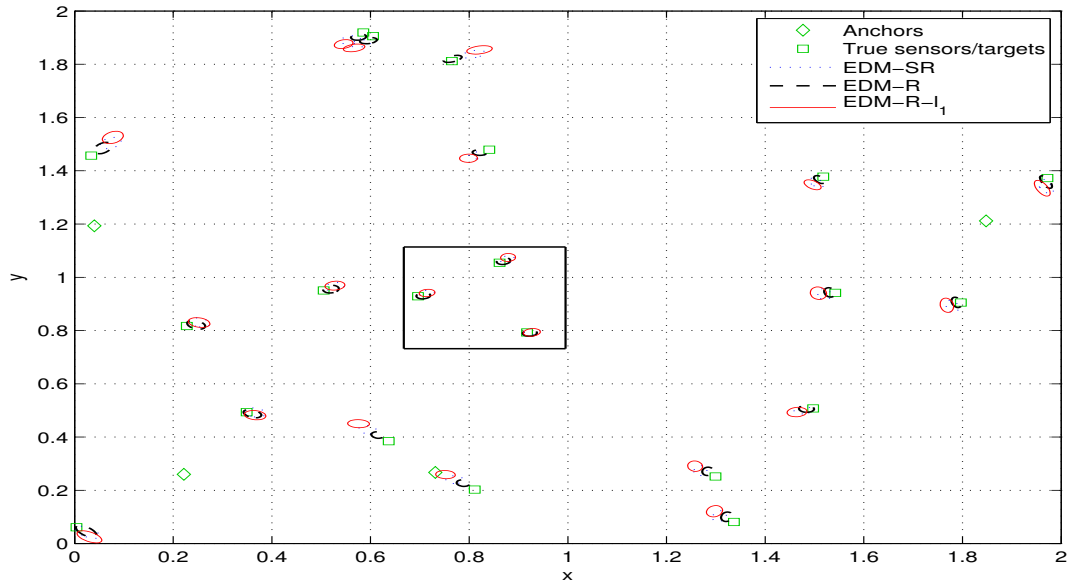
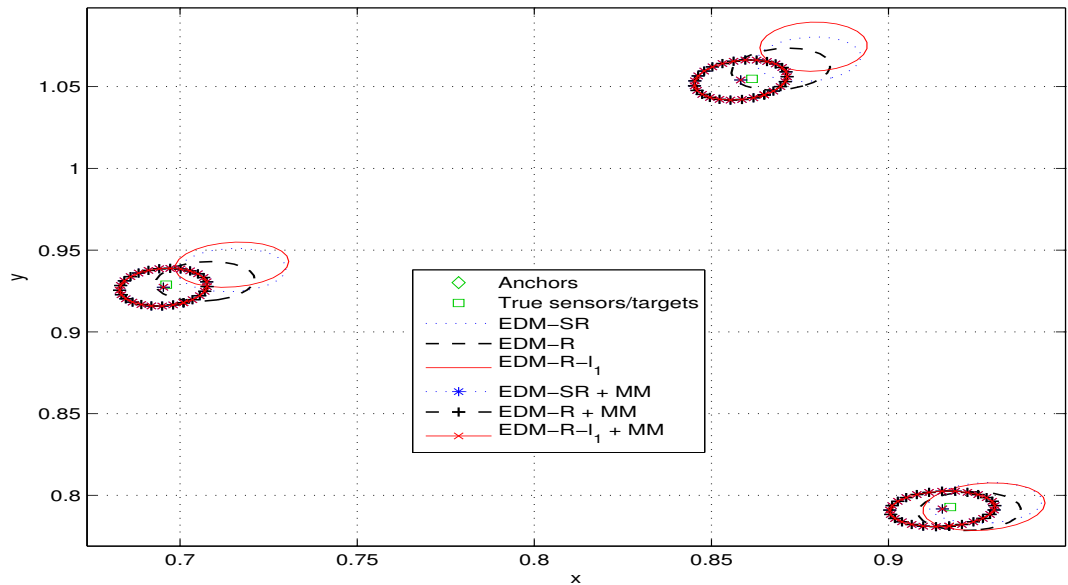


FIGURE 3.4: Comparison of initialization and refinement methods in the startup phase of SLAT.

very similar means and covariances. These are only displayed in the detail view of Figure 3.5(b), as they are too small to be shown in Figure 3.5(a). In the presence of outliers (Figure 3.6), the uncertainty ellipsoids of EDM-SR+wMM are bigger than for other methods and the means of the estimated positions are shifted. Since EDM-R- l_1 and EDM-R initializations converge to global extrema most of the time, the means of the positions estimated by weighted MM still approach the true positions and their uncertainty ellipsoids are much smaller than for EDM-SR+wMM. In the presence of outliers this example shows that EDM-R- l_1 +wMM is clearly superior to the other methods.



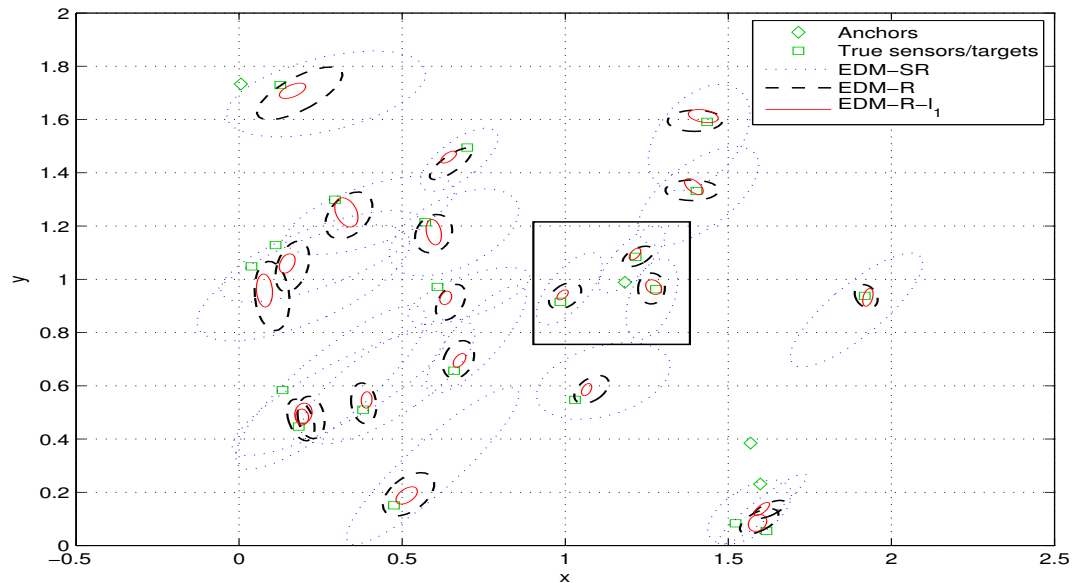
(a) Whole constellation



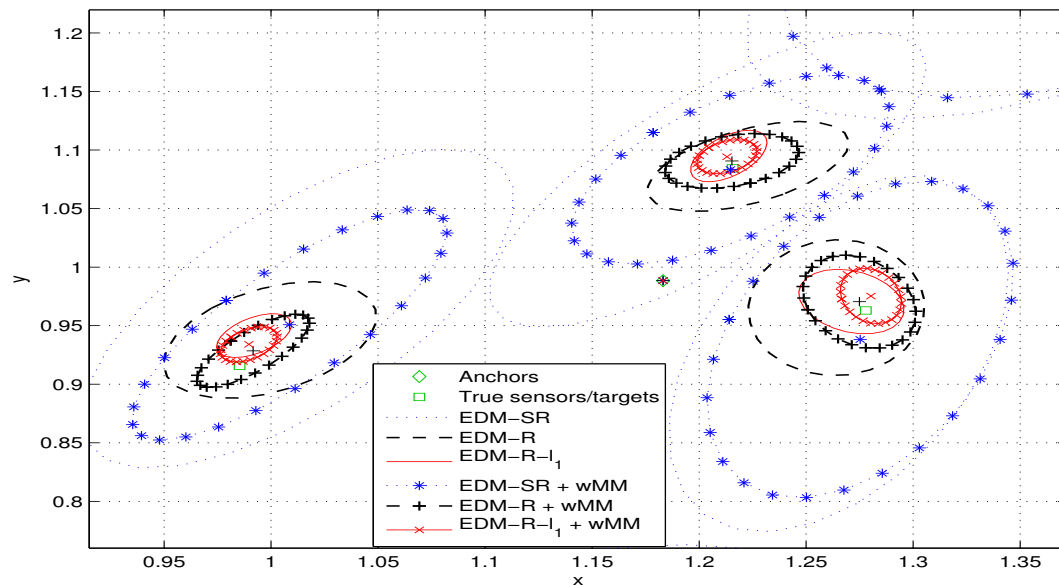
(b) Detail view

FIGURE 3.5: Mean and uncertainty ellipsoids in the startup phase with different initialization methods. No outliers, $\sigma_{\text{gaussian}} = 0.025$.

A Note on Practical Computational Complexity of EDM Initialization The experiments were conducted on a machine with an Intel Xeon 2.93 GHz Quad-Core CPU and 8 GB of RAM, using Matlab 7.1, CVX 1.2 and Yalmip 3/SeDuMi 1.1 as a general-purpose SDP solver. CPU times are similar for EDM-SR, EDM-R and EDM-R- ℓ_1 , under 5 seconds for the example described above with $h = 25$ unknown positions and empirically increasing with $h^{4.5}$ for larger values of n (< 100). This gives a notion of what network sizes are currently practical for the EDM initialization methods, while keeping in mind that CPU times are known to be unreliable surrogates for intrinsic



(a) Whole constellation



(b) Detail view (including an anchor at (1.18; 0.99))

FIGURE 3.6: Mean and uncertainty ellipsoids in the startup phase with different initialization methods. Selective Gaussian Noise (outlier), $\sigma_{\text{outlier}} = 0.8/\sigma_{\text{gaussian}} = 0.02$.

computational complexity due to dependencies on factors such as machine hardware architecture, operating system, efficiency of numerical libraries, and solver preprocessing. No attempt was taken to formulate the EDM completion problems in the most efficient way possible for the SDP solver. For MM-type iterative algorithms, extremely large problem sizes can be efficiently handled using contemporary numerical algorithms and computing platforms. In the experiments each iteration takes up to about 1 millisecond.

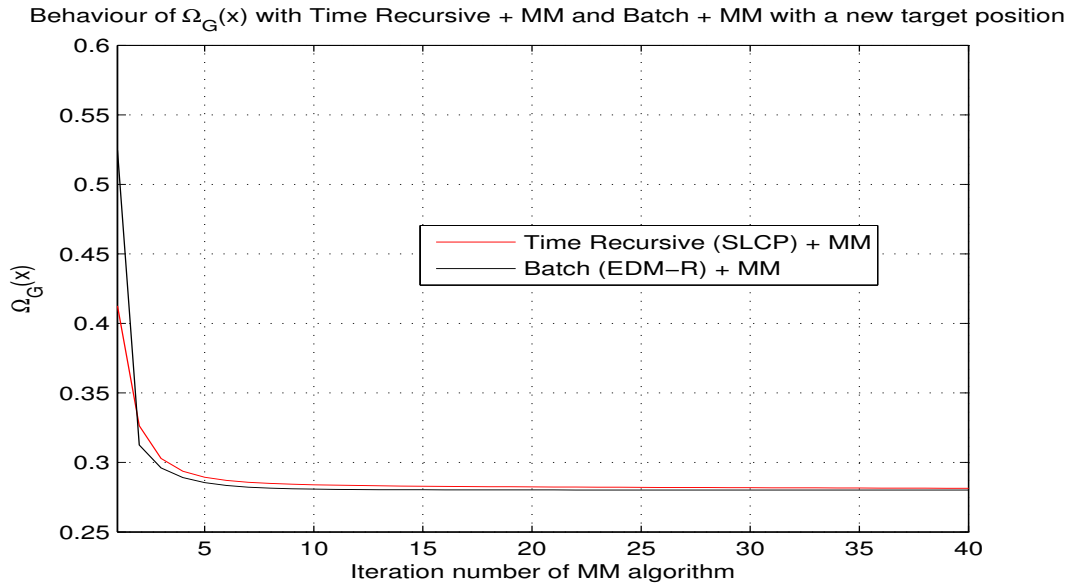


FIGURE 3.7: Evolution of Gaussian cost function $\Omega_G(\mathbf{x})$ during refinement for EDM-R+MM and SLCP+MM approaches, with $\sigma_{\text{gaussian}} = 0.04$.

Example 3 [Global Assessment of the Updating Phase (Time-Recursive Algorithms)] This example assesses the performance of the full time-recursive procedure (updating phase), comprising SLCP or $SL\ell_1$ initialization followed by refinement. The network scenario has 16 unknown sensors, 4 anchors and 10 target locations, all randomly positioned. A new target sighting (the 11th one) becomes available and is processed incrementally, i.e., the position is estimated through SLCP or $SL\ell_1$ by fixing all the remaining ones, then all estimates are jointly refined. Results are benchmarked against refinement with full batch initialization, which makes a fresh start to the process without using any previous knowledge at every new target position to be estimated, solving different and increasingly large EDM completion problems for ML initialization.

As explained in Section 3.4.4, this type of incremental approach was used in [37] with the SR-LS algorithm of [46] and MM refinement for Gaussian noise. However, SLCP is used here instead of SR-LS because, as shown in [45], it increases the convergence speed of subsequent iterative methods and also alleviates the problem of convergence to local extrema of the ML cost function by providing better initial points than SR-LS does. Figure 3.7 shows the evolution of the Gaussian cost function $\Omega_G(\mathbf{x})$ during refinement after ranges to the 11th target position are sensed ($\sigma_{\text{gaussian}} = 0.04$ m). The time-recursive (SLCP)+MM approach takes advantage of previously estimated positions to start with a lower cost than batch (EDM-R)+MM, but it reaches the same final error value.

The same network scenario is adopted in the presence of outliers. Figure 3.8 shows the evolution of cost function $\Omega_L(\mathbf{x})$ during refinement for Laplacian outliers ($\sigma_{\text{laplacian}} = 0.1$

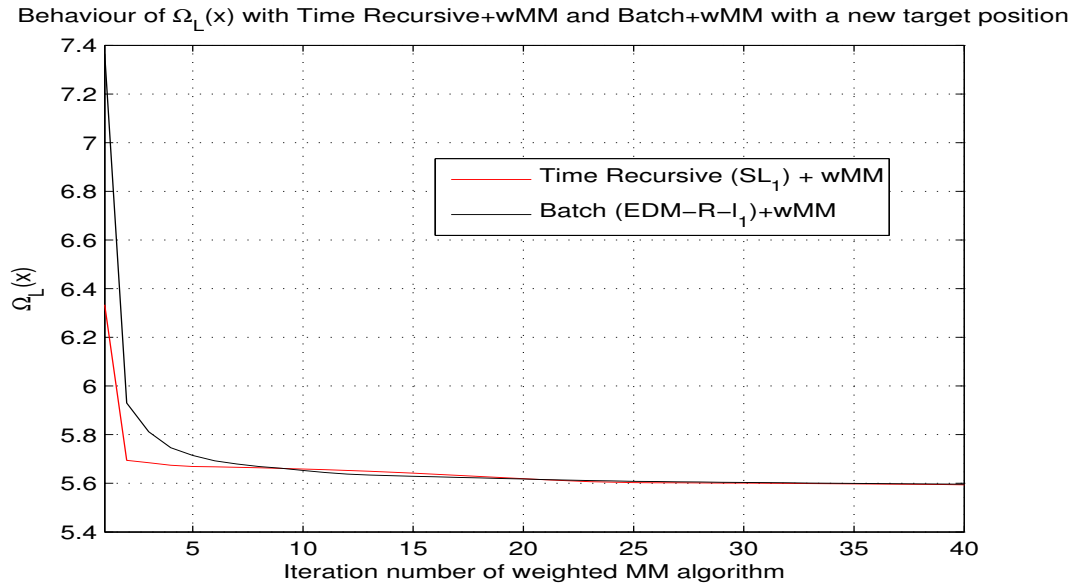


FIGURE 3.8: Evolution of Laplacian cost function $\Omega_L(\mathbf{x})$ during refinement for EDM-R- l_1 +wMM and SL l_1 +wMM approaches, with $\sigma_{\text{laplacian}} = 0.1$.

m), whose behavior is similar to the Gaussian case of Figure 3.7. In both Gaussian and Laplacian settings refinement yields similar accuracy and convergence speed after batch or time-recursive initializations. Therefore, time-recursive updating is seen to retain the essential features of the EDM-based approach to SLAT, namely, a very limited need for *a priori* spatial information and fast convergence, at a fraction of the computational cost.

3.7 Real Indoor Experiments

The present section illustrates the performance of proposed algorithms in a real world experimental setup explained in Section 2.9, where the statistics of perturbations are unknown and the true locations of sensors are only approximately known (to an accuracy on the order of 2 cm) [52]. In the following, results will be presented relative to tracking a Pioneer P3-DX robot and a human in a test environment shown in Figure 2.9. The same RMSE metric defined in (3.27) is used, without averaging over Monte Carlo runs.

Experiment 1: In the first experiment, 8 listeners are deployed around the lab and on the ceiling in a 4 m by 4 m area and a beacon is attached to a Pioneer P3-DX mobile robot programmed to follow a circular trajectory. As the robot moves, the beacon periodically emits signals which allow some of the sensors and anchors to measure their distances to the robot. The sensors and anchors send their measurements to a desktop machine to process them in batch and time recursive algorithms. Note that no measurements are collected between sensors. Through the trajectory of 1.5 minutes, 18 positions

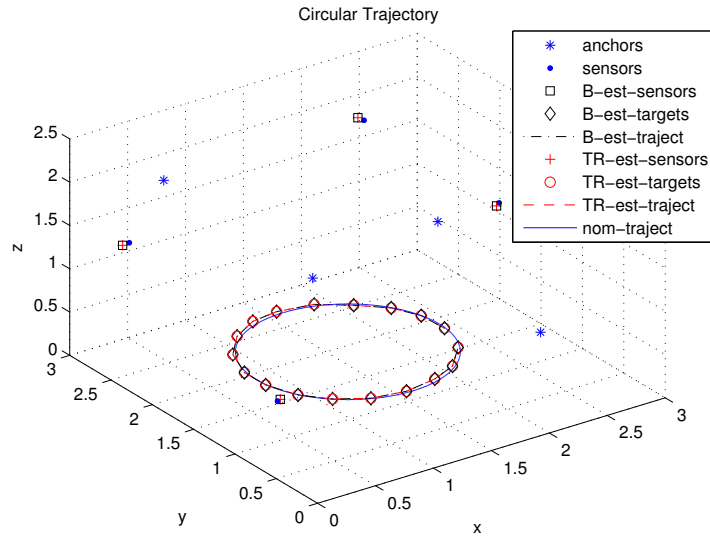


FIGURE 3.9: Circular trajectory of Pioneer P3-DX. B-est and TR-est refer to estimation from full batch (EDM-R + MM) and the time recursive $((EDM-R + MM) + SLNN + MM)$ procedures, respectively.

of the robot are observed. The ground truth of sensors and beacon/robot positions are obtained using manual measurements. On average 7 sensors heard beacon signals from each target position. The algorithm is able to accurately localize a network of 4 anchors, 4 sensors and 18 target positions with an RMSE of 4.1 cm. The geometrical configuration of these sensor and target positions has intrinsic reflection ambiguities that are not resolved with anchors because the robot moves in the same z -coordinate through the circular trajectory. Therefore, some of the sensor positions are estimated at the mirror of their real positions with respect to the robot z -coordinate. For this particular setup, the intrinsic reflection ambiguity is readily solved by projecting them to the positive z -axis with respect to the estimated robot z -coordinate.

Figure 3.9 shows sensor/anchor positions and the 3D nominal and estimated target trajectories. Dark symbols represent estimated positions from the full batch (18 target positions), while red symbols display the estimated positions from an initial batch (first 15 target positions), followed by three time recursive updates for the three last target positions. At each time recursive update, it is assumed that a new target range measurement is obtained by the sensors and the new position is estimated by fixing the previously estimated positions while minimizing (2.37). The newly estimated target position and all positions estimated previously are given as an initial point to start MM. Therefore, Figure 3.9 presents not only the last three target positions estimated in updating initializations, but also all positions refined by MM step.

Experiment 2: In this experiment, the robot moves along a straight line, followed by a half circle, a straight line, and a full circle for approximately 2 minutes, generating 24

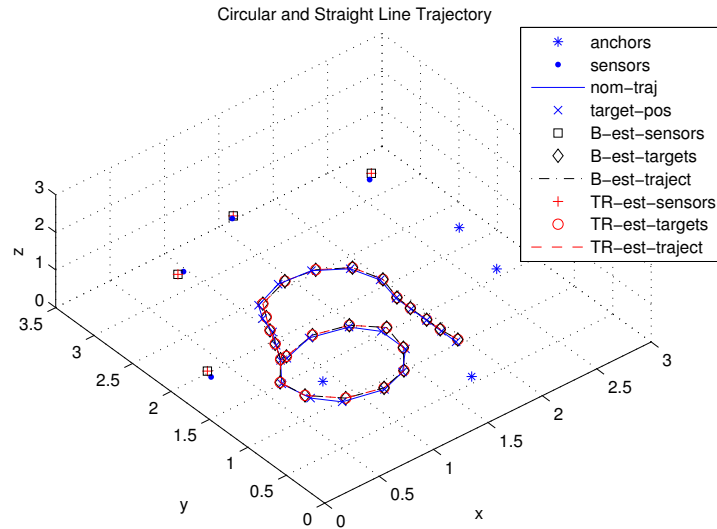


FIGURE 3.10: Piecewise linear/circular trajectory of Pioneer P3-DX. B-est and TR-est refer to estimation from full batch (EDM-R + MM) and the time recursive ((EDM-R + MM) + SLNN + MM) procedures, respectively.

target positions. The RMSE of this setup (4 anchors, 4 sensors and 24 target positions) is 3.95 cm which is slightly better than the previous experiment due to the larger batch dimension (24 target positions). Figure 2.10 shows the sensor/anchor node positions, as well as the nominal and estimated target trajectories for both the batch and time recursive approaches. The latter pertains to the last three target positions, as described in Experiment 1. The time recursive procedure attains the same accuracy as the batch algorithm, with the advantage of lower computational complexity.

Experiment 3: In this experiment, a human carries the beacon, generating 18 target sightings along a somewhat erratic trajectory (the human moves to the positions that have ground truths). Figure 3.11 depicts the sensor/anchor positions, the nominal and the estimated target trajectories. Since the human carries the beacon in different z-coordinates, there is no symmetry, thus no intrinsic ambiguity in this case. The RMSE of this network of 4 anchors, 4 sensors and 18 target positions is 3.88 cm.

3.8 Conclusion

In this chapter, a ML-based technique is presented to solve a SLAT problem using a two-phase approach under Gaussian or Laplacian noise. A MM method is proposed to iteratively maximize the non-convex likelihood function, for which a good initial point is required. Therefore, two initialization schemes, EDM completion and SLCP/SLNN/SL- ℓ_1 s are investigated that bypass the need for strong priors on sensor/target positions.

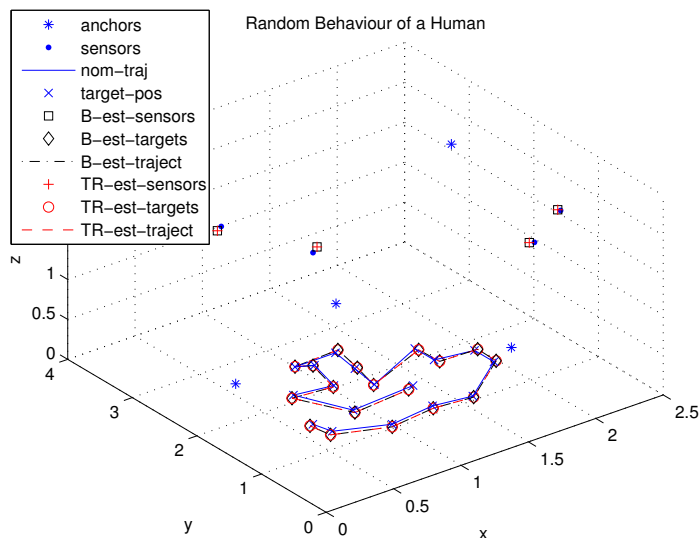


FIGURE 3.11: Trajectory of a human target.

After the first batch of measurements is obtained, EDM completion is used for the first initialization of the sensor network topology. In the experiments this was accomplished reasonably fast (a few seconds) for scenarios with up to about 30 unknown positions. As EDM completion is not scalable, after startup an alternative, lightweight, incremental initialization scheme is resorted as additional target range measurements become available. The SLCP/SLNN or $SL-\ell_1$ family of time recursive methods use the already estimated positions at each time a new position is to be estimated; afterwards the newly estimated position and the already estimated ones are given as an initialization to the optimization methods. Anchors are used to avoid some inherent ambiguities of the sensor/target localization problem using range measurements.

Simulation results showed that proposed scheme nearly attains the CRLB under moderate Gaussian noise. In the presence of outliers, both EDM-R- ℓ_1 and $SL-\ell_1$ provide more accurate initial position estimates than other existing methods. Moreover, when used as input to iterative refinement methods they provide a good starting point that reduces the probability of convergence to undesirable extrema, yielding improved overall estimation performance. Hence, with this methodology, a processing structure is obtained that is robust to outliers and provides a scalable and accurate solution to the SLAT problem. Importantly, the algorithms based on ℓ_1 norm optimization exhibited robust behaviour in simulation not only for Laplacian outliers, but also for an alternative outlier generation technique that did not match the underlying Laplacian modelling assumptions.

The proposed algorithms are tested in a real 3D indoor environment. It is observed that

the range estimation accuracy depends on the distance and the facing angle of sensor-target pair, which affects the accuracy of the algorithms. Additionally, for particular setups, intrinsic ambiguities can not be resolved with anchors. It is demonstrated experimentally that the proposed scheme can track a target and localize sensors to within about 4 cm accuracy in a 3D indoor environment using mixed ultrasound-RF ranging.

Chapter 4

Sensor Network Localization in the Presence of Unknown Turn-Around Time or Transmit Power

In this chapter, cooperative sensor network localization with nuisance parameters, i.e. unknown turn-around time for TOA based and unknown transmit power for RSS based systems will be addressed. Mathematically, these problems are closely related to the ones addressed in Chapter 3, with additional difficulties. Therefore, similar techniques are resorted to solve them.

4.1 TOA based Sensor Network Localization with Unknown Turn-Around Time

4.1.1 Introduction

As the TOA measurements are time-based, clock synchronization among different nodes affects localization algorithms. Moreover, because of the stringent cost and power constraints of WSNs, low-cost clocks are normally employed. This makes time-based localization and synchronization tightly coupled and challenging. To address this problem, in this section, the Two-Way Time-of-Arrival (TW-TOA) protocol is adopted, where the anchor node sends the ranging request and the target node responds back. The time of flight of the signal is proportional to the distance between target-anchor if there is

no delay in the response time of the target, or if that delay, called turn-around time, is correctly included in the reply packet and subtracted at the node originating the ranging request. Although, broadcast mode, pairwise distances are obtained one at a time, is less obvious than the one for TOA based systems, this way, TW-TOA based systems can exploit unsynchronized clocks as shown in Figure 4.1. However, in practical scenarios, calibration of nodes to determine the turn-around time is costly and difficult [97, 98]. In addition, the responding target might deceive the anchor by reporting a wrong turn-around time. Therefore, localization algorithms should tackle this issue which is solved within the context of cooperative localization in this section. In this scheme, not only are TW-TOAs between target nodes and anchor nodes measured, but also the target nodes themselves are involved and collect TW-TOA measurements from each other.

In [99], an UWB ranging-based localization strategy which is immune to an internal ranging attack, a false timestamp report, is proposed using TW-TOA protocol. For example, a compromised sensor node tampers its timestamp report to deceive its processing time in order to falsely decrease or enlarge distance measurements, or a sensor node submits an inaccurate timestamp report due to the clock drift. The authors resort to TDOA type algorithms to solve the synchronization and localization problem. In [100, 101], the authors first propose closed-form LS estimators for joint synchronization and a single target localization using the TW-TOA protocol in which clock offset and skew are unknown. And then the authors propose an Asymmetric Trip Ranging (ATR) protocol, where anchors are not only able to communicate with the target, but also listen to the other anchor-target communications. An asynchronous position measurement system is proposed in [102] and another LS based method is solved for indoor localization of a single target by using the differential TOA. The target node position and clock offset are estimated by a weighted least-squares estimator in a computationally efficient way in [103]. A generalized total LS algorithm is developed for the joint synchronization and localization of an unknown node in [104]. The authors consider hierarchical hop-by-hop time synchronization and localization where only one node needs to be localized and synchronized to the anchors at a time. Recently, an LS based approach using hybrid TW-TOA and TDOA in cooperative networks is proposed for the joint estimation of unknown turn-around times and node locations [105]. The authors did not consider TW-TOA measurements between targets to improve the accuracy. All mentioned methods either estimate a single target position or estimate each target position at a time by a linearization-based LS. Therefore, the main contribution of this section is an accurate SDP method which localizes multiple targets simultaneously in the presence of unknown turn-around time in a cooperative network.

To find the MLE for the sensor network localization problem with unknown turn-around times, it is necessary to solve a nonlinear and nonconvex optimization problem. To avoid

this difficulty, the original MLE is transformed into an approximate NLS problem using squared range measurements. Then, relaxation techniques are applied to convert the NLS problem into a convex optimization problem by resorting to EDM completion. Through this, the target turn-around times are considered as nuisance parameters and estimated jointly with the target locations. The resulting problem is globally solvable, but it is sub-optimal and hence cannot achieve the best possible performance under all conditions.

The remainder of this section is organized as follows. Section 4.1.2 formalizes the problem and formulates the proposed EDM completion. Simulations and computational complexity analysis are given in Section 4.1.3. Conclusions are drawn in Section 4.1.4.

4.1.2 Problem Formulation

This section formulates the cooperative localization problem using TW-TOA measurements, where the target locations and turn-around times are unknown. Two sets of TW-TOA measurements are available to the estimator: target-anchor and target-target measurements. Let $\mathbf{s}_j \in \mathbb{R}^n$, $j \in \mathcal{S} = \{1, \dots, h\}$ and $\mathbf{a}_i \in \mathbb{R}^n$, $i \in \mathcal{A} = \{h+1, \dots, h+m\}$ denote h target and m anchor locations, respectively. The cooperative TW-TOA measurement (converted to distance) [106], when the i -th node interrogates the j -th node, is expressed as

$$d_{ij} = T_j + 2\hat{d}_{ij} + w_{ij}, \quad j \in \mathcal{S}, \quad i \in \mathcal{B}_j \cup \mathcal{C}_j \quad (4.1)$$

where T_j is the turn-around time of the j -th target (converted to distance), $\hat{d}_{ij} = \|\mathbf{s}_i - \mathbf{s}_j\|$, $i \in \mathcal{C}_j$ and $\hat{d}_{ij} = \|\mathbf{a}_i - \mathbf{s}_j\|$, $i \in \mathcal{B}_j$. Sets \mathcal{B}_j and \mathcal{C}_j are defined in (3.1) and (3.2), respectively. Note that, here, \mathcal{C}_j contains the index set of targets (called as sensors in (3.2)) that communicate with the j -th target. In addition, w_{ij} are modeled as i.i.d. zero mean Gaussian random variables with standard deviation σ_{ij} . Consequently, there are in total $n \times h + h$ unknown elements that should be estimated, including the target locations and the turn-around times defined as $\mathbf{S} = [\mathbf{s}_1, \dots, \mathbf{s}_h] \in \mathbb{R}^{n \times h}$ and $\mathbf{T} = [T_1, \dots, T_h]^T \in \mathbb{R}^h$, respectively.

In practical scenarios, we can assume that a target sends a ranging request to another target, which responds back. When the communication initiator gets the response, it then sends a final packet as if it had been interrogated. In this way, with three communications, two TW-TOA measurements are obtained as shown in Figure 4.1(a). Whenever an anchor sends a ranging request to a target, that target not only responds back to the ranging message but also sends its TW-TOA measurements obtained with respect to the other targets with which it has communicated. As a result, all TW-TOA measurements are conveyed to the central node via anchors.

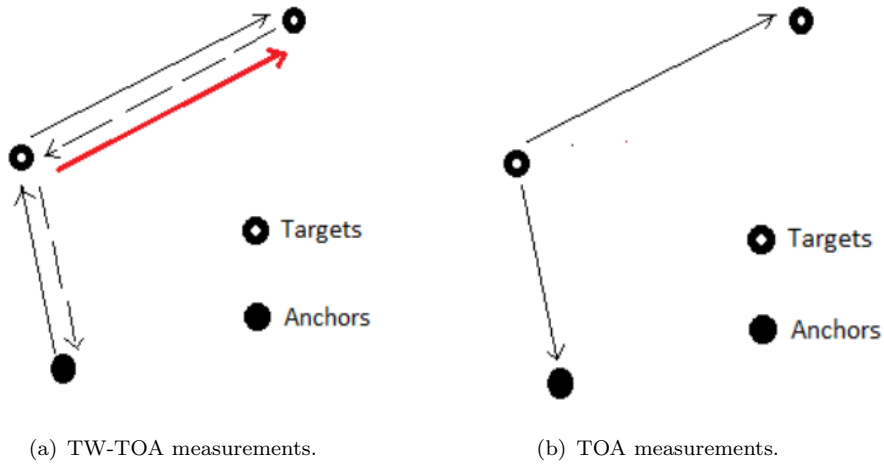


FIGURE 4.1: Two TW-TOAs are obtained in three communications between target nodes. TOA measurements are estimated accurately only when the clocks of the nodes are synchronized.

4.1.2.1 EDM Formulation

By moving T_j to the left hand side (LHS) of the equation and squaring both sides, (4.1) can be reformulated as

$$d_{ij}^2 - 2d_{ij}T_j + T_j^2 = 4\hat{d}_{ij}^2 + 4\hat{d}_{ij}w_{ij} + w_{ij}^2. \quad (4.2)$$

For sufficiently small noise, w_{ij}^2 in the right-hand side of (4.2) can be neglected and (4.2) is written as

$$d_{ij}^2 - 2d_{ij}T_j + T_j^2 = 4\hat{d}_{ij}^2 + \epsilon_{ij}, \quad (4.3)$$

where $\epsilon_{ij} = 4\hat{d}_{ij}w_{ij}$ is a zero-mean Gaussian noise with standard deviation $4\hat{d}_{ij}\sigma_{ij}$. The NLS formulation that matches predicted (\hat{d}_{ij}, T_j) vs. observed d_{ij} ranges is

$$\underset{\mathbf{S}, \mathbf{T}}{\text{minimize}} \quad \sum_{j \in \mathcal{S}} \sum_{i \in \mathcal{B}_j \cup \mathcal{C}_j} (d_{ij}^2 - 2d_{ij}T_j + T_j^2 - 4\hat{d}_{ij}^2)^2. \quad (4.4)$$

The unknown squared distances can be arranged into a single symmetric EDM matrix of size $(h + m) \times (h + m)$, with elements $E_{ij} = \hat{d}_{ij}^2$, and satisfying the properties of the EDM cone \mathcal{E} [23, 38] given in (3.6).

Introducing a vector epigraph variable $\mathbf{K} = [K_1, \dots, K_h]^T$ yields the following relaxed EDM problem:

$$\begin{aligned}
 & \underset{\mathbf{E}, \mathbf{T}, \mathbf{K}}{\text{minimize}} && \sum_{j \in \mathcal{S}} \sum_{i \in \mathcal{B}_j \cup \mathcal{C}_j} (d_{ij}^2 - 2d_{ij}T_j + K_j - 4E_{ij})^2 \\
 & \text{subject to} && \mathbf{E} \in \mathcal{E}, \quad \mathbf{E}(\mathcal{A}) = \mathbf{A} \\
 & && K_j \geq T_j^2, \quad T_j \geq 0, \quad \text{and } \gamma_j \geq K_j.
 \end{aligned} \tag{4.5}$$

The constraint $\mathbf{E}(\mathcal{A}) = \mathbf{A}$ enforces the known *a priori* spatial information related with anchors in the appropriate EDM submatrix. In (4.5) the desired nonlinear equality constraint $K_j = T_j^2$ is relaxed to an inequality to obtain a convex optimization problem. However, the relaxation can cause K_j to become arbitrarily large, which is undesirable because estimated locations become arbitrarily far apart. To mitigate this difficulty, large K_j values might be penalized by adding a regularization term to the objective [23, 91]. However, this is sensitive to the penalization term [107]. Another way is to upper bound K_j by a constant γ_j , which might be chosen with respect to prior knowledge of system specifications, i.e., knowledge of the maximum possible value of turn-around time or according to the method proposed in Section 4.1.2.2.

Note that the solution of (4.5) is a distance matrix \mathbf{E} . Detailed explanations of how to estimate the spatial coordinates of the targets from EDM and the usage of anchors are given in Section 3.4.2.1.

4.1.2.2 Estimate of γ_j

To provide a reasonably good upper bound, γ_j , for the variable K_j , (4.3) can be approximated by dropping the noise term when $i \in \mathcal{B}_j$ as

$$d_{ij}^2 - 2d_{ij}T_j + T_j^2 = 4\|\mathbf{a}_i\|^2 - 8\mathbf{a}_i^T \mathbf{s}_j + 4\|\mathbf{s}_j\|^2, \tag{4.6}$$

and rearranging terms as

$$d_{ij}^2 - 4\|\mathbf{a}_i\|^2 = -8\mathbf{a}_i^T \mathbf{s}_j + 4\|\mathbf{s}_j\|^2 + 2d_{ij}T_j - T_j^2, \tag{4.7}$$

which can be written as $b_{ij} = \mathbf{H}_{ij}\mathbf{y}_j$, where $b_{ij} = d_{ij}^2 - 4\|\mathbf{a}_i\|^2$, $\mathbf{H}_{ij} = [1, -8\mathbf{a}_i^T, 2d_{ij}]$ and $\mathbf{y}_j = [4\|\mathbf{s}_j\|^2 - T_j^2, \mathbf{s}_j, T_j]^T$. The vector \mathbf{b}_j and matrix \mathbf{H}_j are constructed from b_{ij} and \mathbf{H}_{ij} , $i \in \mathcal{B}_j$, such that $\mathbf{b}_j = \mathbf{H}_j\mathbf{y}_j$. If \mathbf{H}_j has full column rank, coarse estimates of \mathbf{s}_j and T_j are obtained from the LS solution

$$\hat{\mathbf{y}}_j = (\mathbf{H}_j^T \mathbf{H}_j)^{-1} \mathbf{H}_j^T \mathbf{b}_j. \tag{4.8}$$

Through simulations it was observed that the accuracy of position estimation is better than the turn-around time estimation with this method. Therefore, estimated turn-around times are calculated as $\tilde{T}_j = (\sum_{i \in \mathcal{B}_j} (d_{ij} - 2\tilde{d}_{ij})) / |\mathcal{B}_j|$, where \tilde{d}_{ij} is the estimate of \hat{d}_{ij} from the estimated target position $\hat{\mathbf{s}}_j$, and $|\mathcal{B}_j|$ is the cardinality of \mathcal{B}_j . The upper bound in (4.5) is set as $\gamma_j = \tilde{T}_j^2$. Note that to solve (4.8), at least 4 (2D) or 5 (3D) anchors are needed. The estimator first estimates the locations and turn-around times of targets that are connected to a sufficient number of anchors, and it uses the estimated position of the neighboring targets as virtual anchors for the remaining ones. When these conditions are not satisfied, the estimator simply assigns a constant to γ_j based on prior knowledge of maximum turn-around times.

Note that, ideally, one would like γ_j to be large enough (but no larger) so that the true values of $K_j = T_j^2$ for a given network setup are included in the feasible set of (4.5). Even though the method above for setting γ_j does not really guarantee that, simulation results show that it is a good heuristic.

4.1.3 Simulations

In this section, computer simulations are performed to evaluate the performance of the proposed algorithm which will be called “EDM” in the figures. The comparison metric is the total RMSE defined as in (3.27). To assess the fundamental hardness of the position estimation, error plots also show the average CRLB with known (“CRLB-Known-T”) and unknown turn-around times (“CRLB”) for each noise variance. The derivation of the CRLB is given in Appendix H.1 and it follows the same reasoning as in [16].

To compare the proposed algorithm with MLE, Matlab’s function *lsqnonlin* is initialized with the output of the proposed method and with random initialization, denoted below as EDM-MLE and RAND-MLE, respectively. Additionally, results for EDM localization with true turn-around time (“EDM-Known-T”) will be provided. In every realization of the network, the turn-around time is randomly drawn from [1, 100] ns and the measurement noise assumed i.i.d. Gaussian, with $\sigma_{ij} = \sigma \in [0.01, 18]$ m.

Example 1 [Random network] A fully connected (all anchors and targets are within communication range) randomly distributed network in $[-80, 80] \text{ m} \times [-80, 80] \text{ m}$ consisting of 6 targets and 8 anchors is generated at each Monte Carlo run for each noise level. Figure 4.2 shows the RMSE of different approaches. The accuracy of the proposed method is good and the degradation in performance due to unknown turn-around time is small when compared to EDM-Known-T. Additionally, EDM-MLE attains the CRLB. The RMSE of RAND-MLE is the worst one.

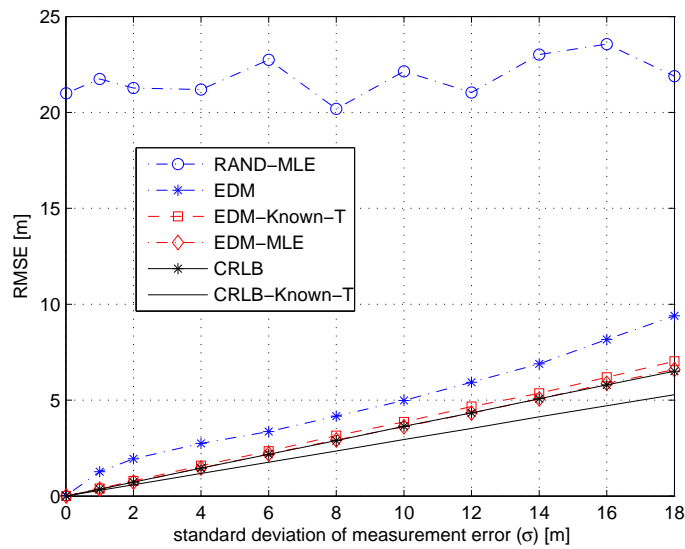


FIGURE 4.2: RMSE comparisons in a fully connected randomly distributed network.

Example 2 [Structured network] The behavior of the algorithms is examined for a *structured network*, in which $\mathbf{a}_i \in \{[\pm 50, \pm 50]^T, [0, \pm 70]^T, [\pm 70, 0]^T\}$ m and $\mathbf{s}_i \in \{[\pm 20, 40]^T, [0, \pm 40]^T, [0, 0]^T, [20, 40]^T\}$, i.e., when all 6 targets are in the convex hull of 8 anchors and they are fully connected. As shown in Figure 4.3, the accuracy of EDM is good and EDM-MLE attains the CRLB. However, for this scenario RAND-MLE also achieves the CRLB because the cost function appears to have a unique minimum.

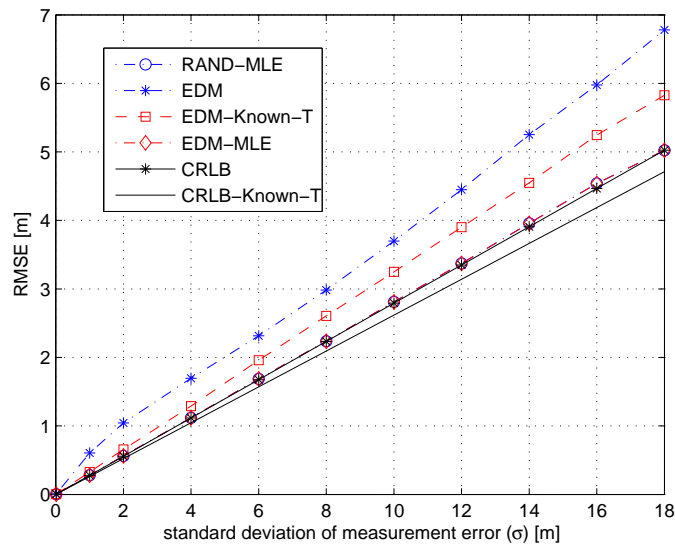


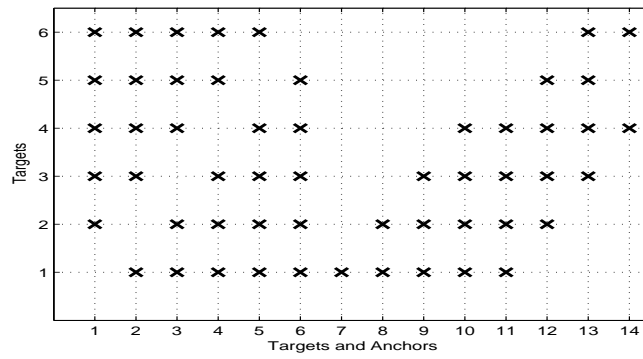
FIGURE 4.3: RMSE comparisons in a fully connected *structured network*.

Example 3 [The sample mean and uncertainty ellipsoids] The sample mean and the uncertainty ellipsoids of EDM and EDM-Known-T are given in Figure 4.4(b) when $\sigma = 10$ m for the *structured network*. The connectivity matrix for the network is shown in Figure 4.4(a), where the 5th and 6th targets are only connected to two anchors and all others communicate with five anchors. Although two anchors are not enough for the 5th and 6th targets to be localized in 2D, all positions are eventually determined with good accuracy through cooperation, as the remaining targets are within range of a sufficient number of anchors. Figure 4.4(c) shows the RMSE comparisons for this network. With limited connectivity to anchors the localization problem becomes harder, similarly to what is known to occur even with full connectivity when some of the targets lie outside the convex hull of the set of anchors. This is seen, e.g., in the significant degradation of RAND-MLE for strong observation noise levels ($\sigma > 10$ m). However, EDM still provides good accuracy. Moreover, EDM-MLE attains the CRLB.

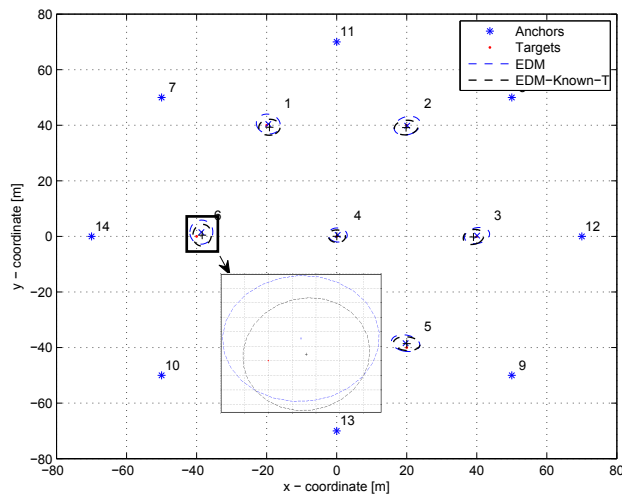
A Note on Practical Computational Complexity: The worst case computational complexity of SDP based algorithms for sensor network localization is bounded by $O((h + m)^6)$ [35]. For the proposed algorithm, CPU time empirically increases with $(h + m)^{4.5}$. The experiments were conducted on a laptop with Intel Core i5-2430M 2.4 GHz CPU and 4 GB of RAM, using MATLAB 7.11, CVX 1.22 and SeDuMi as a general purpose SDP solver. The CPU time to solve the proposed method is about 0.5 seconds for this network.

4.1.4 Conclusion

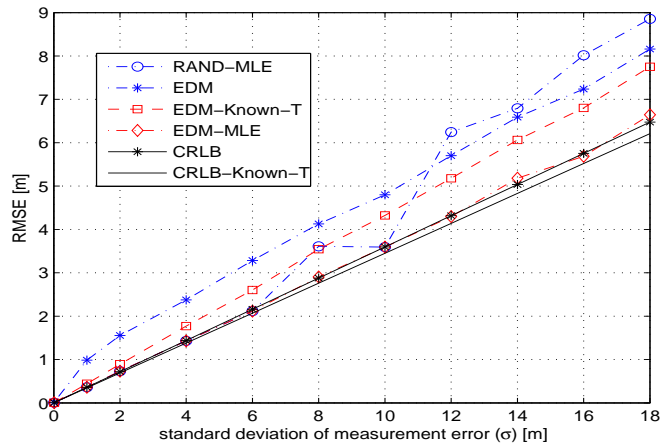
This section discussed the localization of multiple targets when target turn-around times are not known in TOA based cooperative sensor networks under the TW-TOA protocol. The turn around times are assumed as nuisance parameters and jointly estimated with target locations. To avoid the difficulty of solving the original nonconvex and nonlinear problem, it is approximately solved by using the squared range measurements and EDM completion. Simulations showed that the accuracy of the proposed method is good and also when it is used as an initialization of MLE, the latter attains the CRLB. More importantly, it is observed that the cooperation among targets provides accurate localization even if some targets are connected to few anchors.



(a) The connectivity matrix.



(b) The sample mean and uncertainty ellipsoids.



(c) The RMSE comparisons.

FIGURE 4.4: RMSE comparisons, sample mean and uncertainty ellipsoids of localization when the 5th and 6th targets of a *structured network* are connected to only two anchors.

4.2 RSS based Sensor Network Localization with Unknown Transmit Power

4.2.1 Introduction

The RSS measurement model is a function of the transmit power of the source node as given in (4.9), which depends on its battery and antenna gain and might change with time. And the anchor/receiver nodes are only able to find the location of a source node from RSS measurements if transmit power of the source is known. Consequently, each source node has to report its transmit power to anchor nodes during RSS measurements which requires additional hardware and software in both anchor nodes and source nodes making the network more complex. Thus, localization using RSS in the practical case, where transmit powers are different and unknown, is currently an open problem. Therefore, this issue is addressed within the context of cooperative localization in this section. In the proposed setup, not only are RSSs between source nodes and anchor nodes measured, but also the source nodes themselves are involved and collect RSS measurements from each other.

One of the common solutions is to eliminate the dependency of the transmit power from the RSS measurement model by using the differential RSS between a source node and two anchor nodes [108] which enhances the noise and degrades the accuracy. Another very recent method is to estimate the transmit power of the source along with its location [109, 110] which uses SDP similar to the proposed method with less accuracy and more computational complexity. Therefore, the main contribution of this section is to provide a SDP method which is more accurate and less complex than the recently published method.

Similar to Section 4.1, to find the MLE for the sensor network localization problem with unknown transmit powers, it is necessary to solve a nonlinear and nonconvex optimization problem which is transformed into an approximate NLS problem. Then, relaxation techniques are applied to convert the NLS problem into a convex optimization problem by resorting to EDM completion. Through this, the source transmit powers are considered as nuisance parameters and estimated jointly with the source locations.

The remainder of this section is organized as follows. Section 4.2.2 formalizes the problem. Simulations and computational complexity analysis are given in Section 4.2.3. Conclusions are drawn in Section 4.2.4.

4.2.2 Problem Formulation

This section formulates the cooperative RSS based localization problem in which there are more than two source nodes with unknown locations, and moreover, source nodes can communicate not only with anchor nodes but also with each other. The power of the received signal from each source can be measured at both anchor nodes and other source nodes. In other words, two sets of RSS measurements are available to the estimator: source-anchor and source-source measurements. Let $\mathbf{s}_j \in \mathbb{R}^h$, $j \in \mathcal{S} = \{1, \dots, h\}$ and $\mathbf{a}_i \in \mathbb{R}^n$, $i \in \mathcal{A} = \{h+1, \dots, h+m\}$ denote h source and m anchor locations, respectively. The RSS measurement model is expressed as

$$P_{ij} = P_j - 10\beta \log_{10} \hat{d}_{ij} + w_{ij}, \quad j \in \mathcal{S}, \quad i \in \mathcal{B}_j \cup \mathcal{C}_j, \quad (4.9)$$

where P_j [dBm] is the reference power at a reference distance (1m) from the j -th source, β is the path loss exponent that measures the rate at which the RSS decreases with distance and it depends on the specific propagation environment. In addition, the random effect of shadowing is modelled by w_{ij} which is a zero mean Gaussian random variable with standard deviation σ_{ij} [8]. Moreover, $\hat{d}_{ij} = \|\mathbf{s}_i - \mathbf{s}_j\|$, $i \in \mathcal{C}_j$ and $\hat{d}_{ij} = \|\mathbf{a}_i - \mathbf{s}_j\|$, $i \in \mathcal{B}_j$. Sets \mathcal{B}_j and \mathcal{C}_j are defined in (3.1) and (3.2), respectively. Consequently, there are in total $n \times h + h$ elements that should be estimated including the source node locations and the transmit powers of the source nodes defined as $\mathbf{S} = [\mathbf{s}_1, \dots, \mathbf{s}_h] \in \mathbb{R}^{n \times h}$ and $\mathbf{P} = [P_1, \dots, P_h]^T \in \mathbb{R}^h$, respectively.

By rearranging the logarithmic term and dividing both sides by 5β , (4.9) can be reformulated [110] as

$$\hat{d}_{ij}^2 \lambda_{ij} = \alpha_j 10^{\frac{w_{ij}}{5\beta}}, \quad (4.10)$$

where $\lambda_{ij} = 10^{\frac{P_{ij}}{5\beta}}$ and $\alpha_j = 10^{\frac{P_j}{5\beta}}$. For sufficiently small noise, the right hand side (RHS) of (4.10) can be approximated using the first order Taylor series expansion as

$$\hat{d}_{ij}^2 \lambda_{ij} = \alpha_j \left(1 + \frac{\ln 10}{5\beta} w_{ij}\right), \quad (4.11)$$

and this can be rewritten as

$$\hat{d}_{ij}^2 \lambda_{ij} = \alpha_j + \epsilon_{ij}, \quad (4.12)$$

where ϵ_{ij} is a zero mean Gaussian random variable with standard deviation $\alpha_j \frac{\ln 10}{5\beta} \sigma_{ij}$. The corresponding NLS estimator of the unknown parameters \mathbf{S} and α is

$$\underset{\mathbf{S}, \alpha}{\text{minimize}} \quad \sum_{j \in \mathcal{S}} \sum_{i \in \mathcal{B}_j \cup \mathcal{C}_j} (\hat{d}_{ij}^2 \lambda_{ij} - \alpha_j)^2. \quad (4.13)$$

The unknown squared distances can be arranged into a single symmetric EDM matrix of size $(h + m) \times (h + m)$, with elements $E_{ij} = \hat{d}_{ij}^2$, and satisfying the properties of the EDM cone \mathcal{E} [23, 38]. Therefore, the nearest EDM problem is formulated as

$$\begin{aligned} & \underset{\mathbf{E}, \alpha}{\text{minimize}} && \sum_{j \in \mathcal{S}} \sum_{i \in \mathcal{B}_j \cup \mathcal{C}_j} (E_{ij} \lambda_{ij} - \alpha_j)^2 \\ & \text{subject to} && \mathbf{E} \in \mathcal{E}, \mathbf{E}(\mathcal{A}) = \mathbf{A}. \end{aligned} \quad (4.14)$$

Note that the solution of (4.14) is a distance matrix \mathbf{E} . Estimation of the spatial coordinates of the sources from EDM is explained in Section 3.4.2.1.

4.2.3 Simulations

In this section, computer simulations are performed to evaluate the performance of the proposed algorithm which will be called “EDM” in the figures. The comparison metric is the total RMSE defined as in (3.27). To assess the fundamental hardness of the position estimation, error plots also show the total CRLB with known (“CRLB”) and unknown transmit power (“CRLB-Unknown-P”) derived in Appendix H.2 for each noise variance. Throughout the simulations the value of the path loss exponent β is assumed known and set to 4. The standard deviation of shadowing is $\sigma_{ij} = \sigma \in [1 \text{ } 8]$ [dB].

To compare the proposed algorithm with MLE, Matlab’s function *lsqnonlin* is initialized with true values of the positions and transmit power of sources, denoted below as “MLE”. Additionally, the results will be benchmarked with a recently published method “SDP-URSS” [110] which resorts to similar formulations but uses different semidefinite relaxations.

Example 1 [Regular network] In the first scenario, five anchor nodes were placed regularly on the corners and in the center of a square 20 m by 20 m and ten source nodes were distributed in a square area 19 m by 19 m inside the convex hull of the anchor nodes, i.e. $\mathbf{S} = [2 \ 19; 4 \ 3; 6 \ 4; 6 \ 10; 12 \ 2; 14 \ 4; 15 \ 7; 15 \ 16; 16 \ 3; 18 \ 18]$ m as shown in Figure 4.7. The corresponding reference powers are $\mathbf{P} = -[3.92; 11.55; 9.48; 19.47; 5.11; 19.63; 12.42; 14.65; 2.51; 10]$ [dBm]. Full connectivity was assumed, meaning that each source node was connected to all anchor nodes and also to all other source nodes. Figure 4.5 shows that the RMSE of EDM and SDP-URSS are almost the same and they are close to MLE and CRLB.

Example 2 [Irregular network] In the second scenario, the location of the source nodes is the same as in Example 1, but the anchor nodes are placed irregularly as

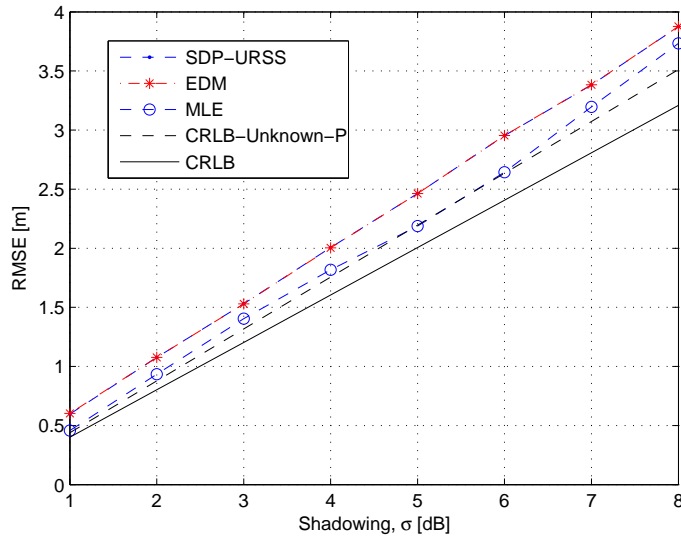


FIGURE 4.5: RMSE comparisons for the first scenario where the sources are inside the convex hull of the anchors.

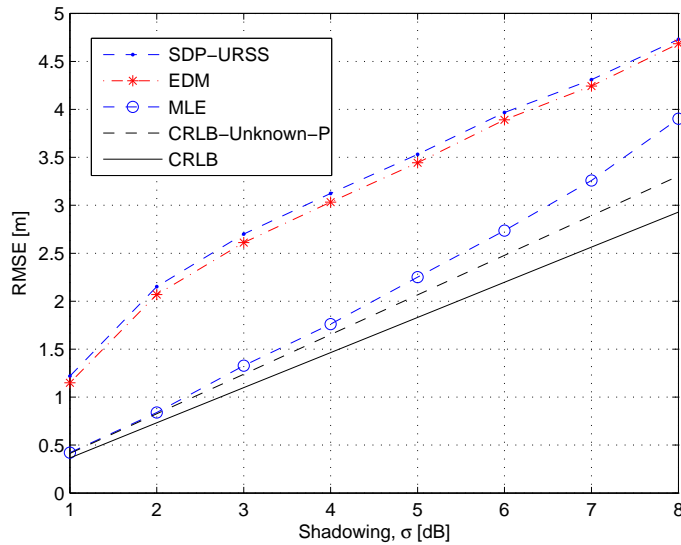


FIGURE 4.6: RMSE comparisons for the second scenario where the sources are not inside the convex hull of the anchors

$\mathbf{A} = [22; 4\ 16; 10\ 10; 12\ 14; 17\ 5]$ m. For this irregular scenario EDM outperforms SDP-URSS, as shown in Figure 4.6. Note that, the performance of the proposed method and the state of the art method is far from the ML estimator for this scenario because they converge to local minima more often when some of the sources lie outside the convex hull of the anchors. Moreover, MLE attains the CRLB only at small noise levels.

A Note on Practical Computational Complexity: The worst case computational complexity of SDP based algorithms for sensor network localization is bounded by $O((h + m)^6)$

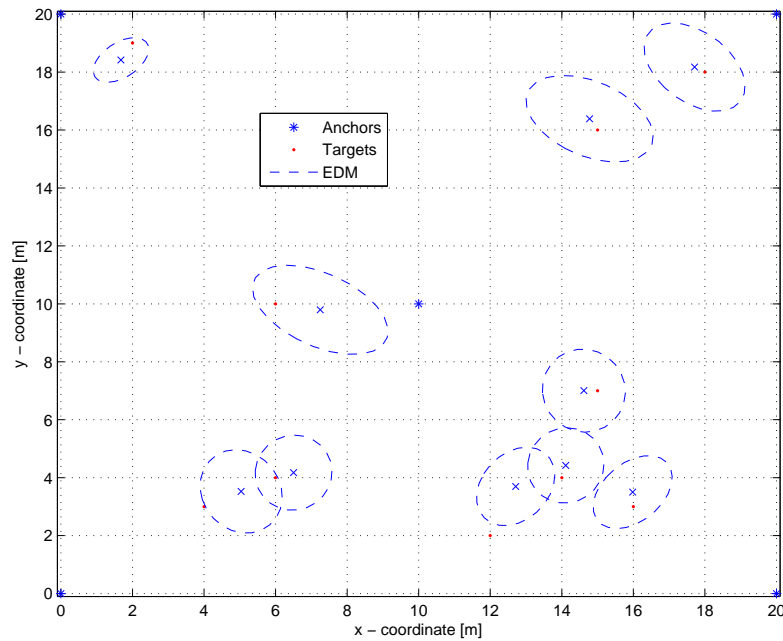


FIGURE 4.7: Sample mean (shown as crosses) and uncertainty ellipsoids of EDM when sources $[\mathbf{s}_1 \ \mathbf{s}_{10}] = [2 \ 19; 18 \ 18]$ are connected to only two anchors.

[35]. In detail, without imposing any structure on matrix variables [68] and following the formulation given in Section 2.6: for EDM and SDP-URSS, the (k, l) pairs are $(k \simeq (h + m)^2 + h, l \simeq h + m)$, $(k \simeq 3h + h^2 + L, l \simeq L)$, respectively such that $\mathcal{O}_{EDM} = ((h + m)^2 + h)^2(h + m)^2$ and $\mathcal{O}_{SDP-URSS} = (3h + h^2 + L)^2 L^2$, where L is the total number of connections. For full connectivity $L = h(m + (h - 1)/2)$.

Similar to TOA based cooperative sensor network localization, for the proposed algorithm, CPU time empirically increases with $(h + m)^{4.5}$. The CPU time used by EDM and SDP-URSS is about 0.3 and 0.7 seconds, respectively for this network.

Example 3 [The sample mean and uncertainty ellipsoids] The sample mean and uncertainty ellipsoids of EDM are given in Figure 4.7 when $\sigma = 4$ [dB] for the first scenario. Two of the sources ($[\mathbf{s}_1 \ \mathbf{s}_{10}] = [2 \ 19; 18 \ 18]$ m) are only connected to two anchors and all others communicate with five anchors. With the limited connectivity to anchors the localization problem becomes harder, similarly to what is known to occur even with full connectivity when some of the sources lie outside the convex hull of the set of anchors. Moreover, although two anchors are not enough for those sources to be localized in 2D, all positions are eventually determined with good accuracy through cooperation, as the remaining sources are within range of a sufficient number of anchors.

4.2.4 Conclusion

The localization of multiple sources is studied when there is no “a priori” information on the source transmit power in RSS based cooperative sensor networks. A variation of EDM completion is derived by applying approximations and relaxations to ML. Although the ML estimator outperforms other algorithms, finding its global minimum involves complex computations and requires a good initialization. However, the proposed SDP approach having a quite close performance to ML for regular networks can be solved efficiently without any initialization and with ease of implementation if a convex solver is available. Its performance is close to CRLB at some scenarios. Additionally, EDM outperforms the state of the art method in two ways: it is more accurate and it requires less computational operations. Moreover, the cooperation among sources provides accurate localization even if some sources are connected to few anchors.

Chapter 5

A Polar Decomposition Approach for Exact Source Localization from Squared Range Differences

5.1 Introduction

This chapter addresses source localization based on the TDOA measurement model, for which only the differences of measured arrival times between sensing nodes are required.

Classical TDOA-based self-localization in navigation applications can be realized by intersecting a set of hyperbolas that are contour lines of constant range difference between the source and various beacons. Because of errors in TDOA measurements, these hyperbolas will not intersect at a single point, which leads to mathematically inconsistent localization equations. A common goal is to find an estimate of the source location that minimizes those inconsistencies.

In the literature, there are mainly four approaches to solve the nonlinear system of equations defining the hyperbolic localization problem [111].

The first traditional approach is the reorganization of the nonlinear terms and introduction of additional variables to attain linear equations that can be solved in closed form by LS [70]. Closed-form solutions are usually less computationally burdensome than iterative or ML methods which will be explained in the following paragraph. Nevertheless, the reorganized linear equations are only suitable in practice for sufficiently small measurement noise.

The second approach is based on the nonlinear LS framework where Taylor-series expansion is used for linearization and the solution is obtained iteratively [112]. When the TDOA measurements have Gaussian distribution, the global minimum of the objective function corresponds to the ML location estimate, which has proven asymptotic consistency and efficiency. Although optimum estimation performance can be attained, it requires a sufficiently precise initialization.

Recently, various SDR methods, each with its own advantages and drawbacks, were proposed to solve different variations of the hyperbolic localization problem. An approximate ML formulation of the TDOA localization is presented in [113], based on an effective relaxation method to transform the original nonconvex optimization problem into a convex one. However, for accurate results all pairwise TDOA measurements between pairs of nodes have to be exhaustively incorporated into a cost function for minimization, which potentially leads to high computational complexity.

An approximate and iterative localization method that can be implemented in a distributed manner is introduced in [114]. It is based on the popular approach of Projection Onto Convex Sets (POCS), modified to accommodate the unbounded hyperbolic sets that arise in TDOA localization. Numerical simulations show that hyperbolic POCS has several desirable features, such as the ability to accurately locate sources outside of the convex hull spanned by the sensors.

In the present work, an exact LS technique denoted *Bisection-KKT* is proposed for the source localization problem using the square of noisy range difference measurements. Although the problem is nonconvex, the formulation shows that it can be efficiently and globally solved by switching from Cartesian to polar/spherical coordinates. Besides that, two more search based methods are derived. The methods have low computational complexity and several numerical examples suggest their accuracies are good. Note that algorithms which use plain range differences might provide better accuracy at the expense of an additional computational complexity.

The organization of this chapter is as follows. Section 5.2 formulates the squared TDOAs based source localization problem, introduces the techniques and discusses their pros and cons. Simulation results are presented in Section 5.3 to evaluate the location estimation performance of the proposed estimators by comparing them with other existing methods. Finally, conclusions are drawn in Section 5.4.

5.2 Problem Formulation

Let $\mathbf{x} \in \mathbb{R}^n$ be the unknown source position, $\mathbf{a}_i \in \mathbb{R}^n$, $i = 1, \dots, m$ be known sensor positions (anchors) and assume there exists an additional reference sensor (sensor 0) located at the origin. The noiseless range difference between sensor i and sensor 0, which also defines a hyperbola with foci \mathbf{a}_i and \mathbf{a}_0 , is given by

$$d_i = \|\mathbf{x} - \mathbf{a}_i\| - \|\mathbf{x}\|, \quad \text{for } i = 1, \dots, m.$$

In the presence of noise-induced inconsistencies a natural choice is to minimize the sum of residuals between measured range differences and those predicted by a hypothesized source location. However, the source localization problem can also be solved by picking the source location as the minimizer of a so-called equation error, i.e., the minimizer of the difference between values of functions of the measured range differences and functions of a hypothesized source location [42] which leads to exact solution with the proposed formulations. Specifically, the modified residual is

$$\|\mathbf{x} - \mathbf{a}_i\|^2 - (d_i + \|\mathbf{x}\|)^2 = -2\mathbf{a}_i^T \mathbf{x} - 2d_i \|\mathbf{x}\| - d_i^2 + \|\mathbf{a}_i\|^2$$

yielding the following LS criterion [46]:

$$\underset{\mathbf{x}}{\text{minimize}} \quad \sum_{i=1}^m (-2\mathbf{x}^T \mathbf{a}_i - 2\|\mathbf{x}\|d_i + g_i)^2 \quad (5.1)$$

where $g_i = \|\mathbf{a}_i\|^2 - d_i^2$.

Expanding (5.1) and dropping constant terms, it can be represented more compactly as

$$\underset{\mathbf{x}}{\text{minimize}} \quad \mathbf{x}^T \mathbf{A} \mathbf{x} + \mathbf{f}^T \|\mathbf{x}\| \mathbf{x} + \mathbf{s}^T \mathbf{x} + e \|\mathbf{x}\| \quad (5.2)$$

where

$$\mathbf{A} = \sum_{i=1}^m (4\mathbf{a}_i \mathbf{a}_i^T + 4d_i^2 \mathbf{I}), \quad \mathbf{f} = \sum_{i=1}^m 8d_i \mathbf{a}_i, \quad e = \sum_{i=1}^m -4d_i g_i, \quad \mathbf{s} = \sum_{i=1}^m -4\mathbf{a}_i g_i.$$

Expressing the source location in terms of its range and bearing, i.e., $\{\mathbf{x} = r\mathbf{u} : r \geq 0$ and $\|\mathbf{u}\| = 1\}$, (5.2) can be written as the following constrained optimization problem:

$$\begin{aligned} & \underset{r, \mathbf{u}}{\text{minimize}} \quad f(r, \mathbf{u}) = r^2(\mathbf{u}^T \mathbf{A} \mathbf{u} + \mathbf{f}^T \mathbf{u}) + r(\mathbf{s}^T \mathbf{u} + e) \\ & \text{subject to} \quad r \geq 0, \|\mathbf{u}\| = 1. \end{aligned} \quad (5.3)$$

For a given \mathbf{u} , (5.3) is a quadratic cost function whose unconstrained optimal solution with respect to r is readily found in closed form from the first order stationary condition

$$\nabla_r f(r, \mathbf{u}) = 2r\mathbf{u}^T \mathbf{A}\mathbf{u} + 2r\mathbf{f}^T \mathbf{u} + \mathbf{s}^T \mathbf{u} + e = 0$$

and

$$r^* = -\frac{e + \mathbf{s}^T \mathbf{u}}{2(\mathbf{u}^T \mathbf{A}\mathbf{u} + \mathbf{f}^T \mathbf{u})}, \quad \text{for } e + \mathbf{s}^T \mathbf{u} < 0. \quad (5.4)$$

Substituting the optimal r in (5.3) leads to

$$p^* = \begin{aligned} & \underset{\mathbf{u}}{\text{maximize}} && \frac{(e + \mathbf{s}^T \mathbf{u})^2}{4(\mathbf{u}^T \mathbf{A}\mathbf{u} + \mathbf{f}^T \mathbf{u})} \\ & \text{subject to} && \|\mathbf{u}\| = 1, \quad e + \mathbf{s}^T \mathbf{u} < 0. \end{aligned} \quad (5.5)$$

Problem (5.5) can be solved in three ways:

5.2.1 Direct Search Method

The straightforward approach to solve (5.5) is one or two dimensional search to obtain an optimal \mathbf{u} that gives the minimum value of (5.5) when $n = 2$ or $n = 3$, respectively. For instance, for 2D \mathbf{u} vector is equivalent to $[\cos \theta \quad \sin \theta]^T$, where θ belongs to the interval $(0, 2\pi]$ and for 3D, $\mathbf{u} = [\sin \theta \cos \psi \quad \sin \theta \sin \psi \quad \cos \theta]^T$, where $\theta \in (0, \pi]$ and $\psi \in (0, 2\pi]$. It is a trivial method and if the search is fine enough, it finds a good approximation to the source location. However, Direct Search takes a considerable amount of time to attain the desired accuracy. Instead, Lipschitz Optimization is initially resorted to detect the smaller interval that is known to contain the global maximum of (5.5) for a given accuracy ϵ [115]. Afterwards, further direct search might be performed in that interval.

5.2.2 Lipschitz Optimization

Lipschitz Optimization considers the problem of finding the global minimum/maximum of a function g defined on the closed interval $[l, u]$. By assuming knowledge of a bound on the rate of the change of the function, Lipschitz constant L , for every $y \in [l, u]$, the following inequality holds

$$\|g(x) - g(y)\| \leq L\|x - y\|, \quad \text{for all } x \in [l, u].$$

This assumption can be used to place a lower or upper bound on the function in any closed interval whose endpoints have been evaluated, i.e., it leads to a piecewise linear

function that approximates $g(x)$ from below/above and gives the rule to further divide the interval into smaller pieces and convergence to the global minimum/maximum at a finite number of iterations [115, 116].

Lipschitz Constant L: The main challenge of Lipschitz Optimization is to find the Lipschitz constant, L , which is obtained for $g(\mathbf{u}) = \frac{(e + \mathbf{s}^T \mathbf{u})^2}{4(\mathbf{u}^T \mathbf{A} \mathbf{u} + \mathbf{f}^T \mathbf{u})}$ as follows:

The gradient of $g(\mathbf{u})$ is

$$\nabla_{\mathbf{u}} g(\mathbf{u}) = \frac{(e + \mathbf{s}^T \mathbf{u}) \mathbf{s}}{2(\mathbf{u}^T \mathbf{A} \mathbf{u} + \mathbf{f}^T \mathbf{u})} - \frac{(e + \mathbf{s}^T \mathbf{u})^2 (2\mathbf{A} \mathbf{u} + \mathbf{f})}{4(\mathbf{u}^T \mathbf{A} \mathbf{u} + \mathbf{f}^T \mathbf{u})^2}. \quad (5.6)$$

Using the triangle inequality, positive homogeneity and Cauchy-Schwartz inequality [63], it is calculated that

$$\|\nabla_{\mathbf{u}} g(\mathbf{u})\| \leq L = \frac{(\|e\| + \|\mathbf{s}\|)\|\mathbf{s}\|}{K} + \frac{(\|e\| + \|\mathbf{s}\|)^2(2\|\mathbf{A}\| + \|\mathbf{f}\|)}{K^2}, \quad (5.7)$$

where K is the solution of

$$\begin{aligned} & \underset{r, \mathbf{u}}{\text{minimize}} && 2(\mathbf{u}^T \mathbf{A} \mathbf{u} + \mathbf{f}^T \mathbf{u}) \\ & \text{subject to} && \|\mathbf{u}\| = 1, \quad e + \mathbf{s}^T \mathbf{u} < 0. \end{aligned} \quad (5.8)$$

Problem (5.8) has a similar closed form solution shown in the next section.

However, the bound on the Lipschitz constant obtained from (5.7) is usually loose, leading to an excessively fine search grid and therefore unnecessarily large computational complexity. An alternative good heuristic is proposed: the term $\frac{(e + \mathbf{s}^T \mathbf{u})}{2(\mathbf{u}^T \mathbf{A} \mathbf{u} + \mathbf{f}^T \mathbf{u})}$ in (5.6) is equal to $-r^*$ in (5.4). Therefore, replacing that term with $-r^*$ in (5.6) and using the triangle inequality, positive homogeneity and Cauchy-Schwartz inequality leads to a tighter Lipschitz constant. But what is $-r^*$ or a sufficiently good upper bound on that quantity? Since a knowledge of the area where the sensors and the source are deployed is known, one can guess an upper bound on r^* .

Deciding the search interval: The constraints of (5.5) constitute a region that is an intersection of a circle and a half-space. Lipschitz optimization method searches the global maximum on the interval corresponding to this region, which is easily decided by trivial algebraic manipulations.

5.2.3 Bisection Method

Before showing the application of the bisection method to (5.5), an interval, known to contain the optimal value of (5.5) and where the bisection search is done is defined.

Problem (5.5) can be equivalently stated as

$$\begin{aligned}
 & \underset{\mathbf{u}, \mathbf{v}}{\text{maximize}} && \frac{(e + \mathbf{s}^T \mathbf{u})^2}{4(\mathbf{v}^T \mathbf{A} \mathbf{v} + \mathbf{f}^T \mathbf{v})} \\
 & \text{subject to} && \|\mathbf{u}\| = 1, \quad e + \mathbf{s}^T \mathbf{u} < 0, \\
 & && \|\mathbf{v}\| = 1, \quad e + \mathbf{s}^T \mathbf{v} < 0, \\
 & && \mathbf{u} = \mathbf{v},
 \end{aligned} \tag{5.9}$$

and the last equality constraint is dropped to obtain a relaxed form

$$\begin{aligned}
 & \underset{\mathbf{u}, \mathbf{v}}{\text{maximize}} && \frac{(e + \mathbf{s}^T \mathbf{u})^2}{4(\mathbf{v}^T \mathbf{A} \mathbf{v} + \mathbf{f}^T \mathbf{v})} \\
 & \text{subject to} && \|\mathbf{u}\| = 1, \quad e + \mathbf{s}^T \mathbf{u} < 0, \\
 & && \|\mathbf{v}\| = 1, \quad e + \mathbf{s}^T \mathbf{v} < 0.
 \end{aligned} \tag{5.10}$$

The optimization problem (5.10) can be expanded into two problems to separately maximize the numerator and minimize the denominator. The ratio of their optimum values gives the upper bound of the interval, ub . For the lower bound, lb , 0 or $-ub$ might be chosen.

The bisection method checks if $p^* \geq t$ at the midpoint of the interval, $t = (ub + lb)/2$, and updates the interval at each iteration until its length is below a given threshold. The feasibility problem is

$$\begin{aligned}
 & \text{find} && \mathbf{u} \\
 & \text{subject to} && \frac{(e + \mathbf{s}^T \mathbf{u})^2}{4(\mathbf{u}^T \mathbf{A} \mathbf{u} + \mathbf{f}^T \mathbf{u})} \geq t, \\
 & && \|\mathbf{u}\| = 1, \quad e + \mathbf{s}^T \mathbf{u} < 0,
 \end{aligned} \tag{5.11}$$

equivalently,

$$\begin{aligned}
 & \text{find} && \mathbf{u} \\
 & \text{subject to} && \mathbf{u}^T \mathbf{M} \mathbf{u} + 2\mathbf{b}^T \mathbf{u} + \delta \leq 0, \\
 & && \|\mathbf{u}\| = 1, \quad e + \mathbf{s}^T \mathbf{u} < 0,
 \end{aligned} \tag{5.12}$$

where $\mathbf{M} = 4t\mathbf{A} - \mathbf{s}\mathbf{s}^T$, $2\mathbf{b} = 4t\mathbf{f} - 2e\mathbf{s}$ and $\delta = -e^2$. However, this is equivalent to checking if the optimal value of the following optimization problem is less than 0 or not

$$\begin{aligned}
 & \underset{\mathbf{u}}{\text{minimize}} && \mathbf{u}^T \mathbf{M} \mathbf{u} + 2\mathbf{b}^T \mathbf{u} + \delta \\
 & \text{subject to} && \|\mathbf{u}\| = 1, \quad e + \mathbf{s}^T \mathbf{u} < 0.
 \end{aligned} \tag{5.13}$$

Problem (5.13) is a variation of the trust region subproblem, for which optimality conditions and approaches to obtain the global minimizer are known [117]. An efficient method will be introduced to exactly solve (5.13) using KKT conditions in the sequel.

Since \mathbf{M} is a symmetric matrix, it is decomposed as $\mathbf{M} = \mathbf{Q}\mathbf{D}\mathbf{Q}^T$ with \mathbf{D} diagonal matrix and $\mathbf{Q}\mathbf{Q}^T = \mathbf{Q}^T\mathbf{Q} = \mathbf{I}$ to re-express (5.13) as

$$\begin{aligned} & \underset{\mathbf{v}}{\text{minimize}} && \mathbf{v}^T\mathbf{D}\mathbf{v} + 2\mathbf{c}^T\mathbf{v} + \delta \\ & \text{subject to} && \|\mathbf{v}\| = 1, \quad e + \mathbf{s}^T\mathbf{Q}\mathbf{v} < 0, \end{aligned} \quad (5.14)$$

where $\mathbf{v} = \mathbf{Q}^T\mathbf{u}$ and $\mathbf{c} = \mathbf{Q}^T\mathbf{b}$.

For any optimization problem with differentiable objective and constraint functions for which strong duality holds, any set of primal and dual optimal points must satisfy the KKT conditions [23]. The Lagrangian of (5.14) with the dual variable λ and γ is defined as

$$L(\mathbf{v}, \lambda, \gamma) = \mathbf{v}^T\mathbf{D}\mathbf{v} + 2\mathbf{c}^T\mathbf{v} + \delta + \lambda(\mathbf{v}^T\mathbf{v} - 1) + \gamma(e + \mathbf{s}^T\mathbf{Q}\mathbf{v}). \quad (5.15)$$

The KKT conditions

$$e + \mathbf{s}^T\mathbf{Q}\mathbf{v}^* < 0, \quad (5.16)$$

$$\mathbf{v}^{*T}\mathbf{v}^* = 1, \quad (5.17)$$

$$\gamma^* \geq 0, \quad (5.18)$$

$$\gamma^*(e + \mathbf{s}^T\mathbf{Q}\mathbf{v}^*) = 0, \quad (5.19)$$

$$\nabla_{\mathbf{v}}L(\mathbf{v}^*, \lambda^*, \gamma^*) = 0 \quad (5.20)$$

are satisfied by the primal-dual optimal points $(\mathbf{v}^*, \lambda^*, \gamma^*)$. From the conditions (5.16), (5.18) and (5.19), it is obvious that $\gamma^* = 0$ and

$$\nabla_{\mathbf{v}}L(\mathbf{v}, \lambda) = (\mathbf{D} + \lambda\mathbf{I})\mathbf{v} + \mathbf{c} = 0, \quad (5.21)$$

$$\mathbf{v}^T\mathbf{v} = \mathbf{c}^T(\mathbf{D} + \lambda\mathbf{I})^{-T}(\mathbf{D} + \lambda\mathbf{I})^{-1}\mathbf{c} = 1. \quad (5.22)$$

Since $\mathbf{D} = \text{diag}([\sigma_1 \dots \sigma_m])$ where σ_i denotes an eigenvalue of \mathbf{M} and λ can be found by calculating the roots of the polynomial

$$\sum_{i=1}^m \frac{c_i^2}{(\sigma_i + \lambda)^2} = 1.$$

For example for 2D, we have a 4th-degree polynomial

$$\begin{aligned} & \lambda^4 + 2(\sigma_1 + \sigma_2)\lambda^3 + (4\sigma_1\sigma_2 + \sigma_2^2 + \sigma_1^2 - c_1^2 - c_2^2)\lambda^2 + \\ & 2(\sigma_1^2\sigma_2 + \sigma_1\sigma_2^2 - \sigma_2c_1^2 - \sigma_1c_2^2)\lambda + \sigma_1^2\sigma_2^2 - c_1^2\sigma_2^2 - c_2^2\sigma_1^2 = 0, \end{aligned}$$

whose four roots correspond to four possibilities for critical points $\mathbf{v} = -(\mathbf{D} + \lambda\mathbf{I})^{-1}\mathbf{c}$. Evaluating the objective function of (5.14) with the constraint $e + \mathbf{s}^T\mathbf{Q}\mathbf{v} < 0$ at these

TABLE 5.1: RMSE comparisons of SEARCH, KKT, SRD-LS and SI for near field case.

σ_{gaussian}	SEARCH	KKT	SRD-LS	SI
1e-4	0.0215	0.0190	0.0204	0.0230
1e-3	0.0574	0.0572	0.0568	0.0603
1e-2	0.1646	0.1646	0.1647	0.1808
1e-1	0.5604	0.5604	0.5605	0.6117

points, the global minimum can be obtained. It is an exact and very fast method. The major requirement is to calculate the roots of a polynomial of degree 4 (for 2D) or 6 (for 3D). This method will be called *Bisection-KKT*.

5.3 Simulations and Comparisons with Existing Methods

An exact solution to the problem of source localization using squared range differences (SRD-LS) is given in [46], solving a quadratic objective function subject to two quadratic constraints. Another popular approximate solution to (5.1), the so-called Spherical Interpolation (SI) method, is based on closed-form linear techniques [42]. In the sequel, the proposed methods are contrasted with SRD-LS and SI. Additionally, in the examples, SEARCH refers to *Direct Search* and *Lipschitz Optimization*. KKT refers to *Bisection-KKT*, respectively.

Example 1: To investigate the accuracy of the methods, two physical scenarios are set with a source located in the near field and far field of the sensor networks. The performance metric is RMSE defined in (2.66). The number of Monte Carlo runs is 1000 for each noise level.

Near Field Case: In this part of the example, the methods will be compared using five anchors plus a reference sensor at the origin. In each Monte Carlo run the anchor locations \mathbf{a}_i and the source \mathbf{x} were randomly generated from a uniform distribution over the square $[-10, 10] \times [-10, 10]$ m. The observed range-difference measurements were obtained by adding a normal random variable with mean zero and standard deviation $\sigma_{\text{gaussian}} \in [10^{-4}, 10^{-1}]$ m to the exact range differences. Figure 5.1 shows the positions of anchors, hyperbolas defined by each anchor-reference sensor pair and real source position and its estimation by KKT and SRD-LS at one Monte Carlo run of Near Field case. The true and estimated source position appear at the intersection of left branches of hyperbolas. Table 5.1 lists the RMSE of the methods. The RMSE of exact methods SEARCH, KKT and SRD-LS are more or less the same with a slight superiority of KKT and better than the approximate method SI.

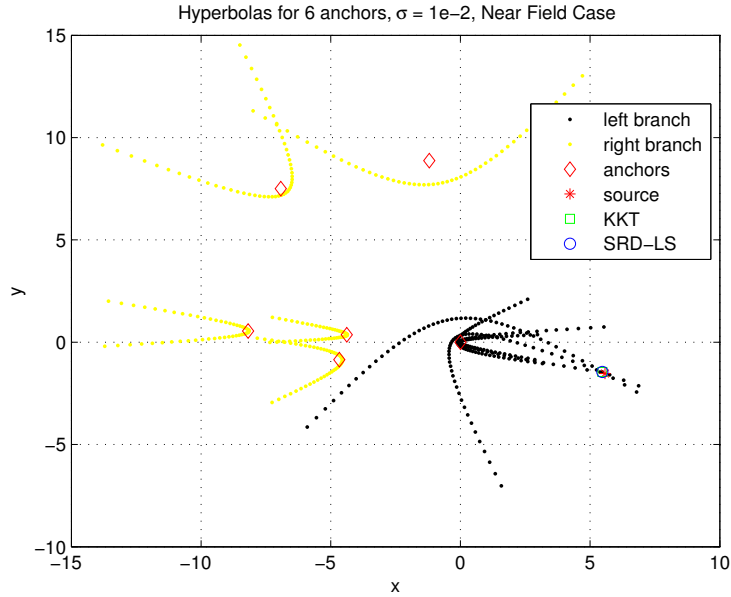


FIGURE 5.1: Hyperbolas and the source position estimated by KKT and SRD-LS methods.

TABLE 5.2: RMSE comparisons of SEARCH, KKT, SRD-LS and SI for far field case.

σ_{gaussian}	SEARCH	KKT	SRD-LS	SI
1e-4	0.3156	0.3222	0.3224	0.3270
1e-3	1.1821	1.1823	1.1834	1.2154
1e-2	3.6724	3.6725	3.6724	3.8401
1e-1	13.303	13.303	13.303	13.397

Far Field Case: An array with 11 sensors (including sensor 0) is considered. In each run, the coordinates of the 10 sensors that are not located at the origin were randomly generated from a uniform distribution over the square $[-10 \ 10] \times [-10 \ 10]$ m and the coordinates of the source were randomly generated from a uniform distribution over the square $[-200 \ -190] \times [-200 \ -190]$ m. The observed range-difference measurements were obtained as described above. Table 5.2 shows the RMSE of the methods for $\sigma_{\text{gaussian}} \in [10^{-4}, 10^{-1}]$ m. Again the results of the exact methods are nearly identical and better than the approximate one. The RMSEs are considerably higher than in Table 5.1, as the source is now predominantly located outside of the convex hull of the anchors, and localizing it becomes harder.

Example 2: This example is provided for direct comparison with Example 3 in [46]. Consider an array of $m = 5$ sensors in the plane ($n = 2$) whose coordinates are given by $\mathbf{a}_1 = (-5, -13)^T$ m, $\mathbf{a}_2 = (-12, 1)^T$ m, $\mathbf{a}_3 = (-1, -5)^T$ m, $\mathbf{a}_4 = (-9, -12)^T$ m, $\mathbf{a}_5 = (-3, -12)^T$ m. The source coordinates are $\mathbf{x} = (-5, 11)^T$ m. The observed range differences were obtained by adding white Gaussian noise with standard deviation 0.2 m

to the exact range differences. The exact range-differences and their noisy observations are given by

Exact: 11.9170 0.1235 4.4094 11.2622 11.0037

Noisy: 11.8829 0.1803 4.6399 11.2402 10.8183.

SRD-LS has a two-step solution procedure based on search and root finding techniques on defined intervals. When the first step fails, i.e., when the last component of a solution vector is negative, it invokes the second step that satisfies necessary optimality conditions. The first step often fails for problems with high noise levels. The estimated source positions given by each method are

$$\mathbf{x}_{\text{first step SRD-LS}} = (-7.1645, -12.2497)^T,$$

$$\mathbf{x}_{\text{SI}} = (-6.5644, -6.0209)^T,$$

$$\mathbf{x}_{\text{SEARCH}} = (-4.9800, 10.2834)^T,$$

$$\mathbf{x}_{\text{KKT}} = (-4.9798, 10.2786)^T \text{ and}$$

$$\mathbf{x}_{\text{second step SRD-LS}} = (-4.9798, 10.2786)^T.$$

For this setup SRD-LS is unable to give an accurate result without the second step. It is worth to point out that proposed methods do not need any special procedure to check if the solution is correct or not or take a decision among intervals, except calculating the bounds of the bisection interval.

5.4 Conclusion

TDOA based source localization leads to a nonconvex optimization problem whose exact solution or global minimum is difficult to find. To cope with this difficulty, squared range differences are used which leads to another (approximate) nonconvex optimization problem whose solution can be efficiently and globally obtained. Several techniques are proposed to find its global minimum. The proposed method KKT, which resorts to bisection method and KKT conditions, attains the exact solution with simple formulations when the source position is expressed in polar coordinates. Additionally, simulations show that the accuracies of the proposed methods are good and diminish for far-field case due to the source being outside of the convex hull of the anchors.

Chapter 6

Conclusion and Outlook

6.1 Conclusion

This thesis proposed several robust algorithms for source localization and sensor network localization under different measurement models (TOA, TDOA and RSS) and noise assumptions (Gaussian and Laplacian). The common theme is to determine the unknown positions by solving optimization problems that provide a solid framework even under challenging geometries and strong measurement noise, where the intuition behind heuristic/geometric methods might fail. A strong emphasis is placed on formulating relaxed convex problems, whose global minima may be determined easily, efficiently, and reliably with general-purpose solvers. Simulation results show that these relaxed problems yield very good localization accuracy, often close to the CRLB. In some cases these relaxations are used as initialization to true MLE methods, in which case convergence to undesirable minima of the latter is almost completely avoided, and near-optimal performance is consistently obtained. On a practical note, the proposed algorithmic constructions for localization are easy to implement, often involving the solution of a single optimization problem, thus making them very well suited for rapid prototyping. This contrasts with other high-performance (near-MLE) approaches available in the literature, which involve a number of relatively elaborate steps that require considerable effort to set up and tune. Detailed conclusions for the various methods are given next.

The nonconvex ML based source localization problem using TOA measurements was tackled for Gaussian and Laplacian noise models in 2D and higher space dimensions. The proposed range based source localization algorithms have a flavor of AOA localization. SLCP is derived by formulating the original problem as an optimization problem in the complex plane. And then it takes advantage of the nearly convex nature of the resulting cost function and constraint set to obtain a SDP relaxation. This essentially involves

dropping a rank constraint, which was found in simulations that it has a negligible impact on the accuracy of the solution in many scenarios. SLNN is proposed as an extension of SLCP to 3D and higher dimensions by formulating it as an optimization problem using nuclear norms and SDR. Similarly, source localization is solved by resorting to ℓ_1 -norm when the noise on the observations is Laplacian, i.e., outliers case. The key insight for this setup is to reformulate the non-differentiable log-likelihood function for Laplacian noise as a reweighted version of the Gaussian log-likelihood where the weights become optimization variables.

Simulation results show that, for Gaussian noise, the proposed algorithms are more accurate than linearization approaches and those relying on squared ranges. Broadly, their accuracy is comparable to state-of-the-art relaxation-based methods and to (nonrelaxed) ML methods. In the presence of outliers the ℓ_1 -based algorithms clearly outperform all the remaining ones. Overall, SL- ℓ_1 SD emerged as a versatile algorithm that delivers very good performance under different types of disturbance and whose moderate complexity scales favorably with the number of anchors and the ambient space dimension. Experimental results demonstrated the feasibility of the algorithms in a practical centralized indoor localization testbed.

An ML-based technique is presented to solve a SLAT problem using a two-phase approach under Gaussian or Laplacian noise. A MM method is proposed to iteratively maximize the nonconvex likelihood function, for which a good initial point is required. To that end, two initialization schemes are investigated based on EDM completion and source localization (SLCP/SLNN/SL- ℓ_1 s) that bypass the need for strong priors on sensor/target positions. After acquiring an initial block of range measurements for the startup phase, a SNL method based on EDM completion was used to estimate the node positions and some of the target locations. As EDM completion is not scalable, after startup, an alternative, lightweight, incremental initialization scheme is used as additional target range measurements become available. The SLCP/SLNN or SL- ℓ_1 s time-recursive methods fix the already estimated positions whenever a new one is to be determined; afterwards all positions are given as initialization to the likelihood refinement methods. With this methodology, a good initialization and a scalable solution for the SLAT problem is guaranteed. Moreover, the details of the proposed cost functions are different for Gaussian and Laplacian cases, but robustness to range errors is gained relative to other methods by matching plain distances (as opposed to squared ones, which are more tractable and popular, but lead to worse accuracy) and using consistent cost functions at each step of both cases.

Simulation results showed that the SLAT method nearly attains the CRLB under moderate Gaussian noise. In the presence of outliers, both EDM-R- ℓ_1 and SL- ℓ_1 provide

more accurate initial position estimates than other existing methods. Importantly, the algorithms based on ℓ_1 -norm optimization exhibited robust behaviour in simulation not only for Laplacian outliers, but also for an alternative outlier generation technique that did not match the underlying Laplacian modelling assumptions. It is demonstrated experimentally that the proposed scheme can track a target and localize sensors to within about 4 cm accuracy in a 3D indoor environment using mixed ultrasound-RF ranging.

Our SLAT approach is a type of SNL problem. In other words, in SNL problem, each position in target trajectory can be assumed as an individual target and inter-target and inter-sensor measurements beside sensor-target measurements are collected. Therefore, similar formulations of EDM completion are applied to harder problems of cooperative sensor network localization based on TOA with unknown turn-around time and RSS with unknown transmit power which are still relatively unexplored in the literature. Simulations showed that the MLE initialized with the proposed method for TOA based systems attains the CRLB. The algorithm proposed for RSS case is better than a recently published method both in accuracy and computational complexity. Moreover, the main conclusion is that the cooperation among sources/targets provides accurate localization even if some sources/targets are connected only to few anchors.

This thesis addresses TDOA based source localization which is hard to be solved with plain range differences. Although, squaring measurements is contrary to our preferred methodology, and it does impact performance, the difficulty of solving a nonconvex optimization problem of TDOA based source localization was overcome by reformulating it as an approximate nonconvex optimization problem with squared range differences. At each bisection iteration, the proposed method solves a variation of the trust region sub-problem, for which optimality conditions and approaches to obtain the global minimizer are known. Hence the exact solution is obtained with simple formulation by expressing the source position in polar coordinates. It is shown that the accuracy of the proposed method is good and diminishes when the source is outside of the convex hull of the anchors.

6.2 Outlook

The proposed methods for TOA based SL have very good accuracy with moderate computational complexity. Implementing those algorithms in a faster way is still an open question for us. What's seen from the literature and the performances of the proposed algorithms, TOA based SL under Gaussian noise is a saturated area. However, more accurate and faster methods might be derived for Laplacian noise/outlier/NLOS.

The SLAT algorithm uses modified EDM completion problem as an initialization technique under Gaussian and Laplacian noise. A faster implementation or formulation of EDM completion is still needed for the SLAT algorithm to be more feasible for large-scale real world applications. For the time being, the SLAT algorithm does not consider target dynamics. With the inclusion of target dynamics, more accurate results might be obtained.

The proposed methods for SNL with TOA in the presence of unknown turn-around time and SNL with RSS in the presence of unknown transmit power resort to EDM completion which uses squared measurements. New methods using plain measurements might be derived to obtain more accurate results. Additionally, the former exploit a heuristic to sidestep the difficulty induced by one of those convex relaxations. This issue needs further exploration.

Our algorithm for TDOA based source localization employs squared range differences to avoid the difficulty of solving a harder problem. Can the above proposed methods for TOA based SL be adapted to solve TDOA based SL with plain measurements? This needs more attention.

Lastly, most clocks at sensors are not so precise because the frequency, the rate at which a clock progresses, is never exactly right. Even a frequency deviation of only 0.001% would bring a clock error of about one second per day. Moreover, there is not only a clock offset, due to internal delays or the lack of a common time origin, but also clock drift which is hard to predict because it depends on the deviation from the ideal frequency and on a few environmental parameters, i.e, temperature, power, voltage, and pressure [118]. This makes time-based localization and synchronization tightly coupled and challenging. Chapter 4 discusses this problem only in the existence of clock offsets for cooperative sensor networks. However, it might be interesting to solve joint synchronization and localization with different clock models which consider not only the clock offset but also other clock parameters.

Appendix A

Equivalence of (2.1) and (2.2)

(2.2) can be written as

$$\begin{aligned} & \underset{\mathbf{x}}{\text{minimize}} \quad \underset{\mathbf{y}_i}{\text{minimize}} \quad \sum_{i=1}^m \|\mathbf{x} - \mathbf{y}_i\|^2 \\ & \text{subject to} \quad \|\mathbf{a}_i - \mathbf{y}_i\| = r_i \quad i = 1, \dots, m. \end{aligned} \tag{A.1}$$

Given \mathbf{x} , the inner optimization problem is separable. Defining $\boldsymbol{\eta}_i = \frac{\mathbf{y}_i - \mathbf{a}_i}{r_i}$ it can be solved for $\mathbf{y}_1, \dots, \mathbf{y}_m$ by individually solving the subproblems

$$\begin{aligned} & \underset{\boldsymbol{\eta}_i}{\text{minimize}} \quad \|\mathbf{x} - r_i \boldsymbol{\eta}_i - \mathbf{a}_i\|^2 = \|\mathbf{x} - \mathbf{a}_i\|^2 + r_i^2 \|\boldsymbol{\eta}_i\|^2 - 2r_i \boldsymbol{\eta}_i^T (\mathbf{x} - \mathbf{a}_i) \\ & \text{subject to} \quad \|\boldsymbol{\eta}_i\| = 1, \end{aligned} \tag{A.2}$$

or, equivalently,

$$\begin{aligned} & \underset{\boldsymbol{\eta}_i}{\text{maximize}} \quad \boldsymbol{\eta}_i^T (\mathbf{x} - \mathbf{a}_i) \\ & \text{subject to} \quad \|\boldsymbol{\eta}_i\| = 1, \end{aligned} \tag{A.3}$$

The optimal solution of (A.3) is clearly given by $\boldsymbol{\eta}_i = \frac{\mathbf{x} - \mathbf{a}_i}{\|\mathbf{x} - \mathbf{a}_i\|}$, leading to an optimal cost in (A.2) $\|\mathbf{x} - \mathbf{a}_i\|^2 + r_i^2 - 2r_i \|\mathbf{x} - \mathbf{a}_i\| = (\|\mathbf{x} - \mathbf{a}_i\| - r_i)^2$. Substituting the sum of these optimal costs for $i = 1, \dots, m$ back into (A.1) yields an unconstrained problem whose cost function is given by (2.1).

Appendix B

Proof of Lemma 2.4.1.1

The proof of Lemma 2.4.1.1 relies on a result, interesting in its own right, that characterizes the convex hull of the set of 3×3 rank-1 matrices built from complex vectors with unit-magnitude components.

Lemma B.0.0.1. Let

$$\mathcal{A} = \{\boldsymbol{\theta}\boldsymbol{\theta}^H : \boldsymbol{\theta} \in \mathbb{C}^3, |\theta_i| = 1\}, \quad (\text{B.1})$$

$$\mathcal{B} = \{\boldsymbol{\Phi} \in \mathbb{C}^{3 \times 3} : \boldsymbol{\Phi} \succeq 0, \phi_{ii} = 1\}. \quad (\text{B.2})$$

then $\mathcal{B} = \text{co}(\mathcal{A})$.

Proof. $\text{co}(\mathcal{A}) \subset \mathcal{B}$ is straightforward since \mathcal{B} is convex and $\mathcal{A} \subset \mathcal{B}$. For the reverse direction $\text{co}(\mathcal{A}) \supset \mathcal{B}$ the goal is to find, for every $\boldsymbol{\Phi} \in \mathcal{B}$, matrices $\boldsymbol{\Theta}_i \in \mathcal{A}$ and nonzero scalars $\lambda_i \geq 0$, with $\sum_i \lambda_i = 1$, such that $\boldsymbol{\Phi} = \sum_i \lambda_i \boldsymbol{\Theta}_i$.

Note that both \mathcal{A} and \mathcal{B} are invariant under the (unitary) similarity operation

$$\mathbf{M} \rightarrow \mathbf{P}\mathbf{M}\mathbf{P}^H, \quad (\text{B.3})$$

where \mathbf{P} is the product of a permutation and a diagonal unitary matrix. In other words, rows and columns can be simultaneously permuted and the i -th row and i -th column are multiplied by a unit-magnitude complex number. Thus, it can be assumed without loss of generality that $\boldsymbol{\Phi}$ is of the form

$$\boldsymbol{\Phi} = \begin{bmatrix} 1 & a & b \\ a & 1 & z^* \\ b & z & 1 \end{bmatrix}, \quad 0 \leq a \leq b, \quad z \in \mathbb{C}. \quad (\text{B.4})$$

Since $\Phi \succeq 0$, we must have $a \leq 1$, $b \leq 1$, $|z| \leq 1$ and

$$0 \leq |\Phi| = 1 - a^2 - b^2 - |z|^2 + 2ab \operatorname{Re}\{z\}, \quad (\text{B.5})$$

which, for $z = x + jy$, reads

$$(x - ab)^2 + y^2 \leq (1 - a^2)(1 - b^2). \quad (\text{B.6})$$

For fixed a, b this inequality describes a circle (with interior) in the (x, y) plane, centered on $(ab, 0)$. Since any point in the interior of a circle can be written as a convex combination of two points on its boundary, it can be assumed that there is an equality in (B.6). Thus, from now on it is assumed that

$$z = ab + \sqrt{(1 - a^2)(1 - b^2)}e^{j\varphi}. \quad (\text{B.7})$$

Now the proof is completed by expressing such Φ as a convex combination of two matrices from \mathcal{A} . For given $0 \leq a \leq b \leq 1$ and $\varphi \in [0, 2\pi[$ one wants to find $\alpha, \beta, \gamma, \delta \in [0, 2\pi[$, and $0 \leq \lambda \leq 1$ such that

$$\Phi = \begin{bmatrix} 1 & a & b \\ a & 1 & z^* \\ b & z & 1 \end{bmatrix} = \lambda \begin{bmatrix} 1 \\ e^{j\alpha} \\ e^{j\beta} \end{bmatrix} \begin{bmatrix} 1 & e^{-j\alpha} & e^{-j\beta} \end{bmatrix} + (1 - \lambda) \begin{bmatrix} 1 \\ e^{j\gamma} \\ e^{j\delta} \end{bmatrix} \begin{bmatrix} 1 & e^{-j\gamma} & e^{-j\delta} \end{bmatrix}. \quad (\text{B.8})$$

Thus,

$$a = \lambda e^{j\alpha} + (1 - \lambda)e^{j\gamma}, \quad b = \lambda e^{j\beta} + (1 - \lambda)e^{j\delta}, \quad (\text{B.9})$$

$$z = \lambda e^{j(\beta - \alpha)} + (1 - \lambda)e^{j(\delta - \gamma)}. \quad (\text{B.10})$$

From the first two relations it is obtained

$$e^{j\gamma} = \frac{a - \lambda e^{j\alpha}}{1 - \lambda}, \quad e^{j\delta} = \frac{b - \lambda e^{j\beta}}{1 - \lambda}, \quad (\text{B.11})$$

and replacing these in the third relation yields, after simple manipulations,

$$z = ab + \frac{\lambda}{1 - \lambda}(e^{-j\alpha} - a)(e^{j\beta} - b). \quad (\text{B.12})$$

Before proceeding, a useful lemma from elementary geometry will be stated and proved:

Lemma B.0.0.2. Referring to Figure B.1(a), if A is a point inside a unit circle whose distance to the center is a , RS is any line through A , and PQ is a diameter through A , then

$$AR \cdot AS = AP \cdot AQ = (1 - a)(1 + a) = 1 - a^2. \quad (\text{B.13})$$

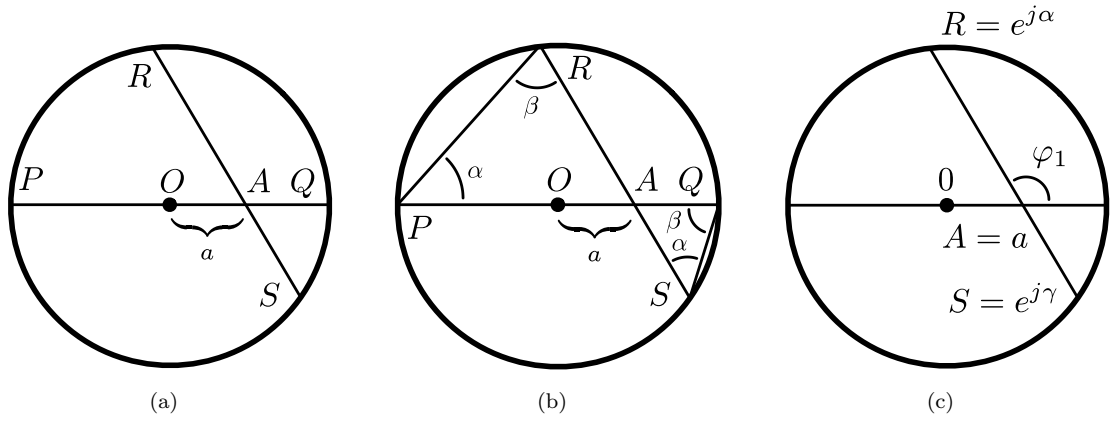


FIGURE B.1: Illustration of geometrical Lemma B.0.0.2 and its application to a convex combination on the unit circle.

Proof. Triangles APR and AQS , depicted in Figure B.1(b), are similar, hence

$$\frac{AP}{AS} = \frac{AR}{AQ}. \quad (\text{B.14})$$

□

The lemma above with parameters is used as depicted in Figure B.1(c). From $A = \lambda R + (1 - \lambda)S$ we have $\frac{AR}{AS} = \frac{1-\lambda}{\lambda}$, and by Lemma B.0.0.2 $AR \cdot AS = 1 - a^2$, hence

$$AR = \sqrt{\frac{1-\lambda}{\lambda}(1-a^2)}, \quad e^{j\alpha} = a + \sqrt{\frac{1-\lambda}{\lambda}(1-a^2)}e^{j\varphi_1}. \quad (\text{B.15})$$

Similarly, with $A = b$, $R = e^{j\beta}$, $S = e^{j\delta}$, and φ_2 instead of φ_1 , the following equality is obtained

$$e^{j\beta} = b + \sqrt{\frac{1-\lambda}{\lambda}(1-b^2)}e^{j\varphi_2}. \quad (\text{B.16})$$

Substituting (B.15), (B.16) back in (B.12) yields

$$z = ab + \sqrt{(1-a^2)(1-b^2)}e^{j(\varphi_2-\varphi_1)}, \quad (\text{B.17})$$

which has the same form as (B.7), obtained from the positive semidefinite condition for matrix Φ in (B.4).

Now it is argued that letting angle α go from 0 to 2π is equivalent to letting φ_1 cover an interval of length 2π as well (Figure B.1(c)). Fixing φ_1 , and consequently α , the two relations in (B.9), together with an arbitrary requirement that $\text{Im}\{e^{j\beta}\} \geq 0$, fix the

values¹ of β , γ , δ , λ , and, in particular, of φ_2 . Thus, $\varphi_2 = f(\varphi_1)$ is a continuous function of φ_1 .

When $\varphi_1 = 0$, φ_2 has a certain value, say, $\varepsilon_0 \in [0, \pi]$ (it can be computed, but is not needed in this proof). For $\varphi_1 = \pi$ it is straightforward to see that $\varphi_2 = \pi - \varepsilon_0$, and for $\varphi_1 = 2\pi$ it is again ε_0 . In particular the continuous function $\varphi_2 - \varphi_1$ takes values from $\varepsilon_0 - 0 = \varepsilon_0$ to $\varepsilon_0 - 2\pi$, i.e., modulo 2π it takes all values in $[0, 2\pi[$. Thus, for any given angle φ in (B.7), let φ_1 be such that $f(\varphi_1) - \varphi_1 = \varphi$, modulo 2π . Then, the corresponding α , β , γ , δ , and λ , as explained above, give the desired decomposition (B.8). \square

Now let us proceed and prove lemma 2.4.1.1 under the assumption of lemma B.0.0.1, thus tacitly assuming $m = 3$. Note that the proof is valid for arbitrary \mathbf{c} , \mathbf{r} in (2.8) and (2.11), i.e., it does not require that the structure for these vectors defined in (2.4) be taken into account.

Proof. Rewrite sets \mathcal{S} in (2.8) and \mathcal{T} in (2.11) using the notation (B.1)

$$\mathcal{S} = \{(\mathbf{c}^H \Theta \mathbf{c}, \mathbf{r}^T \Theta \mathbf{r}) : \Theta \in \mathcal{A}\}, \quad (\text{B.18})$$

$$\mathcal{T} = \{(\mathbf{c}^H \Phi \mathbf{c}, \mathbf{r}^T \Phi \mathbf{r}) : \Phi \in \text{co}(\mathcal{A})\}. \quad (\text{B.19})$$

Obviously $\mathcal{S} \subset \mathcal{T}$. Now let $\alpha \in [0, \frac{\pi}{2}]$ and define

$$(u_1, v_1) = \arg \max_{(u,v) \in \mathcal{T}} \langle (\cos \alpha, \sin \alpha), (u, v) \rangle. \quad (\text{B.20})$$

It is desired to show that

$$\langle (\cos \alpha, \sin \alpha), (u_1, v_1) \rangle = \max_{(u,v) \in \mathcal{S}} \langle (\cos \alpha, \sin \alpha), (u, v) \rangle, \quad (\text{B.21})$$

so that the inner product over \mathcal{S} attains the same maximum value as over the larger set \mathcal{T} , and the support hyperplanes with normal $(\cos \alpha, \sin \alpha)$ thus coincide for the two sets. It is enough to prove that there exists $(u', v') \in \mathcal{S}$ that attains the left-hand side of (B.21).

One can write $\Phi_1 \in \text{co}(\mathcal{A})$ which maximizes (B.20) as

$$\Phi_1 = \sum_i \lambda_i \theta_i \theta_i^H, \quad \lambda_i \geq 0, \quad \sum_i \lambda_i = 1, \quad |\theta_{ik}| = 1, \quad (\text{B.22})$$

¹Equivalently, note that fixing φ_1 fully defines the geometrical construction shown in Figure B.1(c), and thus fixes the values of γ and λ . Then, λ fully defines the corresponding construction for $A = b$ if, in addition, $\text{Im}\{e^{j\beta}\} \geq 0$ is specified, and thus fixes the values of β , δ , and φ_2 .

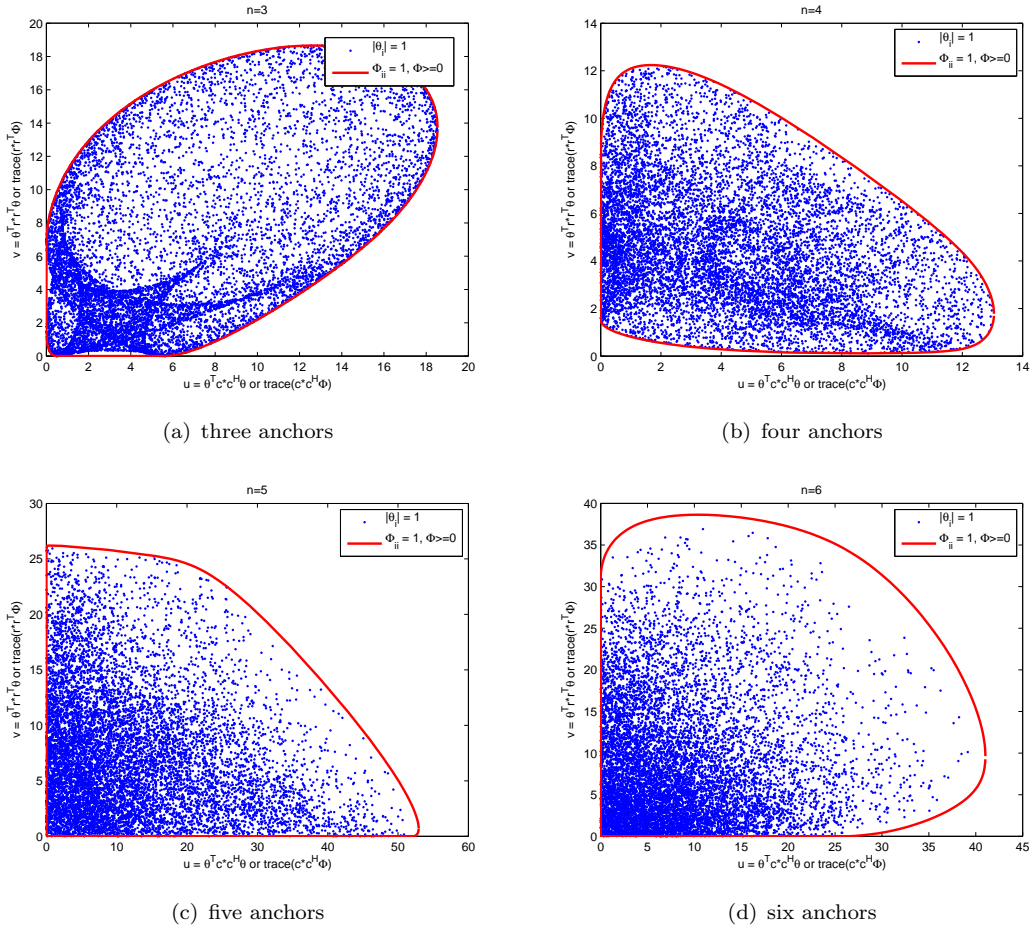


FIGURE B.2: The constraint set \mathcal{S} for randomly generated θ satisfying $|\theta_i| = 1$ and different numbers of randomly placed anchors. For each set the hypothesized convex hull, computed by relaxation of \mathcal{S} , is also depicted.

hence

$$\begin{aligned}
 \langle (\cos \alpha, \sin \alpha), (u_1, v_1) \rangle &= (\sqrt{\cos \alpha} \mathbf{c})^H \Phi_1(\underbrace{\sqrt{\cos \alpha} \mathbf{c}}_{\mathbf{p}}) + (\sqrt{\sin \alpha} \mathbf{r})^T \Phi_1(\underbrace{\sqrt{\sin \alpha} \mathbf{r}}_{\mathbf{q}}) \\
 &= \sum_i \lambda_i (\mathbf{p}^H \theta_i \theta_i^H \mathbf{p} + \mathbf{q}^H \theta_i \theta_i^H \mathbf{q}) = \sum_i \lambda_i (|\mathbf{p}^H \theta_i|^2 + |\mathbf{q}^H \theta_i|^2).
 \end{aligned} \tag{B.23}$$

Let i_0 be the index where the last summation attains its maximum value. Then

$$\langle (\cos \alpha, \sin \alpha), (u_1, v_1) \rangle \leq |\mathbf{p}^H \theta_{i_0}|^2 + |\mathbf{q}^H \theta_{i_0}|^2 = \langle (\cos \alpha, \sin \alpha), (\mathbf{c}^H \theta_{i_0} \theta_{i_0}^H \mathbf{c}, \mathbf{r}^T \theta_{i_0} \theta_{i_0}^H \mathbf{r}) \rangle, \tag{B.24}$$

which completes the proof because the second argument in the inner product is an element of \mathcal{S} .

□

Appendix C

Properties of Single-Source Localization using $\text{SL}\ell_1$

Proof of Lemma 2.4.2.1. To streamline the notation let us define $K_i = \|\mathbf{x} - \mathbf{a}_i\| - r_i$, and apply the KKT condition to the inner optimization problem in (2.20) while fixing \mathbf{x} . The Lagrangian function is

$$L(\boldsymbol{\lambda}, \gamma) = \sum_{i=1}^m \frac{K_i^2}{\lambda_i} + \gamma(\mathbf{1}^T \boldsymbol{\lambda} - 1). \quad (\text{C.1})$$

The KKT conditions are

$$\frac{dL}{d\lambda_i} = -\frac{K_i^2}{\lambda_i^2} + \gamma^* = 0, \quad \mathbf{1}^T \boldsymbol{\lambda} = 1. \quad (\text{C.2})$$

Using (C.2), it is found that $\lambda_i^* = \frac{K_i}{\sum_{i=1}^m K_i}$ as a solution of the inner optimization problem. Plugging the optimal $\boldsymbol{\lambda}$ in the cost function of (2.20) yields $(\sum_i K_i)^2$, thus establishing the equivalence with (2.19). \square

Approximation accuracy of $\boldsymbol{\Pi} = \lim_{\eta \rightarrow \infty} (\boldsymbol{\Lambda} + \eta \mathbf{1}\mathbf{1}^T)^{-1}$. To decide how large η should be, let us first define $\boldsymbol{\Pi}(\eta) = (\boldsymbol{\Lambda} + \eta \mathbf{1}\mathbf{1}^T)^{-1}$. The norm of the difference to the original definition of $\boldsymbol{\Pi}$ in (2.24) is given by

$$\begin{aligned} \|\boldsymbol{\Pi} - \boldsymbol{\Pi}(\eta)\|_F &= \|\boldsymbol{\Lambda}^{-1} \mathbf{1} [(\mathbf{1}^T \boldsymbol{\Lambda}^{-1} \mathbf{1})^{-1} - (\mathbf{1}^T \boldsymbol{\Lambda}^{-1} \mathbf{1} + \eta^{-1})^{-1}] \mathbf{1}^T \boldsymbol{\Lambda}^{-1}\|_F \\ &= \frac{\mathbf{1}^T \boldsymbol{\Lambda}^{-2} \mathbf{1}}{(\mathbf{1}^T \boldsymbol{\Lambda}^{-1} \mathbf{1})(\eta \mathbf{1}^T \boldsymbol{\Lambda}^{-1} \mathbf{1} + 1)}. \end{aligned} \quad (\text{C.3})$$

Now assume the most unfavourable case with identical $\lambda_i = \frac{1}{m}$, such that

$$\|\mathbf{\Pi} - \mathbf{\Pi}(\eta)\|_F = \frac{m}{\eta(m)^2 + 1} \leq \epsilon \Rightarrow \eta \geq \frac{1}{(m)\epsilon} - \frac{1}{(m)^2}. \quad (\text{C.4})$$

For $\epsilon = 10^{-4}$ and $m = 100$, for example, this yields $\eta \geq 10^2 - 10^{-4} \approx 10^2$, which is quite low and does not raise any numerical issues in commonly available convex optimization solvers. \square

Appendix D

Analysis of SLNN

Solution of the inner subproblem (2.33). For any optimization problem with differentiable objective and constraint functions for which strong duality holds, any set of primal and dual optimal points must satisfy the KKT conditions [23]. Define the Lagrangian of (2.33) with dual variable $\mathbf{\Lambda}$ as

$$L(\mathbf{V}, \mathbf{\Lambda}) = \text{tr}(\mathbf{C}^T \mathbf{U} \mathbf{V}) + \text{tr}(\mathbf{\Lambda}^T (\mathbf{V}^T \mathbf{V} - \mathbf{I}_n)). \quad (\text{D.1})$$

The first-order KKT conditions are given by

$$\nabla_{\mathbf{V}} L(\mathbf{V}, \mathbf{\Lambda}) = \mathbf{U}^T \mathbf{C} + \mathbf{V}(\mathbf{\Lambda} + \mathbf{\Lambda}^T) = \mathbf{0}, \quad (\text{D.2})$$

$$\mathbf{V}^T \mathbf{V} = \mathbf{I}_n, \quad (\text{D.3})$$

where (D.2) is obtained by setting to zero the gradient¹ of (D.1) with respect to \mathbf{V} , whereas (D.3) is the original orthogonality constraint in (2.33).

Premultiplying (D.2) with \mathbf{V}^T , taking the trace (i.e., taking the inner product with \mathbf{V}), and using (D.3) yields the optimal value for the cost function

$$\text{tr}(\mathbf{C}^T \mathbf{U} \mathbf{V}) = \text{tr}(\mathbf{V}^T \mathbf{U}^T \mathbf{C}) = -\text{tr}(\mathbf{\Lambda} + \mathbf{\Lambda}^T). \quad (\text{D.4})$$

But from $\mathbf{U}^T \mathbf{C} = -\mathbf{V}(\mathbf{\Lambda} + \mathbf{\Lambda}^T)$ in (D.2) both sides can be squared to get

$$\mathbf{C}^T \mathbf{U} \mathbf{U}^T \mathbf{C} = (\mathbf{\Lambda} + \mathbf{\Lambda}^T)^2. \quad (\text{D.5})$$

Hence, among candidate optimal points satisfying the KKT system, the cost function can be made as small as possible by choosing $\mathbf{\Lambda} + \mathbf{\Lambda}^T$ in (D.4) as a positive semidefinite matrix square root of the left-hand side of (D.5). Replacing this in (D.4) gives the final

¹We use the standard results $\frac{\partial}{\partial \mathbf{X}} \text{tr}(\mathbf{A}^T \mathbf{X}) = \mathbf{A}$ and $\frac{\partial}{\partial \mathbf{X}} \text{tr}(\mathbf{X} \mathbf{B} \mathbf{X}^T) = \mathbf{X}(\mathbf{B} + \mathbf{B}^T)$ [66, 119].

optimal cost

$$\mathrm{tr}(\mathbf{C}^T \mathbf{U} \mathbf{V}) = -\mathrm{tr}((\mathbf{C}^T \mathbf{U} \mathbf{U}^T \mathbf{C})^{\frac{1}{2}}) = -\|\mathbf{C}^T \mathbf{U}\|_N. \quad (\text{D.6})$$

□

Interestingly, note that the more usual Frobenius norm solves the following relaxed version of the inner subproblem (2.33)

$$\begin{aligned} & \underset{\mathbf{V}}{\text{minimize}} && \mathrm{tr}(\mathbf{C}^T \mathbf{U} \mathbf{V}) = \langle \mathbf{V}, \mathbf{U}^T \mathbf{C} \rangle \\ & \text{subject to} && \mathrm{tr}(\mathbf{V}^T \mathbf{V}) = \|\mathbf{V}\|_F^2 = n, \end{aligned} \quad (\text{D.7})$$

which is easily verified by writing the KKT system based on the Lagrange function $\mathrm{tr}(\mathbf{C}^T \mathbf{U} \mathbf{V}) + \lambda(\mathrm{tr}(\mathbf{V}^T \mathbf{V}) - n)$,

$$\mathbf{U}^T \mathbf{C} + 2\lambda \mathbf{V} = 0, \quad \mathrm{tr}(\mathbf{V}^T \mathbf{V}) = n, \quad (\text{D.8})$$

whose solution at the minimum is

$$\mathbf{V} = -\sqrt{n} \frac{\mathbf{U}^T \mathbf{C}}{\|\mathbf{U}^T \mathbf{C}\|_F}, \quad \lambda = \frac{\|\mathbf{U}^T \mathbf{C}\|_F}{2\sqrt{n}}, \quad (\text{D.9})$$

with optimal cost $-\sqrt{n}\|\mathbf{U}^T \mathbf{C}\|_F$. The minimum cost within the expanded domain of this relaxed subproblem will at least be as low as that of (2.33), hence $\|\mathbf{U}^T \mathbf{C}\|_N \leq \sqrt{n}\|\mathbf{U}^T \mathbf{C}\|_F$. On the other hand,

$$\|\mathbf{U}^T \mathbf{C}\|_N = \sqrt{(\sum_i \sigma_i)^2} \geq \sqrt{\sum_i \sigma_i^2} = \|\mathbf{U}^T \mathbf{C}\|_F, \quad (\text{D.10})$$

where σ_i denotes the i -th singular value of $\mathbf{U}^T \mathbf{C}$. Combining the two inequalities the bounds are

$$\|\mathbf{U}^T \mathbf{C}\|_F \leq \|\mathbf{U}^T \mathbf{C}\|_N \leq \sqrt{n}\|\mathbf{U}^T \mathbf{C}\|_F. \quad (\text{D.11})$$

Proof of equivalence between (2.36) and (2.37). First (2.37) is rewritten replacing the linear matrix inequality with an equivalent Schur complement

$$\begin{aligned} & \underset{\mathbf{W}, \mathbf{Z}}{\text{maximize}} && 2 \mathrm{tr}(\mathbf{Z}) + \frac{1}{m} \mathrm{tr}(\mathbf{r} \mathbf{r}^T \mathbf{W}) \\ & \text{subject to} && \mathbf{W} \succeq 0, \quad W_{ii} = 1 \\ & && \mathbf{Z}^2 \preceq \mathbf{C}^T \mathbf{W} \mathbf{C}, \quad \mathbf{Z} \succeq 0. \end{aligned} \quad (\text{D.12})$$

Let p_1^* and p_2^* be the optimal values of problems (2.36) and (D.12), respectively.

Choose a feasible point (\mathbf{Z}, \mathbf{W}) for the second problem, such that $0 \preceq \mathbf{Z}^2 \preceq \mathbf{C}^T \mathbf{W} \mathbf{C}$. This implies² $\mathbf{Z} \preceq (\mathbf{C}^T \mathbf{W} \mathbf{C})^{\frac{1}{2}}$, hence the values of the two objective functions satisfy

$$2 \operatorname{tr}(\mathbf{Z}) + \frac{1}{m} \operatorname{tr}(\mathbf{r} \mathbf{r}^T \mathbf{W}) \leq 2 \operatorname{tr}((\mathbf{C}^T \mathbf{W} \mathbf{C})^{\frac{1}{2}}) + \frac{1}{m} \operatorname{tr}(\mathbf{r} \mathbf{r}^T \mathbf{W}). \quad (\text{D.13})$$

In particular, choosing for (\mathbf{Z}, \mathbf{W}) the unique maximizer of (D.12), inequality (D.13) asserts that $p_1^* \geq p_2^*$.

For the converse choose a feasible point \mathbf{W} for the first problem and consider the eigendecomposition $\mathbf{C}^T \mathbf{W} \mathbf{C} = \mathbf{Q} \mathbf{\Lambda} \mathbf{Q}^T$. Now set $\mathbf{Z} = \mathbf{Q} \mathbf{\Lambda}^{\frac{1}{2}} \mathbf{Q}^T$, so that $\mathbf{Z}^2 = \mathbf{Q} \mathbf{\Lambda} \mathbf{Q}^T = \mathbf{C}^T \mathbf{W} \mathbf{C}$, and (\mathbf{W}, \mathbf{Z}) is therefore feasible for (D.12). For both problems the value of the cost function is

$$2 \operatorname{tr}(\mathbf{\Lambda}^{\frac{1}{2}}) + \frac{1}{m} \operatorname{tr}(\mathbf{r} \mathbf{r}^T \mathbf{W}). \quad (\text{D.14})$$

In particular, choosing for \mathbf{W} the maximizer of (2.36) the construction for \mathbf{Z} yields a feasible point (\mathbf{W}, \mathbf{Z}) for (D.12) where the objective function equals p_1^* . Therefore $p_1^* \leq p_2^*$, and coupling this with the converse inequality above we conclude that $p_1^* = p_2^*$ and the two problems are equivalent. \square

² $\mathbf{A} \succeq \mathbf{B} \succeq 0 \Rightarrow \mathbf{A}^{\frac{1}{2}} \succeq \mathbf{B}^{\frac{1}{2}} \succeq 0$ [120].

Appendix E

Derivation of CRLB for Source Localization Based on TOA

The log of the joint conditional pdf for TOA Source Localization problem for Gaussian case is (up to an additive constant)

$$\log f(\mathbf{r}|\mathbf{x}) = -\frac{1}{2\sigma^2} \sum_j (\|\mathbf{x} - \mathbf{a}_j\| - r_j)^2. \quad (\text{E.1})$$

where \mathbf{x} and \mathbf{r} denote the source position and the concatenation of all range measurements, respectively. The first derivative of (E.1) with respect to \mathbf{x} is

$$\nabla_{\mathbf{x}} \log f(\mathbf{r}|\mathbf{x}) = \frac{1}{\sigma^2} \sum_j (\|\mathbf{x} - \mathbf{a}_j\| - r_j) \frac{\mathbf{x} - \mathbf{a}_j}{\|\mathbf{x} - \mathbf{a}_j\|}. \quad (\text{E.2})$$

The second derivative of (E.1) with respect to \mathbf{x} is

$$\begin{aligned} \nabla_{\mathbf{x}}^2 \log f(\mathbf{r}|\mathbf{x}) = & -\frac{1}{\sigma^2} \sum_j \left[\frac{(\mathbf{x} - \mathbf{a}_j)(\mathbf{x} - \mathbf{a}_j)^T}{\|\mathbf{x} - \mathbf{a}_j\|^2} \right. \\ & \left. + \frac{\|\mathbf{x} - \mathbf{a}_j\| - r_j}{\|\mathbf{x} - \mathbf{a}_j\|} (\mathbf{I}_n - \frac{(\mathbf{x} - \mathbf{a}_j)(\mathbf{x} - \mathbf{a}_j)^T}{\|\mathbf{x} - \mathbf{a}_j\|^2}) \right]. \end{aligned} \quad (\text{E.3})$$

The Fisher information matrix, $F_{\mathbf{x}}$, is obtained by taking the negative expected value of (G.5) with respect to ranges as [71]

$$F_{\mathbf{x}} = -\mathbf{E}_{\mathbf{r}}\{\nabla_{\mathbf{x}}^2 \log f(\mathbf{r}|\mathbf{x})\} = \frac{1}{\sigma^2} \sum_j \frac{(\mathbf{x} - \mathbf{a}_j)(\mathbf{x} - \mathbf{a}_j)^T}{\|\mathbf{x} - \mathbf{a}_j\|^2}. \quad (\text{E.4})$$

The CRLB matrix in (2.67) is taken as the inverse of $F_{\mathbf{x}}$.

Appendix F

Convergence of Weighted Majorization Minimization

To prove (local) convergence of the weighted MM iteration (3.24) the Laplacian cost function (3.4) is first majorized at time t by

$$\Gamma_L^t(\mathbf{x}) = \frac{1}{2} \sum_{j \in \mathcal{S}} \sum_{i \in \mathcal{C}_j} \left\{ u_{ij}^t (f_{ij}(\mathbf{x}) - d_{ij})^2 + \frac{1}{u_{ij}^t} \right\} + \frac{1}{2} \sum_{j \in \mathcal{S}} \sum_{i \in \mathcal{B}_j} \left\{ v_{ij}^t (g_{ij}(\mathbf{x}) - d_{ij})^2 + \frac{1}{v_{ij}^t} \right\}, \quad (\text{F.1})$$

where f_{ij} , g_{ij} and u_{ij}^t , v_{ij}^t are defined in (3.12) and (3.23). The inequality $\Omega_L(\mathbf{x}) \leq \Gamma_L^t(\mathbf{x})$ follows from

$$\begin{aligned} \Gamma_L^t(\mathbf{x}) - \Omega_L(\mathbf{x}) &= \frac{1}{2} \sum_{j \in \mathcal{S}} \sum_{i \in \mathcal{C}_j} \left\{ u_{ij}^t (f_{ij}(\mathbf{x}) - d_{ij})^2 + \frac{1}{u_{ij}^t} - 2|f_{ij}(\mathbf{x}) - d_{ij}| \right\} \\ &\quad + \frac{1}{2} \sum_{j \in \mathcal{S}} \sum_{i \in \mathcal{B}_j} \left\{ v_{ij}^t (g_{ij}(\mathbf{x}) - d_{ij})^2 + \frac{1}{v_{ij}^t} - 2|g_{ij}(\mathbf{x}) - d_{ij}| \right\} \\ &= \frac{1}{2} \sum_{j \in \mathcal{S}} \sum_{i \in \mathcal{C}_j} \left\{ \sqrt{u_{ij}^t} |f_{ij}(\mathbf{x}) - d_{ij}| - \frac{1}{\sqrt{u_{ij}^t}} \right\}^2 \\ &\quad + \frac{1}{2} \sum_{j \in \mathcal{S}} \sum_{i \in \mathcal{B}_j} \left\{ \sqrt{v_{ij}^t} |g_{ij}(\mathbf{x}) - d_{ij}| - \frac{1}{\sqrt{v_{ij}^t}} \right\}^2 \geq 0. \end{aligned} \quad (\text{F.2})$$

It is easy to check that $\Omega_L(\mathbf{x}^t) = \Gamma_L^t(\mathbf{x}^t)$, so $\Gamma_L^t(\mathbf{x})$ has the properties of a true majorization function for the iterate \mathbf{x}^t . Now the same technique used in (3.13) is applied to

majorize (F.1) by a convex quadratic function of \mathbf{x} , yielding

$$\begin{aligned} \Omega_L(\mathbf{x}) \leq & \frac{1}{2} \sum_{j \in \mathcal{S}} \sum_{i \in \mathcal{C}_j} \left\{ u_{ij}^t (f_{ij}^2(\mathbf{x}) - 2d_{ij} f_{ij}(\mathbf{x}^t) - 2d_{ij} \langle \nabla f_{ij}(\mathbf{x}^t), (\mathbf{x} - \mathbf{x}^t) \rangle + d_{ij}^2) + \frac{1}{u_{ij}^t} \right\} \\ & + \frac{1}{2} \sum_{j \in \mathcal{S}} \sum_{i \in \mathcal{B}_j} \left\{ v_{ij}^t (g_{ij}^2(\mathbf{x}) - 2d_{ij} g_{ij}(\mathbf{x}^t) - 2d_{ij} \langle \nabla g_{ij}(\mathbf{x}^t), (\mathbf{x} - \mathbf{x}^t) \rangle + d_{ij}^2) + \frac{1}{v_{ij}^t} \right\}. \end{aligned} \tag{F.3}$$

As before, equality holds for $\mathbf{x} = \mathbf{x}^t$, so the right-hand side of (F.3) is still a valid majorization function. Discarding constant terms the weighted MM iteration (3.24) results.

Appendix G

Derivation of CRLB for Sensor Network Localization

The log of the joint conditional pdf for the SLAT problem is (up to an additive constant)

$$\log f(\mathbf{d}|\mathbf{x}) = -\frac{1}{2\sigma^2} \left\{ \sum_{j \in \mathcal{S}} \sum_{i \in \mathcal{C}_j} (\|\mathbf{x}_i - \mathbf{e}_j\| - d_{ij})^2 + \sum_{j \in \mathcal{S}} \sum_{i \in \mathcal{B}_j} (\|\mathbf{a}_i - \mathbf{e}_j\| - d_{ij})^2 \right\}, \quad (\text{G.1})$$

where, similarly to \mathbf{x} , \mathbf{d} denotes the concatenation of all range measurements. Let us define matrices \mathbf{M}_{ij} and \mathbf{N}_j that extract individual positions or their differences from the vector of concatenated coordinates¹ \mathbf{x} as follows

$$\mathbf{M}_{ij}\mathbf{x} = \mathbf{x}_i - \mathbf{e}_j, \quad \mathbf{N}_j\mathbf{x} = -\mathbf{e}_j. \quad (\text{G.2})$$

Thus, (G.1) is rewritten as

$$\log f(\mathbf{d}|\mathbf{x}) = -\frac{1}{2\sigma^2} \left\{ \sum_{j \in \mathcal{S}} \sum_{i \in \mathcal{C}_j} (\|\mathbf{M}_{ij}\mathbf{x}\| - d_{ij})^2 + \sum_{j \in \mathcal{S}} \sum_{i \in \mathcal{B}_j} (\|\mathbf{a}_i + \mathbf{N}_j\mathbf{x}\| - d_{ij})^2 \right\}. \quad (\text{G.3})$$

¹If sensor positions \mathbf{x}_i and target positions \mathbf{e}_j are concatenated into vector \mathbf{x} according to the order $\mathbf{x}_1, \dots, \mathbf{x}_n, \mathbf{e}_1, \dots, \mathbf{e}_m$, the selection matrices are explicitly given by

$$\mathbf{M}_{ij} = [\mathbf{z}_i^T \otimes \mathbf{I}_2 \quad -\mathbf{v}_j^T \otimes \mathbf{I}_2], \quad \mathbf{N}_j = [\mathbf{0}_{2 \times 2n} \quad -\mathbf{v}_j^T \otimes \mathbf{I}_2],$$

where vector $\mathbf{z}_i \in \mathbb{R}^n$ has 1 in the i -th component and zeros elsewhere, and similarly for $\mathbf{v}_j \in \mathbb{R}^m$.

The first derivative of (G.3) with respect to \mathbf{x} is

$$\begin{aligned} \nabla_{\mathbf{x}} \log f(\mathbf{d}|\mathbf{x}) = & -\frac{1}{\sigma^2} \left\{ \sum_{j \in \mathcal{S}} \sum_{i \in \mathcal{C}_j} (\|\mathbf{M}_{ij}\mathbf{x}\| - d_{ij}) \frac{\mathbf{M}_{ij}^T \mathbf{M}_{ij} \mathbf{x}}{\|\mathbf{M}_{ij}\mathbf{x}\|} \right. \\ & \left. + \sum_{j \in \mathcal{S}} \sum_{i \in \mathcal{B}_j} (\|\mathbf{a}_i + \mathbf{N}_j \mathbf{x}\| - d_{ij}) \frac{\mathbf{N}_j^T (\mathbf{a}_i + \mathbf{N}_j \mathbf{x})}{\|\mathbf{a}_i + \mathbf{N}_j \mathbf{x}\|} \right\}. \end{aligned} \quad (\text{G.4})$$

The second derivative of (G.3) with respect to \mathbf{x} is

$$\begin{aligned} \nabla_{\mathbf{x}}^2 \log f(\mathbf{d}|\mathbf{x}) = & -\frac{1}{\sigma^2} \left\{ \sum_{j \in \mathcal{S}} \sum_{i \in \mathcal{C}_j} \left\{ \frac{\mathbf{M}_{ij}^T \mathbf{M}_{ij} \mathbf{x} \mathbf{x}^T \mathbf{M}_{ij}^T \mathbf{M}_{ij}}{\|\mathbf{M}_{ij}\mathbf{x}\|^2} \right. \right. \\ & \left. \left. + \frac{\|\mathbf{M}_{ij}\mathbf{x}\| - d_{ij}}{\|\mathbf{M}_{ij}\mathbf{x}\|} \left(\mathbf{M}_{ij}^T \mathbf{M}_{ij} - \frac{\mathbf{M}_{ij}^T \mathbf{M}_{ij} \mathbf{x} \mathbf{x}^T \mathbf{M}_{ij}^T \mathbf{M}_{ij}}{\|\mathbf{M}_{ij}\mathbf{x}\|^2} \right) \right\} \right. \\ & \left. + \sum_{j \in \mathcal{S}} \sum_{i \in \mathcal{B}_j} \left\{ \frac{\mathbf{N}_j^T (\mathbf{a}_i + \mathbf{N}_j \mathbf{x}) (\mathbf{a}_i + \mathbf{N}_j \mathbf{x})^T \mathbf{N}_j^T}{\|\mathbf{a}_i + \mathbf{N}_j \mathbf{x}\|^2} + \frac{\|\mathbf{a}_i + \mathbf{N}_j \mathbf{x}\| - d_{ij}}{\|\mathbf{a}_i + \mathbf{N}_j \mathbf{x}\|} \right. \right. \\ & \left. \left. \left(\mathbf{N}_j^T \mathbf{N}_j - \frac{\mathbf{N}_j^T (\mathbf{a}_i + \mathbf{N}_j \mathbf{x}) (\mathbf{a}_i + \mathbf{N}_j \mathbf{x})^T \mathbf{N}_j^T}{\|\mathbf{a}_i + \mathbf{N}_j \mathbf{x}\|^2} \right) \right\} \right\}. \end{aligned} \quad (\text{G.5})$$

The Fisher information matrix, $F_{\mathbf{x}}$, is obtained by taking the negative expected value of (G.5) with respect to ranges as [71]

$$\begin{aligned} F_{\mathbf{x}} = -\text{E}_{\mathbf{d}} \{ \nabla_{\mathbf{x}}^2 \log f(\mathbf{d}|\mathbf{x}) \} = & \frac{1}{\sigma^2} \left\{ \sum_{j \in \mathcal{S}} \sum_{i \in \mathcal{C}_j} \frac{\mathbf{M}_{ij}^T \mathbf{M}_{ij} \mathbf{x} \mathbf{x}^T \mathbf{M}_{ij}^T \mathbf{M}_{ij}}{\|\mathbf{M}_{ij}\mathbf{x}\|^2} \right. \\ & \left. + \sum_{j \in \mathcal{S}} \sum_{i \in \mathcal{B}_j} \frac{\mathbf{N}_j^T (\mathbf{a}_i + \mathbf{N}_j \mathbf{x}) (\mathbf{a}_i + \mathbf{N}_j \mathbf{x})^T \mathbf{N}_j^T}{\|\mathbf{a}_i + \mathbf{N}_j \mathbf{x}\|^2} \right\}. \end{aligned} \quad (\text{G.6})$$

The CRLB matrix in (3.28) is taken as the inverse of $F_{\mathbf{x}}$.

Appendix H

Derivation of CRLB for Sensor Network Localization with Unknown Turn-Around Time or Transmit Power

H.1 TOA based with Unknown Turn-Around Time

The log of the joint conditional pdf for the TOA based cooperative sensor network localization problem with unknown turn-around time is (up to an additive constant)

$$\log f(\mathbf{d}|\mathbf{S}, \mathbf{T}) = -\frac{1}{2\sigma^2} \left\{ \sum_{j \in \mathcal{S}} \sum_{i \in \mathcal{B}_j} (d_{ij} - T_j - 2\|\mathbf{a}_i - \mathbf{s}_j\|)^2 + \sum_{j \in \mathcal{S}} \sum_{i \in \mathcal{C}_j} (d_{ij} - T_j - 2\|\mathbf{s}_i - \mathbf{s}_j\|)^2 \right\}, \quad (\text{H.1})$$

where \mathbf{S} , \mathbf{T} and \mathbf{d} are the concatenation of all target positions, their unknown turn around times (converted to distance) and distance measurements, respectively. The Fisher information matrix¹,

$$\mathbf{F}_{\text{TOA}} = \begin{bmatrix} F_{xx} & F_{yx} & F_{Tx} \\ F_{xy} & F_{yy} & F_{Ty} \\ F_{xT} & F_{yT} & F_{TT} \end{bmatrix}, \quad (\text{H.2})$$

¹The generalization to three-dimensional space is straightforward.

is obtained by taking the negative expected value of the second derivative of (H.1) with respect to \mathbf{S} and \mathbf{T} [71], where

$$\begin{aligned}
 F_{xx} &= \begin{cases} \gamma \left\{ \sum_{k \in \mathcal{B}_j} \frac{(a_{kx} - s_{jx})^2}{\|\mathbf{a}_k - \mathbf{s}_j\|^2} + \sum_{k \in \mathcal{C}_j} \frac{2(s_{kx} - s_{jx})^2}{\|\mathbf{s}_k - \mathbf{s}_j\|^2} \right\} & , i = j \\ -\gamma \frac{2(s_{jx} - s_{ix})^2}{\|\mathbf{s}_j - \mathbf{s}_i\|^2} & , i \neq j \end{cases} \\
 F_{yy} &= \begin{cases} \gamma \left\{ \sum_{k \in \mathcal{B}_j} \frac{(a_{ky} - s_{jy})^2}{\|\mathbf{a}_k - \mathbf{s}_j\|^2} + \sum_{k \in \mathcal{C}_j} \frac{2(s_{ky} - s_{jy})^2}{\|\mathbf{s}_k - \mathbf{s}_j\|^2} \right\} & , i = j \\ -\gamma \frac{2(s_{jy} - s_{iy})^2}{\|\mathbf{s}_j - \mathbf{s}_i\|^2} & , i \neq j \end{cases} \\
 F_{yx} &= \begin{cases} \gamma \left\{ \sum_{k \in \mathcal{B}_j} \frac{(a_{ky} - s_{jy})(a_{kx} - s_{jx})}{\|\mathbf{a}_k - \mathbf{s}_j\|^2} + \sum_{k \in \mathcal{C}_j} \frac{2(s_{ky} - s_{jy})(s_{kx} - s_{jx})}{\|\mathbf{s}_k - \mathbf{s}_j\|^2} \right\} & , i = j \\ -\gamma \frac{2(s_{jy} - s_{iy})(s_{jx} - s_{ix})}{\|\mathbf{s}_j - \mathbf{s}_i\|^2} & , i \neq j \end{cases} \\
 F_{xT} &= \begin{cases} -\rho \left\{ \sum_{k \in \mathcal{B}_j} \frac{(a_{kx} - s_{jx})}{\|\mathbf{a}_k - \mathbf{s}_j\|} + \sum_{k \in \mathcal{C}_j} \frac{(s_{kx} - s_{jx})}{\|\mathbf{s}_k - \mathbf{s}_j\|} \right\} & , i = j \\ \rho \frac{(s_{jx} - s_{ix})}{\|\mathbf{s}_j - \mathbf{s}_i\|} & , i \neq j \end{cases} \\
 F_{yT} &= \begin{cases} -\rho \left\{ \sum_{k \in \mathcal{B}_j} \frac{(a_{ky} - s_{jy})}{\|\mathbf{a}_k - \mathbf{s}_j\|} + \sum_{k \in \mathcal{C}_j} \frac{(s_{ky} - s_{jy})}{\|\mathbf{s}_k - \mathbf{s}_j\|} \right\} & , i = j \\ \rho \frac{(s_{jy} - s_{iy})}{\|\mathbf{s}_j - \mathbf{s}_i\|} & , i \neq j \end{cases} \\
 F_{TT} &= \begin{cases} \frac{1}{\sigma^2} \left\{ \sum_{k \in \mathcal{B}_j} 1 + \sum_{k \in \mathcal{C}_j} 1 \right\} & , i = j \\ 0 & , j \neq i \end{cases}
 \end{aligned}$$

and $\gamma = \frac{4}{(\sigma)^2}$, $\rho = \frac{2}{(\sigma)^2}$. The CRLB for this problem is taken as the inverse of \mathbf{F}_{TOA} .

H.2 RSS based with Unknown Transmit Power

The log of the joint conditional pdf for the RSS based cooperative sensor network localization problem with unknown transmit power is (up to an additive constant)

$$\begin{aligned}
 \log f(\mathbf{q}|\mathbf{S}, \mathbf{P}) &= -\frac{1}{2\sigma^2} \left\{ \sum_{j \in \mathcal{S}} \sum_{i \in \mathcal{B}_j} (P_{ij} - P_j - 10\beta \log_{10}(\|\mathbf{a}_i - \mathbf{s}_j\|))^2 \right. \\
 &\quad \left. + \sum_{j \in \mathcal{S}} \sum_{i \in \mathcal{C}_j} (P_{ij} - P_j - 10\beta \log_{10}(\|\mathbf{s}_i - \mathbf{s}_j\|))^2 \right\}, \tag{H.3}
 \end{aligned}$$

where \mathbf{S} , \mathbf{P} and \mathbf{q} are the concatenation of all source positions, their unknown transmit powers and RSS measurements, respectively. The Fisher information matrix,

$$\mathbf{F}_{\text{RSS}} = \begin{bmatrix} F_{xx} & F_{yx} & F_{Px} \\ F_{xy} & F_{yy} & F_{Py} \\ F_{xp} & F_{yp} & F_{PP} \end{bmatrix}, \tag{H.4}$$

is obtained by taking the negative expected value of the second derivative of (H.3) with respect to \mathbf{S} and \mathbf{P} as [71] where

$$\begin{aligned}
 F_{xx} &= \begin{cases} \gamma \left\{ \sum_{k \in \mathcal{B}_j} \frac{(a_{kx} - s_{jx})^2}{\|\mathbf{a}_k - \mathbf{s}_j\|^4} + \sum_{k \in \mathcal{C}_j} \frac{(s_{kx} - s_{jx})^2}{\|\mathbf{s}_k - \mathbf{s}_j\|^4} \right\} & , i = j \\ -\gamma \frac{(s_{jx} - s_{ix})^2}{\|\mathbf{s}_j - \mathbf{s}_i\|^4} & , i \neq j \end{cases} \\
 F_{yy} &= \begin{cases} \gamma \left\{ \sum_{k \in \mathcal{B}_j} \frac{(a_{ky} - s_{jy})^2}{\|\mathbf{a}_k - \mathbf{s}_j\|^4} + \sum_{k \in \mathcal{C}_j} \frac{(s_{ky} - s_{jy})^2}{\|\mathbf{s}_k - \mathbf{s}_j\|^4} \right\} & , i = j \\ -\gamma \frac{(s_{jy} - s_{iy})^2}{\|\mathbf{s}_j - \mathbf{s}_i\|^4} & , i \neq j \end{cases} \\
 F_{yx} &= \begin{cases} \gamma \left\{ \sum_{k \in \mathcal{B}_j} \frac{(a_{ky} - s_{jy})(a_{kx} - s_{jx})}{\|\mathbf{a}_k - \mathbf{s}_j\|^4} + \sum_{k \in \mathcal{C}_j} \frac{(s_{ky} - s_{jy})(s_{kx} - s_{jx})}{\|\mathbf{s}_k - \mathbf{s}_j\|^4} \right\} & , i = j \\ -\gamma \frac{(s_{jy} - s_{iy})(s_{jx} - s_{ix})}{\|\mathbf{s}_j - \mathbf{s}_i\|^4} & , i \neq j \end{cases} \\
 F_{xP} &= \begin{cases} \rho \left\{ \sum_{k \in \mathcal{B}_j} \frac{a_{kx} - s_{jx}}{\|\mathbf{a}_k - \mathbf{s}_j\|^2} + \sum_{k \in \mathcal{C}_j, j < k} \frac{s_{kx} - s_{jx}}{\|\mathbf{s}_k - \mathbf{s}_j\|^2} \right\} & , i = j \\ -\rho \frac{s_{jx} - s_{ix}}{\|\mathbf{s}_j - \mathbf{s}_i\|^2} & , i < j \end{cases} \\
 F_{yP} &= \begin{cases} \rho \left\{ \sum_{k \in \mathcal{B}_j} \frac{a_{ky} - s_{jy}}{\|\mathbf{a}_k - \mathbf{s}_j\|^2} + \sum_{k \in \mathcal{C}_j, j < k} \frac{s_{ky} - s_{jy}}{\|\mathbf{s}_k - \mathbf{s}_j\|^2} \right\} & , i = j \\ -\rho \frac{s_{jy} - s_{iy}}{\|\mathbf{s}_j - \mathbf{s}_i\|^2} & , i < j \end{cases} \\
 F_{PP} &= \begin{cases} \frac{1}{\sigma^2} \left\{ \sum_{k \in \mathcal{B}_j} 1 + \sum_{k \in \mathcal{C}_j, j < k} 1 \right\} & , i = j \\ 0 & , j \neq i \end{cases}
 \end{aligned}$$

and $\gamma = \frac{(10\beta)^2}{(\ln 10\sigma)^2}$, $\rho = \frac{10\beta}{\ln 10\sigma^2}$. The CRLB for this problem is taken as the inverse of \mathbf{F}_{RSS} .

Bibliography

- [1] A. Savvides, C. C. Han, and M. B. Strivastava. Dynamic fine grained localization in ad-hoc networks of sensors. In *Proceedings of The ACM International Conference on Mobile Computing and Networking (MobiCom'01)*, Rome, Italy, July 2001.
- [2] A. Savvides, M. Srivastava, Lewis Girod, and Deborah Estrin. *Wireless Sensor Networks-Chapter 15 Localization in Sensor Networks*. Springer, New York, USA, 2004.
- [3] J. Bachrach and C. Taylor. *Handbook of Sensor Networks, Chapter Localization in Sensor Networks*. Wiley, New York, USA, 2005.
- [4] S. Gezici and H. V. Poor. Position estimation via ultra-wide-band signals. In *Proceedings of IEEE*, volume 97, pages 386–403, 2009.
- [5] G. Mao, B. Fidan, and B. D. O. Anderson. Wireless sensor network localization techniques. *Computer Networks*, 51(10):2529–2553, January 2007.
- [6] K. W. Cheung, H. C. So, W. K. Ma, and Y. T. Chan. A constrained least squares approach to mobile positioning: algorithms and optimality. *EURASIP Journal on Applied Signal Processing*, 2006:1–23, 2006.
- [7] H. Wymeersch, J. Lien, and M. Z. Win. Cooperative localization in wireless networks. *Proceedings of the IEEE*, 97(2):427–450, February 2009.
- [8] N. Patwari, J. N. Ash, S. Kyperountas, A. O. Hero III, R. L. Moses, and N. S. Correal. Locating the nodes. *IEEE Signal Processing Magazine*, 22(4):54–69, July 2005.
- [9] J. Liu, J. Reich, and F. Zhao. Collaborative in-network processing for target tracking. *EURASIP Journal on Applied Signal Processing*, pages 378–391, 2003.
- [10] J. Hightower and G. Borriello. Location systems for ubiquitous computing. *IEEE Computer*, 34(8):57–66, August 2001.

-
- [11] C. Taylor, H. Shrobe, A. Rahimi, J. Bachrach, and A. Grue. Simultaneous localization, calibration, and tracking in an ad hoc sensor network. In *Proceedings of The International Conference on Information Processing in Sensor Networks (IPSN'06)*, pages 27–33, Nashville, USA, April 2006.
- [12] A. Galstyan, B. Krishnamachari, K. Lerman, and S. Patten. Distributed online localization in sensor networks using a moving target. In *Proceedings of The International Conference on Information Processing in Sensor Networks (IPSN'04)*, pages 61–70, Berkeley, California, USA, April 2004.
- [13] P. Aggarwal and X. Wang. Joint sensor localization and target tracking in sensor networks. *IET Radar Sonar Navigation*, 5(3):225–233, 2011.
- [14] S. Gezici. A survey on wireless position estimation. *Wireless Personal Communications*, 44(3):263–282, February 2008.
- [15] S. Gezici, Z. Tian, G. B. Giannakis, H. Kobayashi, A. F. Molisch, H.V. Poor, and Z. Sahinoglu. Localization via ultra-wideband-radios: A look at positioning aspects for future sensor networks. *IEEE Signal Processing Magazine*, 22:70–84, July 2005.
- [16] N. Patwari, A. Hero, III, M. Perkins, N. S. Correal, and R. J. O’Dea. Relative location estimation in wireless sensor networks. *IEEE Transactions on Signal Processing*, 51(8):2137–2148, 2003.
- [17] G. Carter. Time delay estimation for passive sonar signal processing. *IEEE Transactions on Acoustic, Speech, and Signal Processing*, 29(3):463–470, 1981.
- [18] N. Priyantha, A. Chakraborty, and H. Balakrishnan. A cricket location support system. In *Proceedings of The ACM International Conference on Mobile Computing and Networking (MobiCom'00)*, Boston, Massachusetts, USA, August 2000.
- [19] D. Niculescu and B. Nath. Ad-hoc positioning system using AOA. In *Proceedings of The IEEE Conference on Computer Communications (INFOCOM'03)*, volume 3, pages 1734–1743, 2003.
- [20] Y. Qi. *Wireless Geolocation in a non-line-of-sight environment*. PhD Dissertation, Princeton University, 2004.
- [21] J. Huang, P. Wang, and Q. Wan. CRLBs for WSNs localization in NLOS environments. *EURASIP Journal on Wireless Communications and Networking*, 2011:16.
- [22] V. N. Ekambaram, K. Ramchandran, and R. Sengupta. Scaling laws for cooperative node localization in non-line-of-sight wireless networks. In *IEEE Global Comm. Conf. (GLOBECOM)*, Houston, Texas, USA, December 2011.

- [23] S. Boyd and L. Vandenberghe. *Convex Optimization*. Cambridge University Press, 2004.
- [24] I. Guvenc and C. C. Chong. A survey on TOA based wireless localization and NLOS mitigation techniques. *IEEE Communications Survey and Tutorials*, 11(3):107–124, 2009.
- [25] D. E. Manolakis. Efficient solution and performance analysis of 3-d position estimation by trilateration. *IEEE Transactions on Aerospace and Electronic Systems*, 32(4):1239–1248, October 1996.
- [26] A. H. Sayed, A. Tarighat, and N. Khajehnouri. Network-based wireless location. *IEEE Signal Processing Magazine*, 22:24–40, July 2005.
- [27] B. T. Fang. Simple solutions for hyperbolic and related position fixes. *IEEE Transactions on Aerospace and Electronic Systems*, 26(5):748–758, September 1990.
- [28] P. E. Gill and W. Murray. Algorithms for the solution of the nonlinear least squares problem. *SIAM Journal on Numerical Analysis*, 15(5):977–992, 1978.
- [29] Y. Shang and W. Ruml. Improved MDS-based localization. In *Proceedings of The IEEE Conference on Computer Communications (INFOCOM'04)*, volume 4, pages 2640–2651, Hong-Kong, China, March 2004.
- [30] J. de Leeuw. Convergence of the majorization method for multidimensional scaling. *Journal of Classification*, 5(2):163–180, September 1988.
- [31] J. Costa, N. Patwari, and A. Hero, III. Distributed weighted-multidimensional scaling for node localization in sensor networks. *ACM Transactions on Sensor Networks*, 2(1):39–64, 2006.
- [32] D. J. Torrieri. Statistical theory of passive location systems. *IEEE Transactions on Aerospace and Electronic Systems*, AES20(2):183–198, 1984.
- [33] M. Gavish and A. J. Weiss. Performance analysis of bearing only target location algorithms. *IEEE Transactions on Aerospace and Electronic Systems*, 28(3):817–828, 1992.
- [34] J. J. Caffery and G. L. Stuber. Subscriber location in CDMA cellular networks. *IEEE Transactions on Vehicle Technologies*, 47(2):406–416, May 1998.
- [35] P. Biswas, T. C. Liang, K. C. Toh, and Y. Ye. Semidefinite programming approaches for sensor network localization with noisy distance measurements. *IEEE Transactions on Automation Science and Engineering*, 3:360–371, 2006.

- [36] F. Gustafsson and F. Gunnarsson. Mobile positioning using wireless networks: Possibilities and fundamental limitations based on available wireless network measurements. *IEEE Signal Processing Magazine*, 22(4):41–53, July 2005.
- [37] P. Oğuz-Ekim, J. Gomes, J. Xavier, and P. Oliveira. ML-based sensor network localization and tracking: Batch and time-recursive approaches. In *Proceedings of The European Signal Processing Conference (EUSIPCO'09)*, Glasgow, Scotland, August 2009.
- [38] P. Oğuz-Ekim, J. Gomes, J. Xavier, and P. Oliveira. Robust localization of nodes and time-recursive tracking in sensor networks using noisy range measurements. *IEEE Transactions on Signal Processing*, 59(8):3930–3942, August 2011.
- [39] A. M. C. So and Y. Ye. Theory of semidefinite programming for sensor network localization. *Proceedings of The Sixteenth Annual ACM-SIAM Symposium on Discrete Algorithms*, pages 405–414, 2005.
- [40] L. Doherty, K. S. J. Pister, and E. El Ghaoui. Convex position estimation in wireless sensor networks. In *Proceedings of The IEEE Conference on Computer Communications (INFOCOM'01)*, volume 5, pages 1655–1663, Anchorage, AK, April 2001.
- [41] K. W. Cheung, H. C. So, W. K. Ma, and Y. T. Chan. Least squares algorithms for time of arrival based mobile location. *IEEE Transactions on Signal Processing*, 52(4):1121–1128, April 2004.
- [42] J. O. Smith and J. S. Abel. Closed-form least-squares source location estimation from range-difference measurements. *IEEE Transactions on Acoustic, Speech, and Signal Processing*, 12:1661–1669, Dec 1987.
- [43] W. Dargie and C. Poellabauer. *Fundamentals of Wireless Sensor Networks: Theory and Practice*. Wiley Series on Wireless Communications and Mobile Computing. John Wiley & Sons, 2010.
- [44] T. He, C. Huang, B. M. Blum, J. A. Stankovic, and T. Abdelzaher. Range-free localization schemes for large scale sensor networks. In *Proceedings of The ACM International Conference on Mobile Computing and Networking MobiCom'03*, San Diego, CA, USA, September 2003.
- [45] P. Oğuz-Ekim, J. Gomes, J. Xavier, and P. Oliveira. A convex relaxation for approximate maximum-likelihood 2D source localization from range measurements. In *Proceedings of The International Conference on Acoustic, Speech, and Signal Processing (ICASSP'10)*, pages 2698–2701, Dallas, Texas, USA, March 2010.

- [46] A. Beck, P. Stoica, and J. Li. Exact and approximate solutions of source localization problems. *IEEE Transactions on Signal Processing*, 56(5):1770–1778, May 2008.
- [47] A. Beck, M. Teboulle, and Z. Chikishev. Iterative minimization schemes for solving the single source localization problem. *SIAM Journal on Optimization*, 19(3):1397–1416, 2008.
- [48] E. Xu, Z. Ding, and S. Dasgupta. Wireless source localization based on time of arrival measurement. In *Proceedings of The International Conference on Acoustic, Speech, and Signal Processing (ICASSP'10)*, pages 2842 – 2845, Dallas, Texas, USA, March 2010.
- [49] Y. Chan, H. Hang, and P. Ching. Exact and approximate maximum likelihood localization algorithms. *IEEE Transactions on Signal Processing*, 55(1):10–16, January 2006.
- [50] K. W. Cheung, W. K. Ma, and H. C. So. Accurate approximation algorithm for TOA-based maximum likelihood mobile location using semidefinite programming. In *Proceedings of The International Conference on Acoustic, Speech, and Signal Processing (ICASSP'04)*, volume 2, pages 145–148, Montreal, Canada, May 2004.
- [51] P. Oğuz-Ekim, J. Gomes, J. Xavier, M. Stošić, and P. Oliveira. Approximate maximum likelihood source localization from range measurements through convex relaxation. *submitted to IEEE Transactions on Signal Processing*, arXiv:1111.6755v1, 2011.
- [52] P. Oğuz-Ekim, J. Gomes, J. Xavier, and P. Oliveira. Experimental evaluation of simultaneous 3D localization of sensor nodes and tracking moving targets. In *Proceedings of The European Signal Processing Conference (EUSIPCO'12)*, Bucharest, Romania, August 2012.
- [53] P. Oğuz-Ekim, J. Gomes, M. R. Gholami, E. G. Ström, and P. Oliveira. TW-TOA based cooperative sensor network localization with unknown turn-around time. In *Proceedings of The International Conference on Acoustic, Speech, and Signal Processing (ICASSP'13)*, Vancouver, Canada, May 2013.
- [54] P. Oğuz-Ekim, J. Gomes, and P. Oliveira. RSS based cooperative sensor network localization with unknown transmit power. In *Sinyal İşleme ve İletişim Kurultayı (SIU'13)*, submitted, Girne, Kuzey Kıbrıs Türk Cumhuriyeti, April 2013.
- [55] P. Oğuz-Ekim, J. Gomes, J. Xavier, and P. Oliveira. A polar decomposition approach for exact source localization from squared range differences. *IEEE Signal Processing Letters*, under preparation 2012.

- [56] E. Xu, Z. Ding, and S. Dasgupta. Source localization in wireless sensor networks from signal time of arrival measurements. *IEEE Transactions on Signal Processing*, 59(6):2887–2897, June 2011.
- [57] H. C. So and L. Lin. Linear least squares approach for accurate received signal strength based source localization. *IEEE Transactions on Signal Processing*, 59(8):4035–4040, August 2011.
- [58] A. O. Hero and D. Blatt. Sensor network source localization via projection onto convex sets (POCS). In *Proceedings of The International Conference on Acoustic, Speech, and Signal Processing (ICASSP'05)*, volume 3, pages 689–692, Philadelphia, USA, March 2005.
- [59] F. K. W. Chan and H. C. So. Accurate distributed range-based positioning algorithm for wireless sensor networks. *IEEE Transactions on Signal Processing*, 57(10):4100–4105, 2009.
- [60] A. G. Dimakis, S. Kar, J. M. F. Moura, M. Rabbat, and A. Scaglione. Gossip algorithms for distributed signal processing. *Proceedings of The IEEE*, 98(11):1847–1864, 2010.
- [61] P. Biswas and Y. Ye. Semidefinite programming for ad hoc wireless sensor network localization. In *Proceedings of The International Conference on Information Processing in Sensor Networks (IPSN'04)*, pages 46–54, Berkeley, California, USA, April 2004.
- [62] K. Yang, G. Wang, and Z. Q. Luo. Efficient convex relaxation methods for robust target localization by a sensor network using time differences of arrivals. *IEEE Transactions on Signal Processing*, 57(7):2775–2784, 2010.
- [63] G. Golub and C. van Loan. *Matrix Computations*. Johns Hopkins University Press, Baltimore, MD, third edition, 1996.
- [64] A. Ben-Tal and A. Nemirovski. *Lectures on Modern Convex Optimization: Analysis, Algorithms, and Engineering Applications*. SIAM, 2001.
- [65] Y. Ding, N. Krislock, J. Qian, and H. Wolkowicz. Sensor network localization, Euclidean distance matrix completions, and graph realization. In *Research report CORR 2006-23*, University of Waterloo, Waterloo, ONN2L 3G1, Canada, 2008.
- [66] K. B. Petersen and M. S. Pedersen. The matrix cookbook, October 2008. URL <http://www2.imm.dtu.dk/pubdb/p.php?3274>. Version 20081110.
- [67] A. Ben-Tal and A. Nemirovski. *Lectures on Modern Convex Optimization: Analysis, Algorithms, and Engineering Applications*. SIAM, 2001.

- [68] L. Vandenberghe and S. Boyd. Semidefinite programming. *SIAM Rev.*, 38(1):49–95, 1996.
- [69] E. Larsson and G. Danev. Accuracy comparison of LS and squared-range LS for source localization. *IEEE Transactions on Signal Processing*, 58(2):916–923, 2010.
- [70] Y. T. Chan and K. C. Ho. A simple and efficient estimator for hyperbolic location. *IEEE Transactions on Signal Processing*, 42(8):1905–1915, August 1994.
- [71] S. M. Kay. *Fundamentals of Statistical Signal Processing: Estimation Theory*. Prentice-Hall, Englewood Cliffs, NJ, 1993.
- [72] A. Renaux, P. Foster, P. Larzabal, C. Richmond, and A. Nehorai. A fresh look at the bayesian bounds of the weiss-weinstein family. *IEEE Transactions on Signal Processing*, 39(5):5334–5352, November 2008.
- [73] A. Host-Madsen. On the existence of efficient estimators. *IEEE Transactions on Signal Processing*, 48(11):3028–3031, November 2000.
- [74] A. J. Weiss and J. Picard. Maximum-likelihood position estimation of network nodes using range measurements. *IET Signal Processing*, 2(4):394–404, 2008.
- [75] G. Destino and G. Abreu. On the maximum likelihood approach for source and network localization. *IEEE Transactions on Signal Processing*, 59(10):4954–4970, October 2011.
- [76] L. M. Ni, Y. Liu, Y. C. Lau, and A. P. Patil. LANDMARC: Indoor location sensing using active RFID. *Wireless Networks*, 10:701–710, 2004.
- [77] R. Want, A. Hopper, V. Falcao, and J. Gibbons. The active badge location system. *ACM Transactions on Information Systems (TOIS)*, 10:91–102, 1992.
- [78] A. Ward, A. Jones, and A. Hopper. A new location technique for the active office. *IEEE Personal Communications*, 4:42–47, October 1997.
- [79] A. Conti, D. Dardari, and M. Win. Experimental results on cooperative UWB based positioning systems. In *Proceedings of the IEEE International Conference on Ultra-Wideband (ICUWB'08)*, volume I, pages 191–195, 2008.
- [80] M. Popa, J. Ansari, J. Riihijarvi, and P. Mahonen. Combining Cricket system and inertial navigation for indoor human tracking. In *Proceedings of the IEEE Wireless Communication and Networking Conference (WCNC'08)*, pages 3063–3068, 2008.

- [81] S. Funiak, C. Guestrin, M. Paskin, and R. Sukthankar. Distributed localization of networked cameras. In *Proceedings of The International Conference on Information Processing in Sensor Networks (IPSN'06)*, pages 34–42, Nashville, USA, April 2006.
- [82] R. Rangarajan, R. Raich, and A. Hero, III. Euclidean matrix completion problems in tracking and geo-localization. In *Proceedings of The International Conference on Acoustic, Speech, and Signal Processing (ICASSP'08)*, pages 5324–5327, Las Vegas, Nevada, USA, March 2008.
- [83] J. Teng, H. Snoussi, and C. Richard. Decentralized variational filtering for simultaneous sensor localization and target tracking in binary sensor networks. In *Proceedings of The International Conference on Acoustic, Speech, and Signal Processing (ICASSP'09)*, pages 2233–2236, Taipei, Taiwan, April 2009.
- [84] R. L. Moses, D. Krishnamurthy, and R. Patterson. A self-localization method for wireless sensor networks. *EURASIP Journal on Applied Signal Processing*, 4: 348–358, 2003.
- [85] W. K. Lui, W. K. Ma, H. C. So, and F. K. W. Chan. Semi-definite programming approach to sensor network node localization with anchor position uncertainty. In *Proceedings of The International Conference on Acoustic, Speech, and Signal Processing (ICASSP'09)*, pages 2245–2248, Taipei, Taiwan, April 2009.
- [86] S. Srirangarajan, A. H. Tewfik, and Z. Q. Luo. Distributed sensor network localization with inaccurate anchor positions and noisy distance information. In *Proceedings of The International Conference on Acoustic, Speech, and Signal Processing (ICASSP'07)*, volume 3, pages 521–524, Honolulu, Hawaii, USA, April 2007.
- [87] M. Vemula, M. F. Bugallo, and P. M. Djurić. Sensor self-localization with beacon position uncertainty. *Elsevier Signal Processing*, 89(6):1144–1154, 2009.
- [88] U. A. Khan, S. Kar, and J. M. F. Moura. Distributed sensor localization in random environments using minimal number of anchor nodes. *IEEE Transactions on Signal Processing*, 57(5):2000–2016, 2009.
- [89] D. Hunter and K. Lange. A tutorial on MM algorithms. *The American Statistician*, 58(1):30–37, 2004.
- [90] J. Picard and A. J. Weiss. Accurate geolocation in the presence of outliers using linear programming. In *Proceedings of The European Signal Processing Conference (EUSIPCO'09)*, pages 2077–2081, Glasgow, Scotland, August 2009.

-
- [91] J. Dattorro. *Convex Optimization and Euclidean Distance Geometry*. Meboo publishers, 2005.
- [92] M. S. Lobo, L. Vandenberghe, S. Boyd, and H. Lebet. Applications of second-order cone programming. *Linear Algebra and its Applications*, 284(1-3):193–228, 1998.
- [93] T. K. Moon and W. C. Stirling. *Mathematical Methods and Algorithms for Signal Processing*. Prentice-Hall, 2000.
- [94] P. Rodriguez and B. Wohlberg. Efficient minimization method for a generalized total variational functional. *IEEE Transactions on Image Processing*, 18(2):322–332, 2009.
- [95] C. Chang and A. Sahai. Cramer-Rao-type bounds for localization. *EURASIP Journal on Applied Signal Processing*, 2006:1–13, 2006.
- [96] T. Jia and R. M. Buehrer. A new Cramer-Rao lower bound for TOA-based localization. In *Proceedings of The Military Communications Conference (MILCOM'08)*, pages 1–5, Santiago, California, USA, November 2008.
- [97] Z. Sahinoglu. Improving range accuracy of ieee 802.15.4a radios in the presence of clock frequency offsets. *IEEE Communications Letters*, 15(2):244–246, February 2011.
- [98] J. Y. Lee and R. A. Scholtz. Ranging in a dense multipath environment using an UWB radio link. *IEEE Journal on Selected Areas in Communications*, 20(9):1677–1683, December 2002.
- [99] Y. Wang, G. Leus, and X. Ma. An UWB ranging based localization strategy with internal attack immunity. In *Proceedings of The IEEE International Conference on Ultra-Wideband (ICUWB'10)*, volume 2, pages 1–4, Nanjing, China, September 2010.
- [100] Y. Wang, G. Leus, and X. Ma. Time based localization for asynchronous wireless sensor networks. In *Proceedings of The International Conference on Acoustic, Speech, and Signal Processing (ICASSP'11)*, pages 3284–3287, Prague, Czech Republic, May 2011.
- [101] Y. Wang, X. Ma, and G. Leus. Robust time based localization for asynchronous networks. *IEEE Transactions on Signal Processing*, 59(9):4397–4410, September 2011.

- [102] Y. Zhou, C. L. Law, Y. L. Guan, and F. Chin. Indoor elliptical localization based on asynchronous UWB range measurement. *IEEE Transactions on Instrumentation and Measurement*, 60(1):248–257, January 2011.
- [103] S. Zhu and Z. Ding. Joint time synchronization and localization using TOAs: A linearization based WLS solution. *IEEE Journal on Selected Areas in Communications*, 28(7):1017–1025, September 2010.
- [104] J. Zheng and Y.C. Wu. Joint time synchronization and localization of an unknown node in wireless sensor networks. *IEEE Transactions on Signal Processing*, 58(3):1309–1320, 2010.
- [105] M. R. Gholami, S. Gezici, and E. G. Ström. Improved position estimation using hybrid TW-TOA and TDOA in cooperative networks. *IEEE Transactions on Signal Processing*, 60(7):3770–3785, 2012.
- [106] Z. Sahinoglu and S. Gezici. Enhanced position estimation via node cooperation. In *Proceedings of The IEEE International Conference on Communications (ICC'10)*, pages 1–6, Cape Town, South Africa, July 2010.
- [107] P. Biswas and Y. Ye. A distributed method for solving semidefinite programs arising from ad hoc wireless sensor network localization. *Nonconvex Optimization and its Applications*, 82:69–84, 2006.
- [108] G. Wang and K. Yang. Efficient semidefinite relaxation for energy based source localization in sensor networks. In *Proceedings of The International Conference on Acoustic, Speech, and Signal Processing (ICASSP'09)*, pages 2245–2248, Taipei, Taiwan, April 2009.
- [109] R. M. Vaghefi, M. R. Gholami, and E. G. Ström. RSS-based sensor localization with unknown transmit power. In *Proceedings of The International Conference on Acoustic, Speech, and Signal Processing (ICASSP'11)*, pages 3284–3287, Prague, Czech Republic, May 2011.
- [110] R. M. Vaghefi, M. R. Gholami, R. M. Buehrer, and E. G. Ström. Cooperative received signal strength-based sensor localization with unknown transmit power. *IEEE Transactions on Signal Processing*, digital object identifier: 10.1109/TSP.2012.2232664, December 2012.
- [111] Y. Huang, J. Benesty, G. W. Elko, and R. M. Mersereau. Realtime passive source localization: A practical linear correction least-squares approach. *IEEE Transactions on Signal Processing*, 9(8):943–956, Nov 2002.

- [112] C. Mensing and S. Plass. Positioning algorithms for cellular networks using TDOA. In *Proceedings of The International Conference on Acoustic, Speech, and Signal Processing (ICASSP'06)*, Toulouse, May 2006.
- [113] K. Yang, G. Wang, and Z. Q. Luo. Efficient convex relaxation methods for robust target localization by sensor network using time differences of arrival. *IEEE Transactions on Signal Processing*, 57(7):2775–2784, July 2009.
- [114] M. Rydström, E. G. Ström, and A. Svensson. Robust sensor network positioning based on projections onto circular and hyperbolic convex sets (POCS). In *Proceedings of The IEEE 12th International Workshop on Signal Processing Advances in Wireless Communications (SPAWC'06)*, Cannes, July 2006.
- [115] R. J. Vanderbei. Extension of Piyavskii's algorithm to continuous global optimization. In *Proceedings of The IEEE 12th International Workshop on Signal Processing Advances in Wireless Communications (SPAWC'97)*, Cannes, July 1997.
- [116] D. R. Jones, C. D. Perttunen, and B. E. Stuckman. Lipschitzian optimization without the lipschitz constant. *Journal Of Optimization Theory and Application*, 79(1):157–181, October 1993.
- [117] J. Nocedal and S. J. Wright. *Numerical Optimization*. Springer, New York, USA, 1999.
- [118] B. Denis, J.B. Pierrot, and C. Abou-Rjeily. Joint distributed synchronization and positioning in UWB ad hoc networks using TOA. *IEEE Transactions on Microwave Theory and Techniques*, 54(4):1896–1911, June 2006.
- [119] J. R. Magnus and H. Neudecker. *Matrix Differential Calculus with Applications in Statistics and Econometrics*. Wiley Series in Probability and Statistics. John Wiley & Sons, third edition, 2007.
- [120] R. A. Horn and C. A. Johnson. *Matrix Analysis*. Cambridge University Press, 1990.

Curriculum Vitae

Education:

- **Instituto Superior Técnico-Institute for Systems and Robotics**

PhD in Electrical and Computer Engineering

Research Topic: Localization in Wireless Sensor Networks

October 2007-2013 (Expected)

- **Middle East Technical University, Ankara**

M. Sc in Electrical and Electronics Engineering

Research Topic: Implementation of Northfinding Techniques

September 2003-June 2006

- **Middle East Technical University, Ankara**

B. Sc in Electrical and Electronics Engineering

Specialization: Communication Systems

September 1998-June 2003

Professional Experience:

- **Scientific and Technical Research Council of Turkey (TUBITAK), Ankara**

Defense Industries Research and Development Institute (SAGE)

Full Time Research Engineer

August 2003-June 2006

Publication:

Journal Publications:

- Pınar Oğuz-Ekim, João Gomes, João Xavier, and Paulo Oliveira, *Robust localization of nodes and time-recursive tracking in sensor networks using noisy range measurements*, IEEE Transactions on Signal Processing, vol. 59, no. 8, pp. 3930-3942, August 2011.
- Pınar Oğuz-Ekim, João Gomes, João Xavier, and Paulo Oliveira, *Approximate Maximum Likelihood Source Localization from Range Measurements Through Convex Relaxations*, submitted to IEEE Transactions on Signal Processing.
- Pınar Oğuz-Ekim, João Gomes, João Xavier, and Paulo Oliveira, *A polar decomposition approach for exact source localization from squared range differences* under preparation for IEEE Signal Processing Letters.

Conference Publications:

- Pınar Oğuz-Ekim, Mohammad Reza Gholami, Joao Gomes and Erik Strom, *TW-TOA Cooperative Sensor Network Localization with Unknown Turn Around Time*, Proceedings of The International Conference on Acoustic, Speech, and Signal Processing (ICASSP'13), May 2013.
- Pınar Oğuz-Ekim, João Gomes and Paulo Oliveira, *RSS based Cooperative Sensor Network Localization with Unknown Transmit Power*, submitted to Sinyal İşleme ve İletişim Kurultayı (SIU'13), April 2013.
- Pınar Oğuz-Ekim, João Gomes, João Xavier, and Paulo Oliveira, *Experimental Evaluation of Simultaneous 3D Localization of Sensor Nodes and Tracking of Moving Targets*, Proceedings of The European Signal Processing Conference (EU-SIPCO'12), August 2012, Bucharest/Romania.
- Pınar Oğuz-Ekim, João Gomes, João Xavier, and Paulo Oliveira, *A Convex Relaxation for Approximate Maximum Likelihood 2D Source Localization from Range Measurements*, Proceedings of The International Conference on Acoustic, Speech, and Signal Processing (ICASSP'10), March 2010, Dallas/Texas, USA.

-
- Pınar Oğuz-Ekim, João Gomes, João Xavier, and Paulo Oliveira, *ML Based Sensor Network Localization and Tracking: Batch and Time Recursive Approaches*, Proceedings of The European Signal Processing Conference (EUSIPCO'09), August 2009, Glasgow/Scotland.
 - Pınar Oğuz, Ezgi Gunaydin, Dr. Tolga Sonmez, *Implementing a GNSS Emulator For Navigation Systems*, 6th International ESA Conference on Guidance, Navigation and Control Systems, October 2005, Loutraki / Greece.
 - Pınar Oğuz, Ezgi Gunaydin, Dr. Tolga Sonmez, *Implementing a GPS Emulator For Integrated Navigation Systems*, AIAC 2005-074, 3rd AIAC, August 2005, Ankara / Turkey.
 - Pınar Oğuz, Dr. Tolga Sonmez, *GNSS Benzetimcisi Kullanarak Yonelim Bulumu Gereklenmesi*, SAVTEK, June 2006, Ankara / Turkey.